Workshop of
CODE_BRIGHT USERS

22 May 2024
Barcelona, Spain

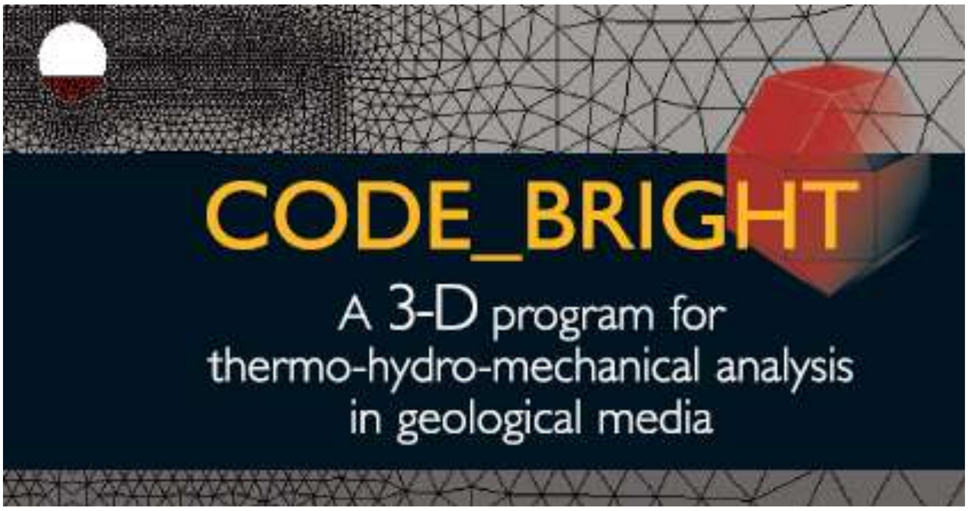

Department of Civil and Environmental Engineering
UPC-BarcelonaTech
Barcelona, Spain

CIMNE
International Center for Numerical Methods in Engineering
Barcelona, Spain

CODE_BRIGHT

A 3-D program for thermo-hydro-mechanical analysis in geological media

WORKSHOP OF CODE_BRIGHT USERS

Barcelona, 22 May 2024

Department of Civil and Environmental Engineering

(UPC-BarcelonaTech, Barcelona, Spain)

CIMNE

(International Center for Numerical Methods in Engineering, Barcelona, Spain)

CONTENTS

CALCULATION OF REACTION RATES INDUCED BY TEMPERATURE CHANGES

Rubén Vidal[*] and Maarten W. Saaltink[*†]

[*] Department of Civil and Environmental Engineering (DECA), School of Civil Engineering,
Universitat Politècnica de Catalunya − BarcelonaTech (UPC),
UPC Campus Nord, Jordi Girona 1-3, Building D2, 08034 Barcelona, Spain
E-mail: ruben.vidal.montes@upc.edu

[†] Associated Unit: Hydrogeology Group
(UPC-CSIC), Barcelona, Spain

Key words: Temperature, Reactive Transport, Analytical Solution, Modelling

ABSTRACT. *Temperature changes can modify the geochemistry and the properties of soils and rocks. This effect can be important in geothermal systems such as in Aquifer Thermal Energy systems (ATES), where heat is injected and extracted with wells into an aquifer. Reactive transport, which includes heat transport, can affect negatively the operation of ATES systems. We present a novel analytical solution that permits to study the thermo-hydro-chemical (THC) processes and to verify complex numerical models. We apply this solution to an ATES pilot project located in Bern, Switzerland.*

1 INTRODUCTION

Temperature has an effect on many properties and chemical processes that take place in the subsurface. Temperature changes affect the reaction kinetics, redox processes, oxidation of organic matter, sorption-desorption of anions and cations and solubility of minerals[i]. Aquifer Thermal Energy Storage (ATES) consists of several wells that simultaneously inject or extract thermal energy into aquifers. The main aim of ATES is to store the excess of energy to reuse it when there is an energy deficit. One of the main advantages of ATES is that can contribute to limit climate change[ii].

We propose a novel analytical solution which considers aqueous reactions and precipitation-dissolution affected by temperature. The aim of this solution is to analyse the thermo-hydro-chemical (THC) processes and to verify complex numerical models. We use this solution in combination of geochemical calculations and the results from TH (thermo-hydraulic) finite elements models to study an ATES system.

2 FORMULATION

The analytical solution is calculated by extending the procedure of De Simoni et al. (2005 and 2007)[iii, iv] with the inclusion of temperature dependencies[v]. The procedure assumes only aqueous and mineral reactions in equilibrium. It consists of four steps: (1) evaluation of the mixing ratios of end-members and temperatures, (2) evaluation of conservative components,

(3) speciation calculations and (4) calculation of reaction rates (r). Following this procedure, the rate for a closed system is reduced to a particular case with only one end-member and without dependence on the mixing ratio[v]:

$$r = r_{mix} + r_{ret} + r_{cond} \tag{1}$$

The rate of the chemical reaction (1) can be decomposed in three rates or processes:

1) Mixing (mixing of waters of different temperature):

$$r_{mix} = -\rho_l \frac{\partial^2 c}{\partial T^2} (\nabla T)^T \phi \mathbf{D} \nabla T^T \tag{2}$$

2) Heat retardation (effect of the retardation of heat front with respect to the front of conservative solutes):

$$r_{ret} = \rho_l \frac{\partial c}{\partial T} (1 - R) \phi \frac{\partial T}{\partial t} \tag{3}$$

3) Heat conduction (differences between heat conduction and solute diffusion):

$$r_{cond} = -\rho_l \frac{\partial c}{\partial T} \nabla \cdot (\phi D_{dif} - C_l^{-1} \lambda) \nabla T \tag{4}$$

Where ρ_l is liquid density, c is concentration of a reactive component, T is temperature, ϕ is porosity, $\mathbf{D}$ is a tensor for dispersion and diffusion coefficients, R is a retardation coefficient for heat, t is time, D_{dif} is a tensor for diffusion coefficient, C_l is volumetric heat capacity for liquid and λ is thermal conductivity.

3 HT-ATES SYSTEM

The power plant of Forsthaus, in Bern (Switzerland), has an excess of heat. In order to reuse this heat, it is planned to implement a High Temperature Aquifer Thermal Energy Storage (HT-ATES) system. This system consists of an injection of hot water at 90°C in a Central well and the extraction of water in four Auxiliary wells during summer. In winter, the Auxiliary wells inject water at 50°C and the Central well extracts water.

We focus on the mixing of 2 waters from the same end-member (same origin), but at different temperatures. One water represents the water of the aquifer and the other the re-injected water from the surface. Both waters are in equilibrium with calcite and dolomite, which are present in the aquifer. The two main reactions are the precipitation or dissolution of calcite and dolomite:

We simplify the procedure of the formulation in 3 steps in order to obtain the reaction rate[v]:

1. Thermo-hydraulic modelling. We calculate the flow rate, temperature and temperature derivatives ($\partial T/\partial t$, ∇T, $\nabla^2 T$) by using the results of the finite element code CODE_BRIGHT[vi].
2. Geochemistry modelling: We calculate the relation between concentration and temperature ($\partial c/\partial T$, $\partial c^2/\partial T^2$) by using the results from geochemical calculations of PHREEQC[vii].
3. Substitution of the variables of steps 1 and 2 in the formula of the reaction rate (1).

We study a simplification of the real case with a single well (Figure 1A). One year of operation consist of a stage of injecting hot water into the well (0 – 216 days) and a stage of extraction (216 – 365 days). The TH model simulates a single well that injects and extracts hot water in a vertical 2D axisymmetrical domain (Figure 1B). The domain consists of a 2.5 m thick sandstone layer on top of a 5 m thick clay layer. Water is injected or extracted at the left boundary which represents the axis of axisymmetry. A liquid pressure and temperature are prescribed at the right boundary. The initial liquid pressure in the full domain is 4.5 MPa and the initial temperature is 15°C (Figure 1B). We simulate injected water by a prescribed heat and water flux boundary condition. Water of 90°C is injected during the injection stage. Water extraction is simulated with boundary conditions of a prescribed water flux. The flow rate in each layer is shown in Figure 1B. The properties of the sandstone and the clay are the same, except for porosity and permeability that are lower in the clay.

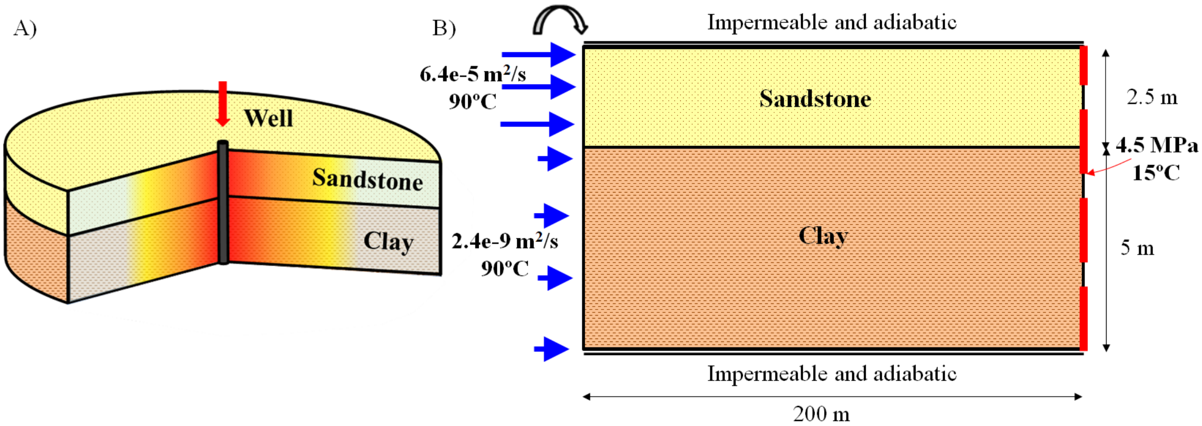

Figure 1. HT-ATES case study (A) and TH model (B).

4 RESULTS

The highest temperature variations take place in the sandstone, which is the most permeable material (Figure 2A). Heat retardation and heat conduction are more relevant than mixing (Figures 2D, 2E, 2F). Reaction rate tends to infinity in the limit between the sandstone and the clay because the effect of heat conduction.

The results of our method have been compared with the results calculated by the coupled thermo-hydro-chemical code RETRASO. We observe a good agreement between the reaction rates for calcite and dolomite of our method and RETRASO (Figures 2B and 2C).

Since the reaction rates for calcite and dolomite are not very significant with the conditions of this case, no important porosity changes are expected.

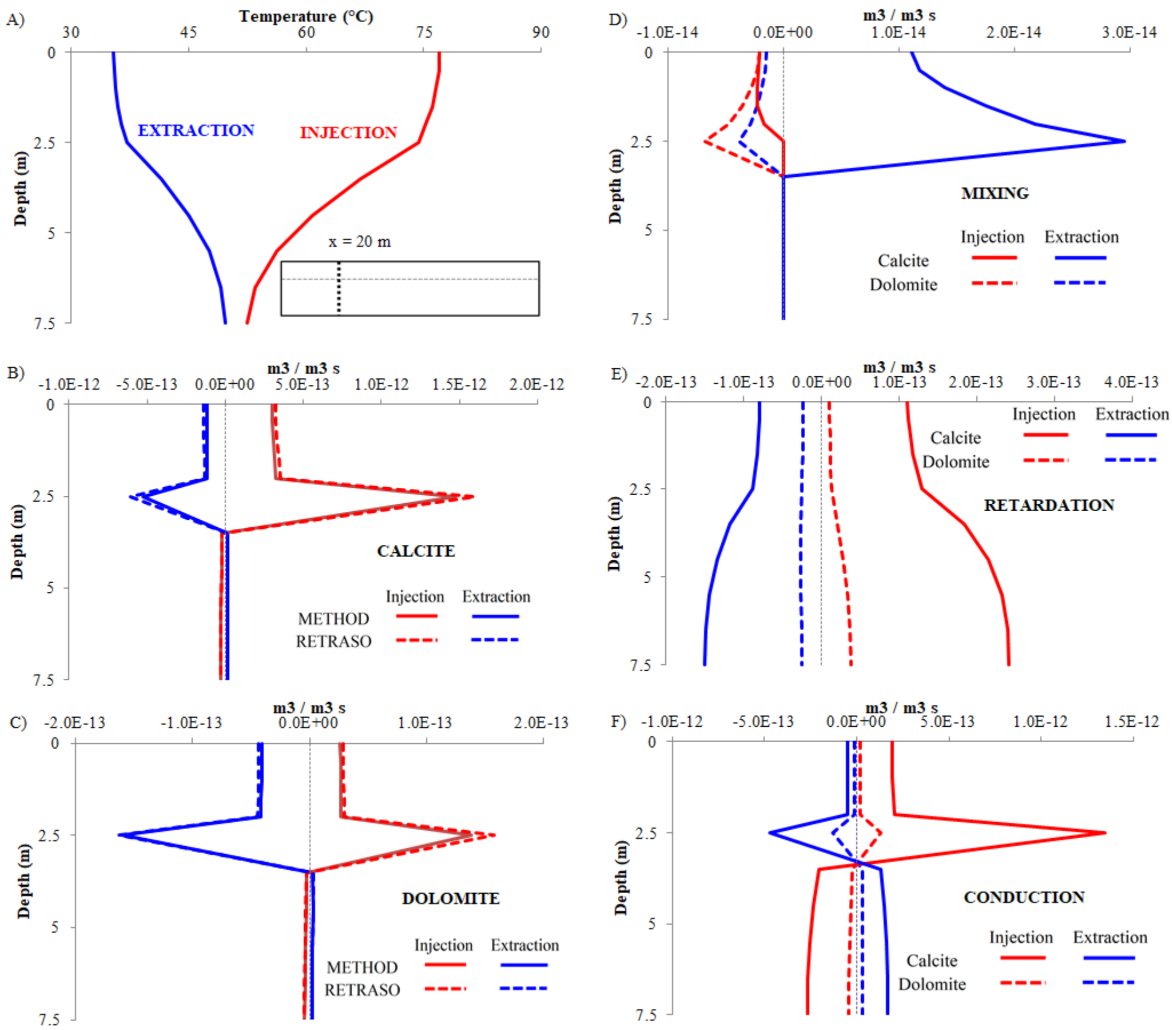

Figure 2. Variation of temperature with depth at 20 m (A). Variation of calcite (B) and dolomite (C) dissolution rate with depth at 20 m with our formulation and RETRASO. Components of the total reaction rate at 20 meters: mixing (D), heat retardation (E) and heat conduction (F). Except in Figure A, positive values mean dissolution, while negative values mean precipitation.

5 CONCLUSIONS

We propose a novel analytical solution that can be used to understand better the THC phenomena. The rate can be separated in three terms or TH processes: mixing, heat retardation and heat conduction. We use this solution in an HT-ATES system in Bern. We study the mixing of 2 waters from the same origin, but at different temperature. In this particular case, mixing is the least relevant process and heat conduction tends to infinite values in the interface between the sandstone and clay.

6 ACNOWLEDGMENTS

This work was financed by the ERANET project HEATSTORE (170153-4401). This project has been subsidized through the ERANET cofund GEOTHERMICA (Project n. 731117), from the European Commission, RVO (the Netherlands), DETEC (Switzerland), FZJ-PTJ (Germany), ADEME (France), EUDP (Denmark), Rannis (Iceland), VEA (Belgium), FRCT (Portugal), and MINECO (Spain). Also, the first author is supported by a grant from the Department of Research and Universities of the Generalitat de Catalunya (2023 FI-3 00208).

REFERENCES

[i] Possemiers, M.; Huysmans M.; Batelaan, O. (2014). Influence of Aquifer Thermal Energy Storage on groundwater quality: A review illustrated by seven case studies from Belgium, Journal of Hydrology: Regional Studies, Volume 2, 2014, Pages 20-34, ISSN 2214-5818, https://doi.org/10.1016/j.ejrh.2014.08.001.

[ii] Bloemendal, M.; Jaxa-Rozen, M.; Olsthoorn, T. (2018). Methods for planning of ATES systems, Applied Energy, Volume 216, 2018, Pages 534-557, ISSN 0306-2619, https://doi.org/10.1016/j.apenergy.2018.02.068.

[iii] De Simoni, M.; Carrera, J.; Sanchez-Vila, X.; Guadagnini, A. (2005). A procedure for the solution of multicomponent reactive transport problems. Water Resources Research, 41, W11410. https://doi.org/10.1029/2005WR004056.De Simoni, M.; Sanchez-Vila, X.; Carrera, J.; Saaltink, M.W. (2007). A mixing ratios-based formulation for multicomponent reactive transport, Water Resour. Res.,43, W07419, doi:10.1029/2006WR005256.

[iv] De Simoni, M.; Sanchez-Vila, X.; Carrera, J.; Saaltink, M.W. (2007). A mixing ratios-based formulation for multicomponent reactive transport, Water Resour. Res.,43, W07419, doi:10.1029/2006WR005256.

[v] Vidal, R.; Saaltink, M.W. (2024). A novel method for decoupling thermo-hydraulic processes from chemical reactions to understand the effect of heat on chemical reaction. *Submitted*.

[vi] Olivella, S.; Gens, A.; Carrera, J.; Alonso, E.E. (1996). Numerical formulation for a simulator (CODE_BRIGHT) for the coupled analysis of saline media. Eng. Comput. 1996 13(7), 87–112. doi:10.1108/02644409610151575.

[vii] Parkhurst, D.L.; Appelo, C.A.J. (2013) Description of Input and Examples for PHREEQC Version 3—A Computer Program for Speciation, Batch-Reaction, One-Dimensional Transport, and Inverse Geochemical Calculations. US Geological Survey Techniques and Methods, Book 6, Chapter A43, 497 p. http://pubs.usgs.gov/tm/06/a43.

Numerical analyses of spherical indenter intrusion into sandstone

Sheng Zhang [a], Alfonso Rodriguez-Dono [a,b*], Zilong Zhou [c], Fei Song [d]

a. Department of Civil and Environmental Engineering, Universitat Politècnica de Catalunya (UPC), Spain, 08034

b. International Centre for Numerical Methods in Engineering (CIMNE), Barcelona, Spain, 08034

c. School of Resources and Safety Engineering, Central South University, Changsha, China, 410083

d. School of Aerospace Engineering and Applied Mechanics, Tongji University, Shanghai, China, 200092

Corresponding author: Alfonso Rodriguez-Dono (alfonso.rodriguez@upc.edu)

Abstract

For a comprehensive understanding of the underlying mechanisms in rock fragmentation under the compression of steel balls during ball milling, this study employs the CODE_BRIGHT finite element software to simulate single and multiple indenters intrusion into rocks. The analysis focuses on the evolution of the stress field in rocks under the influence of intrusion depth and indenter diameter. The results reveal a reduction in both axial and radial stresses with increasing intrusion depth into the rock. Shear stress experiences an initial rise followed by a decline, while circumferential stress demonstrates an initial increase followed by a rapid decrease in the radial direction. The impact of indenter diameter on the stress field within rock diminishes with increasing indenter diameter, following a reduction described by the exponential decay. Compared to single indenter intrusion, the stress field within the rock under dual-indenter intrusion exhibits numerically larger magnitudes and a broader influence range.

Keywords: Spherical indenter; Ball milling; Stress fields; CODE_BRIGHT;

1 Introduction

Rock fragmentation, as pivotal subject topic in rock mechanics research, holds widespread and profound implications in both scientific and engineering domains [1-3]. With ongoing advancements in crushing equipment and techniques, the study of ball milling has garnered significant attention. While significant achievements have been made in this field, the mechanical mechanisms of ball milling for rock fragmentation remaining largely unrevealed [4-6]. This gap is attributed partly to the dynamic variations in both particle and steel ball sizes during the ball milling process. In fact, Eric Forssberg [7] have underscored the existence of three distinct forms of fragmentation – abrasion, compression, and impact – between steel balls and particle in the ball milling (Figure.1). Hence, this study simulates the intrusion of an indenter into rock to simulate the compression of steel balls in a ball mill. By quantifying the evolution of the stress field within the rock.

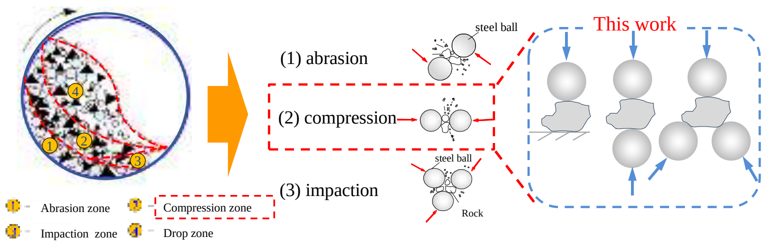

Figure. 1 Fragmentation patterns and primary compression modes of rock within the ball mill

2 Numerical modeling and validation

2.1. Numerical model

（1）Geometric parameters and boundary conditions

Figure 2(a) illustrates schematic diagram of a spherical indenter intrusion into rock, where the indenter diameter ranges from 10 to 500 mm, and the rock specimen has a radius of 50 mm. Displacement constraints are imposed along the model's symmetry axis. The upper boundary is subjected to a vertical loading at a rate of 0.005 mm/s.

(2) Mesh Generation

The mesh elements in the model are configured as quadrilaterals. Considering the localized stress concentration in the indenter-rock contact region, a high-density mesh is employed in this area. In contrast, grids away from the contact region are relatively sparse.

(3) Constitutive Model

The numerical model is delineated into three components (Figure 2). Spherical indenter (Part I) is modeled as an elastic rigid body. The rock (Part III) is characterized as elastic-plastic. During the intrusion process, the contact between the indenter and the rock dynamically evolves. Thus, Part II is modeled as an air gap [8,9], with constitutive model follows a bi-linear elasticity model.

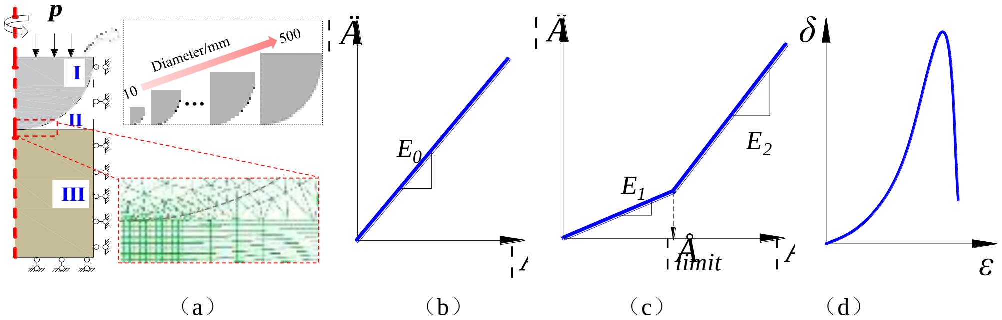

Figure 2 Numerical model and constitutive relationship. (a) Boundary conditions and local meshing (b) Linear elastic model, (c) Bi-linear elasticity model, (d) Elastoplastic model.

2.2. Parameter calibration and validation

Given that the steel balls inside the ball mill are steel material, the parameters of the spherical indenter in the model reference the standard steel parameters. This section use "trial and error" approach to calibrate the parameters for the rock and air gap [10]. The detailed process is depicted in Figure 3， and parameter result list in table 1.

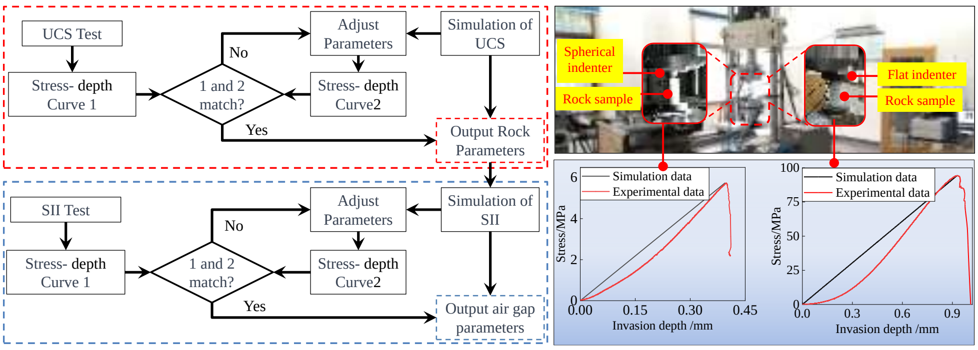

Figure 3 Calibration procedure and experimental comparison

Table 1: Model parameter calibration results for spherical indenter indentation into rock

	Parameter	Value	Unit	Significance
Part I	E_0	300	GPa	Elastic modulus of the indenter
	V_0	0.25	-	Poisson's ratio of the indenter
Part II	E_1	1000	MPa	Young modulus for air gap， if $\varepsilon_v > \varepsilon_{v\,\mathrm{limit}}$
	E_2	1	MPa	Young modulus if $\varepsilon_v < \varepsilon_{v\,\mathrm{limit}}$
	v_1	0.48		Poisson's Ratio

	$\varepsilon_{v\ \mathrm{limit}}$	0.99	Volumetric strain limit to change elastic modulus (positive value)
Part III	E	6.79GPa	Elastic modulus
	v	0.25	Poisson's ratio
	bulk	1.209e8	Bulk modulus
	shear	2.1e8	Shear modulus
	coh	8.30e5	Cohesion
	fric	22	Friction angle
	tens	5.02 e6	Tensile strength

2.3 Simulation scheme

Figure 4 depicts a schematic illustration of a spherical indenter with a radius R intruding to a depth z into the rock. Every point within the rock experiences axial stress (σ_z), radial stress (σ_r), shear stress (τ), and circumferential stress ($\sigma_{r(x)}$) along the radial direction. Based on Figure 4, the numerical simulation scheme is formulated as outlined in Table 2.

Table 2 Model parameters and schemes for SII test

Software	Intrusion mode	Indenter diameter /mm	Intrusion depth /mm	Research theme	Ratio
CODE_BRIGHT	Single indenter	50	0~0.35	Stress field	0.2~10
		10~500	0.10		
	Dual-indenter	50	0~0.35		
		10~500	0.10		

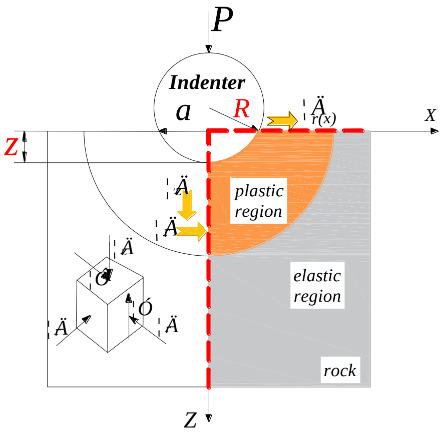

Figure 4 Schematic diagram of spherical indenter intrusion into rock

3 Simulation and comparisons of single indenter intrusion

3.1 Stress field variations with intrusion depth

Both axial and radial stresses decrease with increasing axial depth at a given intrusion depth. Axial and radial stresses beneath the rock increase with the intrusion depth, but the rate of increase diminishes with deeper intrusion, as shown in Figure5.

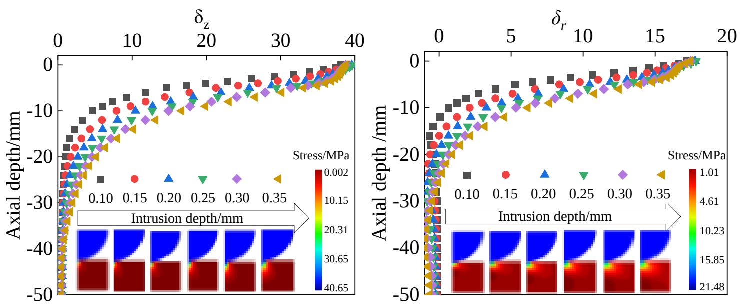

（a） （b）

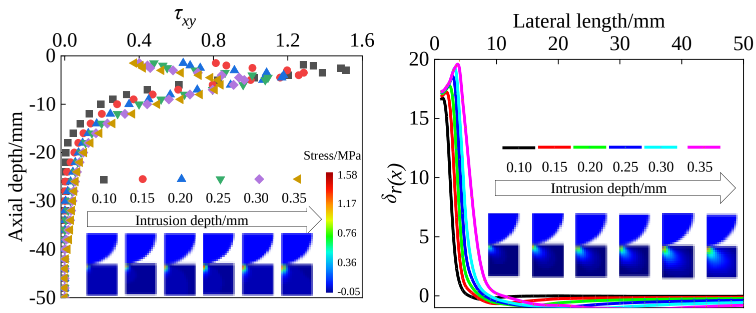

（c） （d）

Figure 5 Evolution of stress fields during intrusion

Shear stress exhibits an initial increase followed by a subsequent decrease with the axial depth at any intrusion depth. Furthermore, At a constant intrusion depth, circumferential stress initially increases in the x-axis direction and then rapidly decreases. As the intrusion depth increases, the circumferential stress values gradually rise.

3.2 Stress field variations with indenter diameter

As the indenter diameter increases, a consistent trend of stress reduction at various positions within the rock. Specifically, both axial and radial stresses decrease with the increasing diameter of the indenter. Shear stress initially increases and then decreases with depth along the axial direction, gradually diminishing with the increase in ball diameter. Radial stresses for any ball diameter exhibit a trend of initial increase followed by a decrease, and as the ball diameter increases, radial stresses gradually decrease.

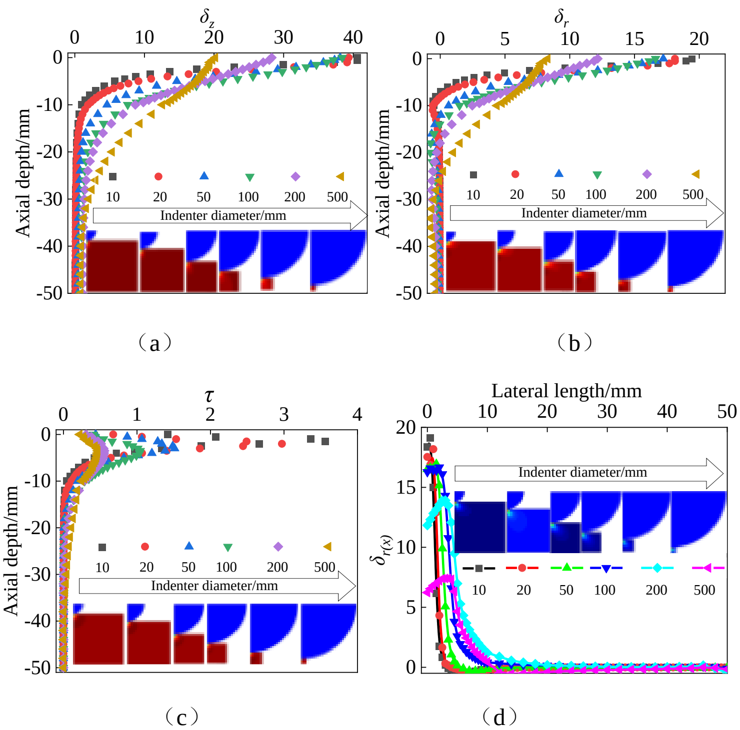

Figure 6 Variation of stress fields during intrusion with indenter diameter.

4 Simulation and comparisons of dual indenters intrusion

4.1 Stress field variations with intrusion depth

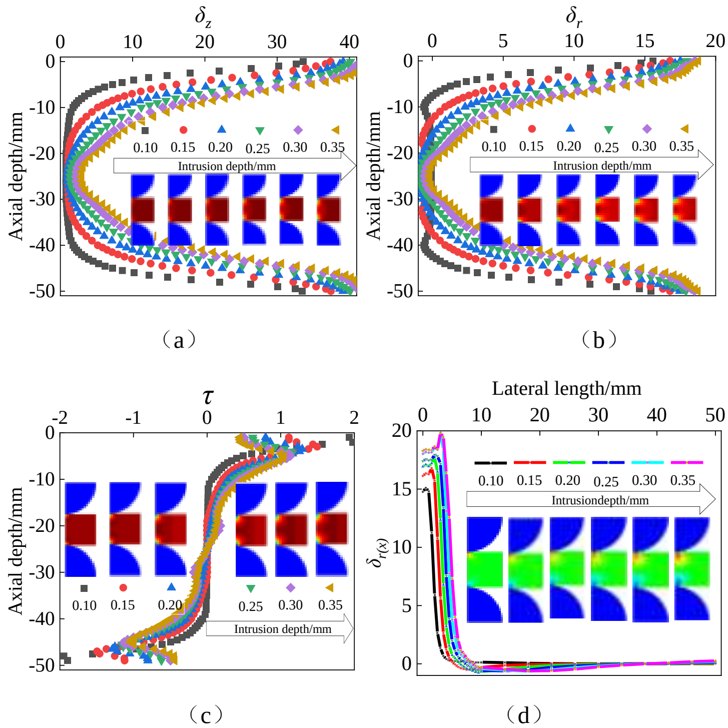

Figure 7 Evolution of stress fields during dual indenters intrusion varying intrusion depth.

Comparing Figure5 reveals that the stress variations with intrusion depth follow a pattern similar to that observed in single indenters intrusion. Both axial and radial stresses exhibit a 'bell-shaped' distribution within the rock during dual indenters intrusion. Circumferential stress values and variation patterns remain nearly unchanged (Figure 7(d))

4.2 Stress field variations with indenter diameter

Figure 8 illustrates the variation of the internal stress field within the rock under dual-indenter intrusion, corresponding to different indenter diameters. Overall, the stress variations within the rock are consistent for different indenter diameters. A comparative analysis with the axial stress during single indenter intrusion into the rock reveals that, with an increase in indenter diameter, the stress values exhibit a notable enhancement compared to the scenario of single indenter intrusion.

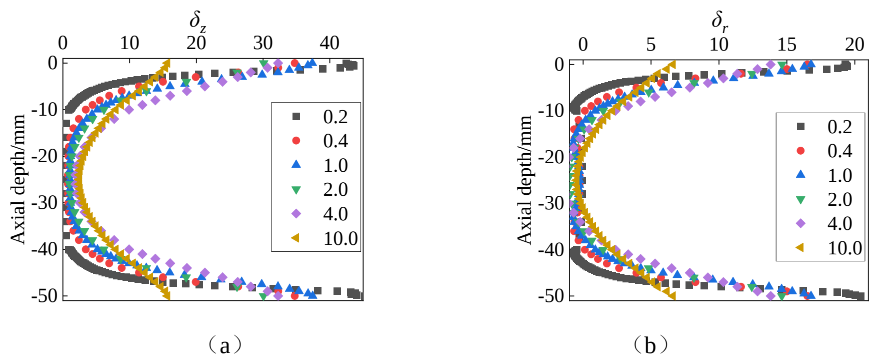

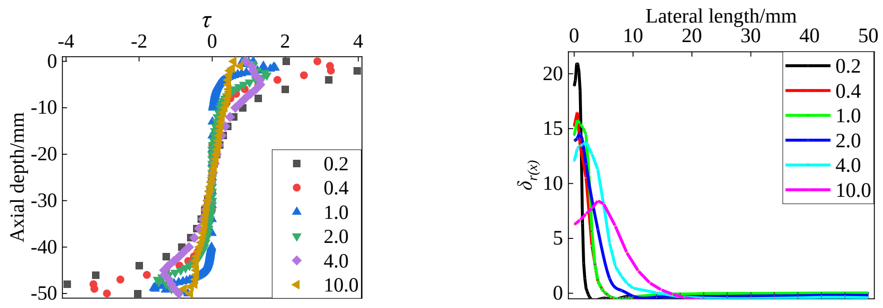

（c）　　　　　　　　　　（d）

Figure 8 Evolution of stress fields during dual indenters intrusion varying indenter diameters.

5 Conclusion

(1) Utilizing bi-linear elasticity relationship for air gap enabled the dynamic simulation of evolving contact interface between rock and indenter.

(2) With increasing intrusion depth, the influence range of axial and radial stresses expands, Shear stress decreases with depth, while circumferential stress initially increases and then rapidly declines in the radial direction.

(3) The impact of the indenter diameter on the stress field within the rock exhibits a decaying exponential relationship as the diameter increases

(4) The changing trends of internal stresses under dual-indenter intrusion mirror those in single-indenter intrusion. the synergistic effect of dual indenters induces greater internal stress and extends the impact range.

References

[1] Taljat B, Pharr G M. Development of pile-up during spherical indentation of elastic–plastic solids[J]. International journal of solids and structures, 2004, 41(14): 3891-3904.

[2] Swadener J G, George E P, Pharr G M. The correlation of the indentation size effect measured with indenters of various shapes[J]. Journal of the Mechanics and Physics of Solids, 2002, 50(4): 681-694.

[3] Zhou Z, Cai X, Li X, et al. Dynamic Response and Energy Evolution of Sandstone Under Coupled Static–Dynamic Compression: Insights from Experimental Study into Deep Rock Engineering Applications[J]. Rock Mechanics and Rock Engineering, 2020, 53: 1305–1331.

[4] Austin L G, Shoji K, Luckie P T. The effect of ball size on mill performance[J]. Powder Technology, 1976, 14(1): 71-79.

[5] Huang P, Ding Y, Wu L, et al. A novel approach of evaluating crushing energy in ball mills using regional total energy[J]. Powder Technology, 2019, 355: 289-299.

[6] Metzger M J, Glasser B J. Simulation of the breakage of bonded agglomerates in a ball mill[J]. Powder Technology, 2013, 237: 286-302.

[7] Bourgeois F S. Single-particle fracture as a basis for microscale modeling of comminution processes[M]. The University of Utah, 1993.

[8] Van der Boom J. Tunnelling in urban areas: the use of lateral walls to protect ancient buildings[J]. 2011.

[9] Olivella S, Jean V, Alfonso R D. CODE_BRIGHT USER'S GUIDE. Barcelona, Spain, Division of Geotechnical Engineering and Geosciences, Department of Civil and Environmental Engineering, Technical University of Catalonia (UPC)[J]. 2020.

[10] Chen P. Effects of microparameters on macroparameters of flat-jointed bonded-particle materials and suggestions on trial-and-error method[J]. Geotechnical and Geological Engineering, 2017, 35: 663-677.

NUMERICAL SIMULATION OF GAS INJECTION IN LOW PERMEABILITY CLAY MATERIALS CONSIDERING DIFFERENT ELEMENT TYPES

Yangyang Mo[1], Alfonso Rodriguez-Dono[1,2,*] and Sebastia Olivella[1,2]

[1] Department of Civil and Environmental Engineering, Universitat Politècnica de Catalunya, Barcelona, Spain

[2] International Centre for Numerical Methods in Engineering (CIMNE), Barcelona, Spain

* Corresponding author: Alfonso Rodriguez-Dono. E-mail: alfonso.rodriguez@upc.edu

Key words: Numerical simulation, HM-coupled, Gas injection, Selective integration method

Abstract. *This study investigates the impact of different element types on hydro-mechanically (HM) coupled geological media using the Heat and Gas Fracking (HGFRAC) model. It is important to note that the types of elements and integration methods used in finite element simulations can significantly influence the results. When comparing quadrilateral and triangular elements, it is observed that quadrilateral elements, due to their bi-linear gradient characteristics, produce a more stable stress field than linear triangular elements. The computational efficiency of the HGFRAC model has been improved through the introduction of the selective integration method for quadrilateral elements. Overall, for HM-coupled gas injection problems, the use of selective integration enhances both stability and cost-efficiency in calculations.*

1 INTRODUCTION

Numerical simulations of gas migration and gas fracturing in clay materials is an important research topic in geological engineering. It is closely related to the secure storage of radioactive waste in underground repositories, analysis of gas fracturing processes and other geological engineering projects involving gas injection.[i, ii] However, there is still a lack of research in several aspects, including the effect of different element types and integration methods on the simulation of coupled multi-physical gas fracturing issues. In addition, numerical simulations often encounter difficulties such as the incompressibility of materials, leading to the locking effect on simulation results.

To date, the current research progress has encompassed extensive experiments and numerical simulations in the exploration of gas injection in clay materials, yielding valuable insights and highlighting specific concerns. Experimental observations indicate that exceeding a certain gas pressure threshold induces gas fracturing, forming localized dilatant pathways in the clay. However, how to accurately simulate the gas fracturing phenomenon in HM-coupled issues remains a challenging task. In previous studies, the accuracy of numerical simulation results of gas flow paths is frequently compromised due to the presence of the locking effect. In this study, various types of finite elements and integration methods are analyzed to effectively address the challenges encountered in contemporary numerical simulations.

2 METHODOLOGY

CODE_BRIGHT is a finite element method (FEM) simulation program developed at the Universitat Politècnica de Catalunya (UPC) that solves the stress equilibrium, conservation of water mass, and conservation of gas mass equations in a coupled manner. The program considers displacement, liquid pressure, gas pressure, temperature, and chemical variables as primary unknowns. The detailed equations employed by CODE_BRIGHT have been previously described.[iii, iv]

This study compares the performance of triangle and quadrilateral elements in the calculations. It should be noted that quadrilateral elements are further subdivided into four types based on their different integration methods, as shown in Fig. 1. According to the integration method, it is divided into two types: “standard integration” and “selective integration”. And for different integration positions, it is divided into two forms: “integrated at Gauss points” (this is equivalent to Gauss quadrature type of integration) and “integrated at the nodes” (this is equivalent to Newton-Cotes quadrature type of integration).

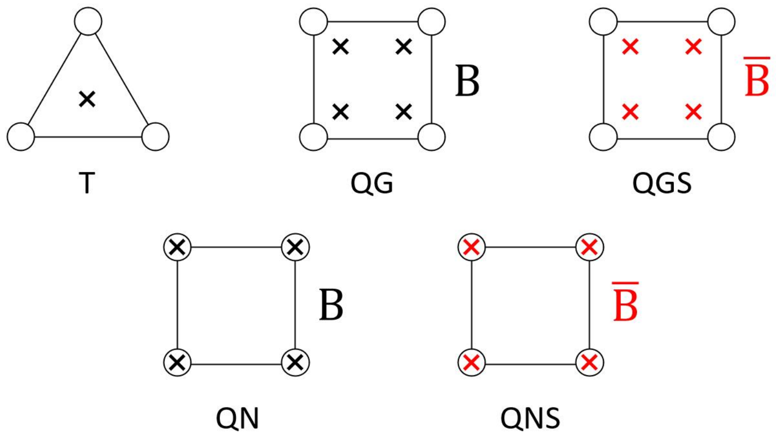

Figure 1: Different types of elements considered in this study: T is triangle with analytical integration, QG is quadrilateral with Gauss integration, QGS is quadrilateral with Gauss selective integration, QN is quadrilateral with nodal integration, and QNS is quadrilateral with nodal selective integration.

3 HGFRAC MODEL

The HGFRAC model, depicted in Fig. 2, represents a gas injection model with specific dimensions and materials. The model consists of a borehole excavated in clay material with a radius $R_b = 0.04\ m$, an interval radius $R_i = 0.03\ m$ and a length $L = 10\ m$. The gas is injected into the interval and then propagates through the clay material (COx). The material properties of the COx can be found elsewhere[v]. Due to the model’s symmetry, only a quarter of the XOY plane is considered for simulation.

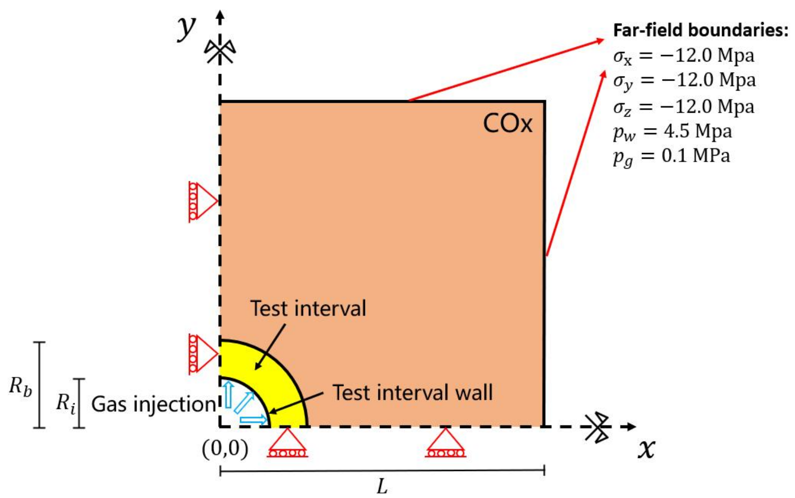

Figure 2: HGFRAC model geometry and boundary conditions.

The complete numerical simulation process consists of four stages. From -2184 hours to -24 hours, the borehole is excavated, and a multiple packer system is installed to monitor water/gas pressure within a specified test interval. During the subsequent 24 hours (i.e., from -24 to 0), the gas pressure and liquid pressure at the clay surface in contact with the interval are prescribed as 0 MPa. Gas injection starts at 0 hours, and the gas flow rate increases linearly from 0 kg/s during the first hour. By the end of the first hour, the gas flow rate reaches 2.75×10^{-6} kg/s. Subsequently, from the 2nd to 720th hour, the gas injection rate remains constant at 2.75×10^{-6} kg/s.

The HGFRAC model has been modelled with different kinds of meshes, as illustrated in Fig. 3. Fig. 3 (a) and (b) depict the use of triangle and quadrilateral elements, respectively, with the same scale for mesh division. Model (a) consists of 5525 nodes and 10755 elements, while model (b) comprises 5351 nodes and 5209 elements.

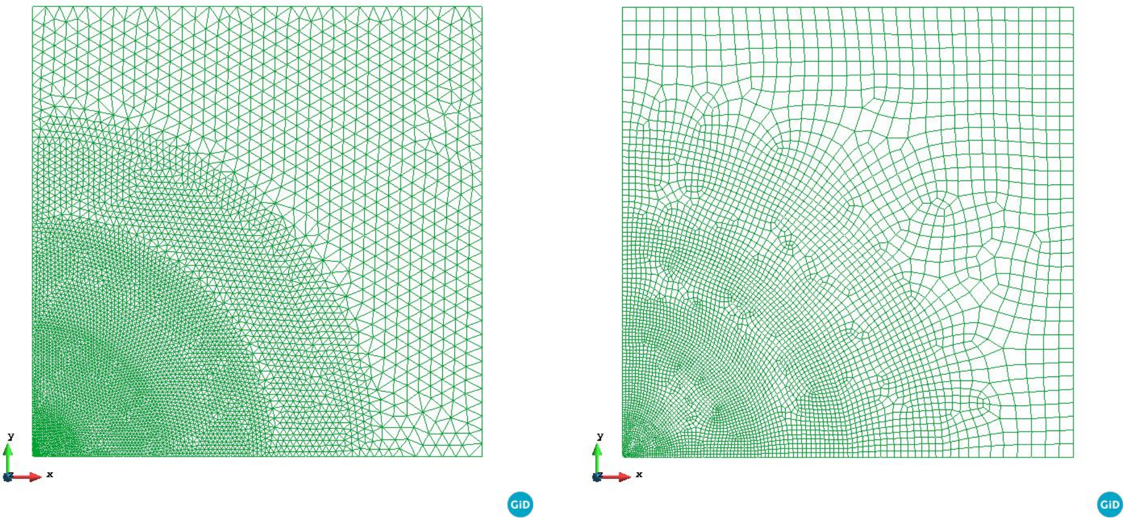

(a) (b)

Figure 3: Mesh configuration: (a) triangular mesh, (b) quadrilateral mesh.

4 RESULTS AND COMPARISON

Fig. 4 depicts the final gas pressure contour fill for the five mentioned element types, along with the addition of an "Elastic+Kozeny" case. A preferential gas flow path can be observed in each model from Fig. 4 (a-e). However, the QG and QN models exhibited instability and the simulation stopped at 360 and 338 hours, respectively. The introduction of the selective integration method in QGS and QNS models shows quite stable and consistent gas flow patterns. In contrast, Fig. 4f shows that the gas flow path is not evident, and the gas pressure only accumulates near the borehole without penetrating into the clay media. This is because, in this case, plastic deformation is limited, causing only a small amount of gas to enter the clay material in the form of diffusion.

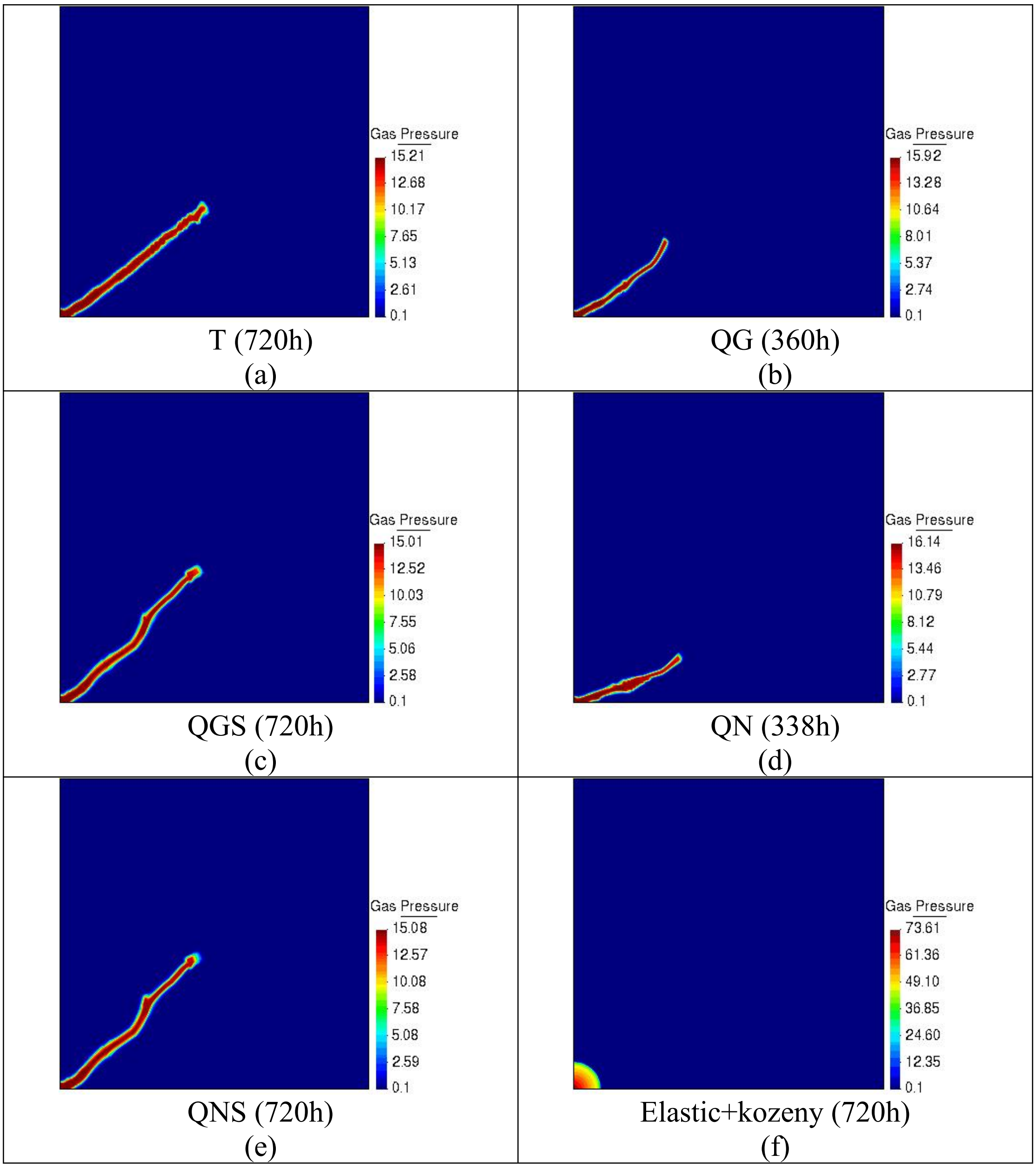

Figure 4. Comparison of gas pressure contour fill in different cases: (a) triangle with analytical integration, (b) quadrilateral with Gauss integration, (c) quadrilateral with Gauss selective integration, (d) quadrilateral with nodal integration, (e) quadrilateral with nodal selective integration, and (f) elastic+kozeny model.

Fig. 5 presents the calculation results of the maximum stress σ_i, minimum stress σ_{iii} and mean effective stress for the five element types. A comparison between the triangle element and the four quadrilateral elements reveals that the accuracy of the stress field is unsatisfactory when using the triangle element, particularly in the vicinity of the gas flow path. The linear triangle element, having only one output value, is naturally less accurate compared to quadrilateral elements, which benefit from linear gradient characteristics. In addition, the triangle element model is prone to the locking effect due to the large gradient variation near the gas preferential path. The volumetric locking phenomenon observed in the linear triangle element can be attributed to the excessive constraints imposed on incompressible materials, severely limiting the range of possible deformation for triangle elements. Among the four types of quadrilateral elements, the stress field has been significantly improved by introducing the selective integration method. Particularly, the QGS and QNS models exhibit more accurate results for the mean effective stress field, while QG and QN still suffer from the locking effect.

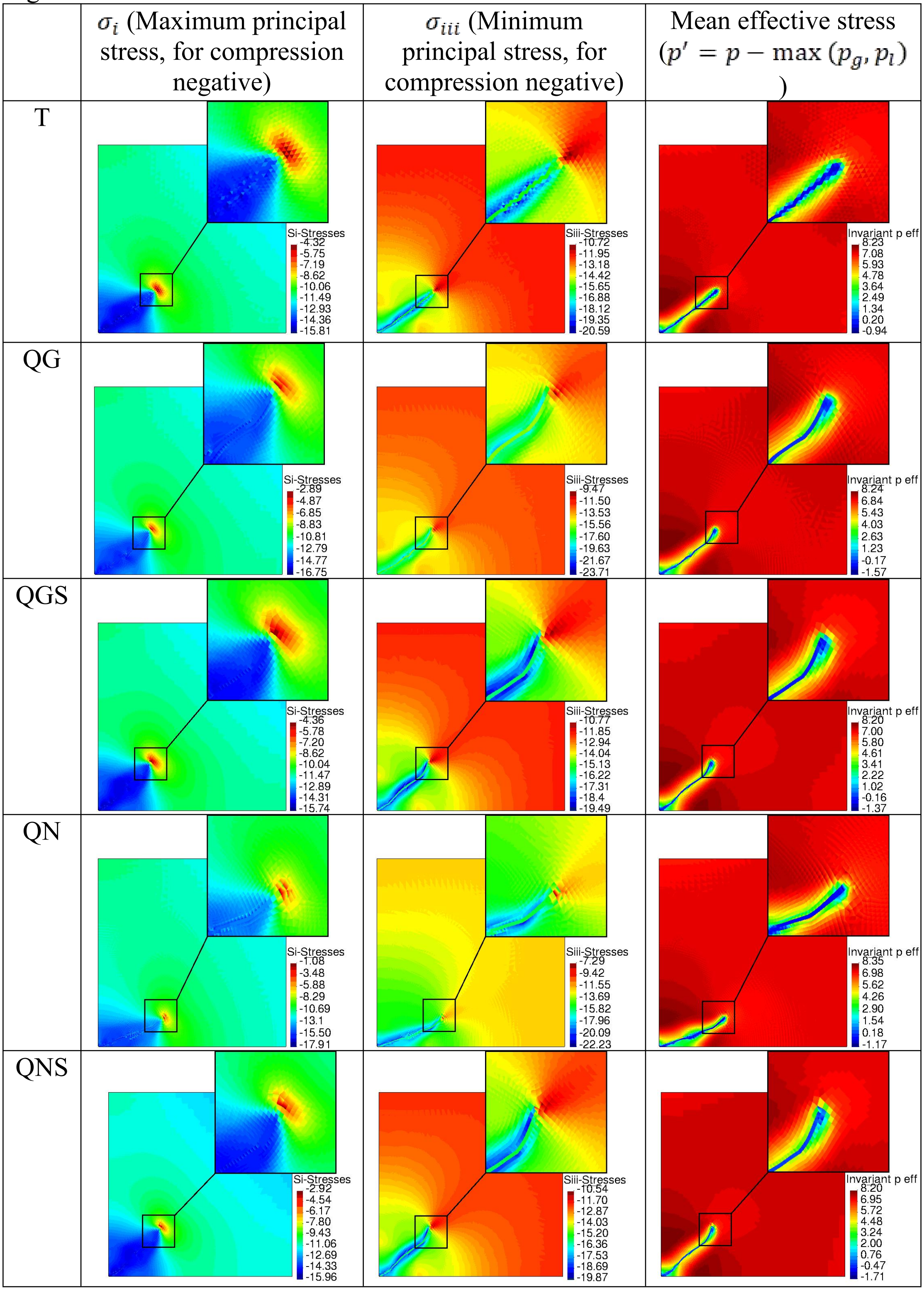

Figure 5. Comparison of stress field with different element type (330 hours). Oscillation of the stress field occurs close to the tip of the crack, but intensity depends on the element type.

5 CONCLUSIONS

The main conclusions of this study can be summarized as follows:

(1) The utilization of triangle elements in simulation has yielded unsatisfactory results, as their stress field is susceptible to the locking effect. In contrast, quadrilateral elements demonstrate higher calculation accuracy compared to triangle elements, although specific explanations are required for different issues.

(2) The selective integration method effectively mitigates the locking effect, leading to improved stability and efficiency in the calculations.

(3) Transitioning from Gauss points to nodal points for integration enhances the calculation stability to a certain extent, but the field results may still encounter challenges associated with the locking effect.

ACKNOWLEDGEMENTS

This research was supported by ANDRA through the DECOVALEX Project (Carlos Plua has led a benchmarking exercise) and by the CODE_BRIGHT Project (International Centre for Numerical Methods in Engineering).

The CODE_BRIGHT project is funded by a Consortium composed by SKB (Sweden), Posiva (Finland), GRS (Germany) and ANDRA (France).

REFERENCES

[i] Senger R, Ewing J, Zhang K, Avis J, Marschall P, Gaus I. Modeling Approaches for Investigating Gas Migration from a Deep Low/Intermediate Level Waste Repository (Switzerland). Transp Porous Media. 2011;90(1): 113-133.

[ii] Yang J, Fall M. Coupled hydro-mechanical modelling of dilatancy controlled gas flow and gas induced fracturing in saturated claystone. Int J Rock Mech Min Sci. 2021;138.

[iii] Olivella S, Gens A, Carrera J, Alonso EE. Numerical formulation for a simulator (CODE-BRIGHT) for the coupled analysis of saline media. Eng Comput. 1996;13(7): 87–112.

[iv] Olivella S, Vaunat J, Rodriguez-Dono A. CODE_BRIGHT USER'S GUIDE. Barcelona, Spain: Division of Geotechnical Engineering and Geosciences, Department of Civil and Environmental Engineering, Technical University of Catalonia (UPC); 2022.

[v] Mo Y, Rodriguez-Dono A, Olivella S. Hydro-Mechanical coupled analysis of gas injection in clay-based materials using different element types. Geomech Energy Envir. 2004: 100541.

MODELLING OF PERMEABILITY AND TRIAXIAL EXPERIMENTS FOR HETEROGENEOUS ANISOTROPIC CLAYSTONE

Yunfeng Zhou*, Alfonso Rodriguez-Dono* and Sebastia Olivella*

* Department of Civil and Environmental Engineering
Universitat Politècnica de Catalunya (UPC)
Campus Nord UPC, 08034 Barcelona, Spain

Key words: Anisotropic heterogeneous model, intrinsic permeability, Young's modulus, claystone, CODE_BRIGHT.

Abstract. *Permeability and triaxial experiments on claystone are simulated using a spatially correlated heterogeneous anisotropic model. A matrix decomposition technique is adopted to generate a structured and random field of porosity. Intrinsic permeability and Young's modulus are a function of porosity, leading to the heterogeneity and anisotropy of these properties. The anisotropy ratios of these two properties are analysed.*

1 INTRODUCTION

Subsurface porous materials often show significant natural variability in their type and spatial distribution. Geostatistical methods are commonly used to quantify this uncertainty, which includes semi-variogram analysis and stochastic simulation [1]. The LU triangular decomposition approach is adopted to reproduce semi-variogram precisely. This approach has been implemented in CODE_BRIGHT to generate a spatially correlated heterogeneous porosity field. Parameters like intrinsic permeability and Young's modulus are functions of porosity, which inherit the heterogeneous features [1]. The correlation length of porosity can be anisotropic, resulting in the anisotropy of intrinsic permeability and Young's modulus. However, when selecting constitutive laws in CODE_BRIGHT, it is important to be careful as the degree of anisotropy might be minimal. Pore shape has a significant effect on the variability of stiffness anisotropy [2].

Numerical intrinsic permeability tests are conducted to measure the ability of water to flow through saturated heterogeneous anisotropic claystone samples under controlled conditions. These tests apply a constant pressure difference across the ends of the sample and monitor the volume of water passing through theses samples over a specific period. Numerical triaxial tests are performed to determine the Young's modulus of these specimens.

2 EXPERIMENT DESCRIPTION

Fig. 1 presents the sample dimension and boundary conditions for numerical intrinsic permeability test and triaxial tests.

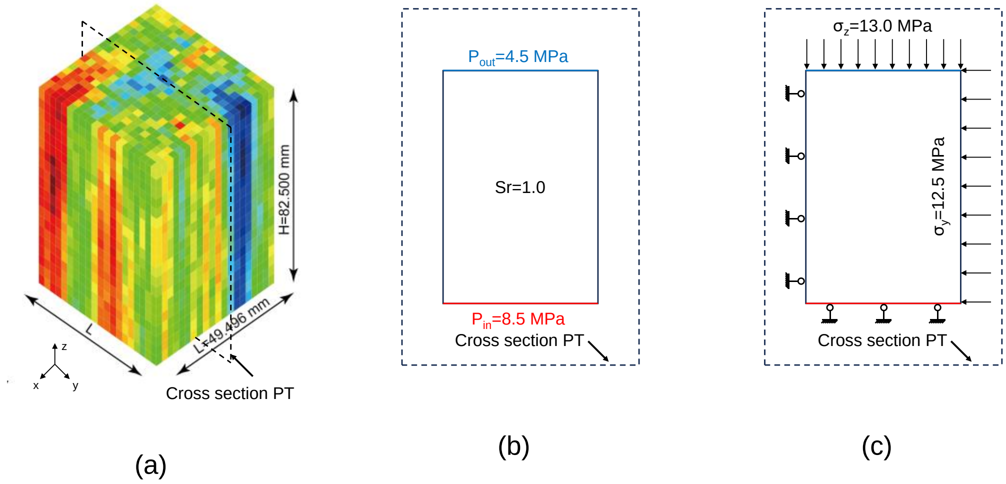

Figure 1 (a) Sample dimension; (b) Boundary conditions of numerical permeability tests; (c) Boundary conditions of numerical triaxial tests.

3 MODEL DESCRIPTION

3.1 Heterogeneous anisotropic model

Stochastic simulations employ semi-variogram models to generate multiple equiprobable images of random variables. The spherical variogram model is adopted in CODE_BRIGHT which is computed in Eq. (1).

$$\gamma(|\boldsymbol{h}|) = \begin{cases} 0, & |\boldsymbol{h}| = 0 \\ C_0 + C_1\left[1.5\dfrac{|\boldsymbol{h}|}{a} - 0.5\left(\dfrac{|\boldsymbol{h}|}{a}\right)^3\right], & 0 < |\boldsymbol{h}| \le a \\ C_0 + C_1, & |\boldsymbol{h}| > a \end{cases} \tag{1}$$

Where C_0 is the nugget, which is due both to measurement errors and to micro-variabilities of the mineralization; a denotes the range, which means that any data value will be correlated with any other value falling within a radius a; $|\boldsymbol{h}|$ is the distance between two elements.

A transformation matrix (Eq. (2)) is used to obtain a random field with an anisotropic correlation length. More details can be referred to Rodriguez-Dono et al [1].

$$\mathbf{T} = \lambda \mathbf{R}_x \mathbf{R}_y \mathbf{R}_z \tag{2}$$

$$\text{with } \lambda = \begin{bmatrix} 1 \\ \lambda_1 \\ \lambda_2 \end{bmatrix} = \begin{bmatrix} 1 \\ a_y/a_x \\ a_z/a_x \end{bmatrix}, \mathbf{R}_x = \begin{bmatrix} 1 & 0 & 0 \\ 0 & \cos(\beta_t) & \sin(\beta_t) \\ 0 & -\sin(\beta_t) & \cos(\beta_t) \end{bmatrix},$$

$$\mathbf{R}_y = \begin{bmatrix} \cos(\gamma_t) & 0 & \sin(\gamma_t) \\ 0 & 1 & 0 \\ -\sin(\gamma_t) & 0 & \cos(\gamma_t) \end{bmatrix}, \mathbf{R}_z = \begin{bmatrix} \cos(\alpha_t) & \sin(\alpha_t) & 0 \\ -\sin(\alpha_t) & \cos(\alpha_t) & 0 \\ 0 & 0 & 1 \end{bmatrix}$$

Where $[\lambda]$ is the matrix for anisotropy ratio, a_x, a_y and a_z are correlation lengths for axis x, y and z, respectively, $\mathbf{R}_x$, $\mathbf{R}_y$ and $\mathbf{R}_z$ are rotation matrices around axis x, y and z, with rotation angle β_t, γ_t and α_t.

3.2 Mechanical and hydraulic constitutive models

The mechanical model is based on linear elasticity and it is a function of porosity which is given in Eq. (3). However, the degree of anisotropy for Young's modulus is not sufficient when Eq. (3) is applied. The stress-strain equation is calculated in Eq. (4) to ensure the degree of anisotropy. C_{ijkl} and H_{ijkl} are functions of porosity and aspect ratio γ. Assuming that the pore shape is the same as oblate spheroid, aspect ratio is defined as the polar radius divided by the equatorial radius.

$$E(\phi) = E_0 + (\phi - \phi_{0E})\frac{dE}{d\phi} \tag{3}$$

Where E_0 is a reference Young's modulus, and ϕ_{0E} represents the reference porosity, $dE/d\phi$ is the Young's modulus variation rate.

$$\varepsilon_{ij} = \left(C_{ijkl} + H_{ijkl}\right)\sigma_{ij}^0 \tag{4}$$

Where C_{ijkl} is the compliance tensor, σ_{ij}^0 is the applied stress, H_{ijkl} refers to the solution of Eshelby's problem. More details can be referred to Sevostianov and Kachanov [3].

The intrinsic permeability is given by Eq. (5) and Eq. (6).

$$k = \frac{k_0(1-\phi_0)^2}{\phi_0^3}\frac{\phi^3}{(1-\phi)^2} \tag{5}$$

$$k = k_0\exp(b_k(\phi - \phi_0)) \tag{6}$$

Where k_0 is the intrinsic permeability corresponding to reference porosity ϕ_0; $b_k$denotes a parameter to calibrate with the experiment data.

The hydro-mechanical parameters are listed in Table 1.

Table 1 Hydro-mechanical properties for claystone.

Parameters		Units	Values
Initial porosity	Average porosity, ϕ_{0avg}	−	0.15
	Variance, C_1	−	See Table 2
Correlation length	a	m	See Table 2
Matrix Permeability, parallel	$k_{11} = k_{22}$	m^2	1×10^{-20}
Matrix Permeability, perpendicular	k_{33}	m^2	1×10^{-20}
Reference porosity	ϕ_0	−	0.15
Calibration parameter	b_k	−	See Table 3
Young's modulus	E_0	MPa	7069
Reference porosity (Eq. (3))	ϕ_{0E}	−	0.15
Young's modulus variation rate	$dE/d\phi$	MPa	-20000
Poisson's ratio	ν	−	0.3
Aspect ratio	γ	−	0.2

Note: The rotation angle is consistent with the bedding plane.

3.3 Simulation schemes

A sensitivity analysis of porosity variance was conducted using Kozeny-Carmen equation (Eq. (5)), and they are listed in Table 2. Samples with different variances are shown in Fig. 2.

Table 2 List of cases to intrinsic permeability tests using Kozeny-Carmen equation (Eq. (5))

Name	Variance (m)	Number of realizations	a_z/a_x	a_y/a_x
CaseK1	4.44×10^{-5}	1	32	1
CaseK2	5.44×10^{-4}	1	32	1
CaseK3	1.60×10^{-3}	1	32	1

Note: a_x is 0.0164 m for all cases.

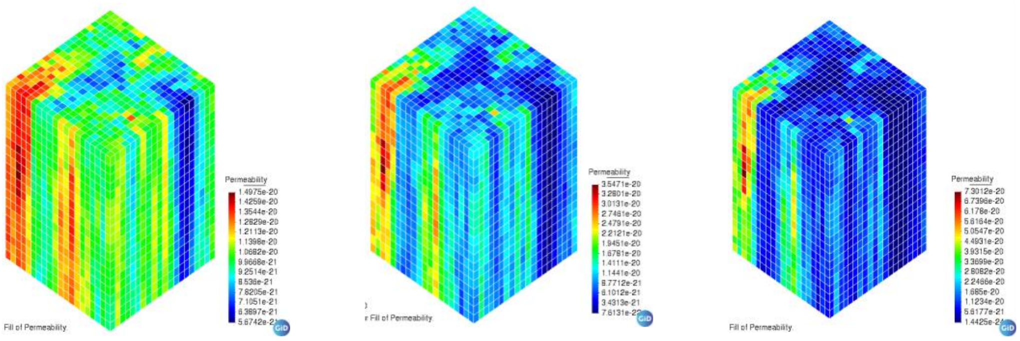

(a) (b) (c)

Figure 2 Samples with different variances for porosity: (a) 4.44×10^{-5} m; (b) 5.44×10^{-4} m; (c) 1.60×10^{-3} m.

Three factors including calibration factor b_k, the number of realizations and correlation length were considered to check the degree of anisotropy of intrinsic permeability, which are listed in Table 3.

Table 3 List of cases to intrinsic permeability tests using the exponential law (Eq. (6))

Name	b_k	Variance (m)	Number of realizations	a_z/a_x	a_y/a_x
CaseE1	1	1.60×10^{-3}	1	32	1
CaseE2	20	1.60×10^{-3}	1	32	1
CaseE3a	40	1.60×10^{-3}	1	32	1
CaseE4	40	1.60×10^{-3}	50	1	1
CaseE3b	40	1.60×10^{-3}	50	32	1

An aspect ratio of 0.2 was used to generate 50 realizations to analyse the anisotropy ratio of Young's modulus.

4 RESULTS

The anisotropy ratio is 1.3 even though the variance is large (CaseK3) when Kozeny-Carmen equation is used. The anisotropy ratio is 2.58 when a relatively large calibration parameter b_k is used (CaseE3a). However, intrinsic permeability in the y direction divided by that in the x direction is 0.83, which should be 1 when correlation lengths in x*O*y plane are the same. The results of CaseE4 show that the number of realizations should be large enough to guarantee the ergodicity of a stochastic process. As shown in Fig. 3(a), the intrinsic permeability is isotropic in the x*O*y plane, and show relatively stable degree of anisotropy when 50 realizations are applied.

When considering a specific aspect ratio (0.2 in this study), the anisotropy ratio is approximately 1.5, and this ratio is independent of the number of realizations (Fig. 3(b)).

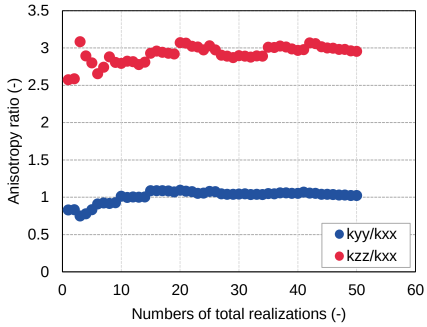

(a)

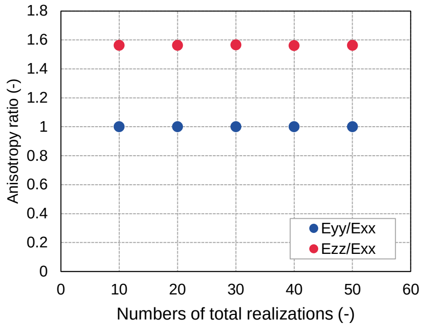

(b)

Figure 3 Anisotropy ratios with respect to numbers of realizations for (a) intrinsic permeability, (b) Young's modulus.

5 CONCLUSIONS

- It is significant to select the appropriate intrinsic permeability laws when generating a heterogeneous random field with anisotropy.
- The number of realizations should be large enough to guarantee the ergodicity of a stochastic process.
- The aspect ratio is necessary to induce anisotropy in Young's modulus. It is noted that the analysis method considering aspect ratio is applicable to linear elasticity. In addition, the anisotropy ratio induced by pore shape is independent of the number of realizations.

REFERENCES

1. Rodriguez-Dono, A., Y. Zhou, and S. Olivella, *A new approach to model geomaterials with heterogeneous properties in thermo-hydro-mechanical coupled problems.* Computers and Geotechnics, 2023. **159**.
2. Griffiths, L., et al., *The influence of pore geometry and orientation on the strength and stiffness of porous rock.* Journal of Structural Geology, 2017. **96**: p. 149-160.
3. Sevostianov, I. and M. Kachanov, *Compliance tensors of ellipsoidal inclusions.* International Journal of Fracture, 1999. **96**(1): p. 3-7.

SIMULATING SOIL REINFORCEMENT INTERACTION USING CODE_BRIGHT

A. Moncada[*†], I.P. Damians[*†‡], S. Olivella[*†] and R.J. Bathurst[§]

[*] Department of Civil and Environmental Engineering (DECA), Universitat Poliècnica de Catalunya (UPC), Campus Nord UPC, 08034 Barcelona, Spain.
e-mail: anibal.moncada@upc.edu

† International Centre for Numerical Methods in Engineering (CIMNE), Campus Nord UPC, 08034 Barcelona, Spain. (http://www.cimne.com)

‡ VSL International Ltd, Barcelona, Spain

§ Geoengineering Centre at Queen's-RMC, Civil Engineering Department, Royal Military College of Canada, Canada.

Key words: Pullout response, reinforced soil, polyester straps, CODE_BRIGHT

Abstract. *Reinforced soil structures (RSS) involve a compacted soil mass with embedded elements, orthogonal to the main stress direction, which act as load bearing components. The compound nature of RSS requires a proper characterization of the soil-reinforcement response, which can vary with on-site conditions and soil and reinforcement properties. The present study details the implementation of numerical models to simulate the laboratory-measured pullout response of polymeric strap reinforcements at constant rate of displacement. Soil-reinforcement interfaces were modelled using continuum elements. Various laboratory conditions were reproduced. After a calibration process, numerical results were found to properly reproduce measured data. The described methodology is part of an ongoing test and modelling campaign focussed on the assessment of on-site conditions on the pullout response of polymeric strap reinforcements.*

1 INTRODUCTION

Reinforced soil structures (RSSs) are characterized by horizontal reinforcement layers placed within a compacted soil mass. Reinforcements can be metallic or polymeric, usually described as inextensible and extensible reinforcements, respectively. The design of RSS includes external and internal stability requirements. More specifically, internal stability criterions include reinforcement rupture, pullout, and connection failure. Rupture, from either reinforcement or connection elements, will depend on the ultimate tensile strength of the used materials and the required tensile load, calculated by means of analytical or numerical methods. In case of pullout, failure will depend in the interaction between soil and reinforcement (i.e., frictional contact in-between materials). In the case of polymeric reinforcements, their extensible characteristics prove an added difficulty when determining said interaction.

According to AASHTO guidelines[i], the pullout resistance (P_r) is a function of the reinforcement surface area (C), width (w), effective length (L_e), applied vertical stress (σ_v), and a friction interaction factor (f') (see Equation 1). The friction interaction factor will depend on a scale effect correction factor (α), related to the extensibility of the reinforcement, and a friction factor (F*), represented by the soil friction angle (ϕ_{soil}) modified using a reduction coefficient (R_i).

$$P_r = f' \left(C\, w\, L_e'\, \sigma_v \right) \tag{1}$$

$$f' = \alpha F^* = \alpha R_i \tan(\phi_{soil}) \tag{2}$$

For geosynthetic materials, R_i has a default value of 0.67. In the case of polymeric strips, values of up to R_i = 0.8 could be used in the absence of product-specific data[ii,iii]. The soil-reinforcement friction interaction (determined by the reduction factor C_i) can be obtained by measuring the required pullout force in constant rate of displacement extraction test.

2 TEST EQUIPEMENT

Pullout tests were warried out using a 1250-mm-long, 500-mm-wide, 750-mm-high rigid steel box. Dimensions are in compliance with international design standards[iv,v]. The front and back of the pullout box have openings to allow the connection to a clamp-pulling system and/or measuring devices (e.g., extensometers). Material is placed and compacted through the top of the pullout box. Once filled, the top opening is closed with a reaction plate which allows the application of vertical loads to simulated varying soil depths. A constant rate of displacement of 1 mm/min is achieved by placing a cord extensometer to the head of the reinforcement, attached to a steel clamp, which in turn is pulled horizontally by a hydraulic jack (see Figure 1). The displacement at the end of the reinforcement (i.e., at the back of the pullout bot) were measured by a second extensometer. The pullout force was measured at the head of the hydraulic jack using a load cell. Tests were carried out considering equivalent depths of 0.35-, 3-, and 7-m. The pullout criteria were two. First, if the stress-displacement of the front-end of the reinforcement showed and plateau with respect to stress with increasing displacements, or second, if the back-end of the reinforcement suffered displacements greater than 25 mm.

Table 1 shows material properties, including those required in the numerical modelling. Soil properties were determined via direct shear tests. Reinforcement stiffness was determined using constant-rate-of-strain ultimate tensile strength test results.

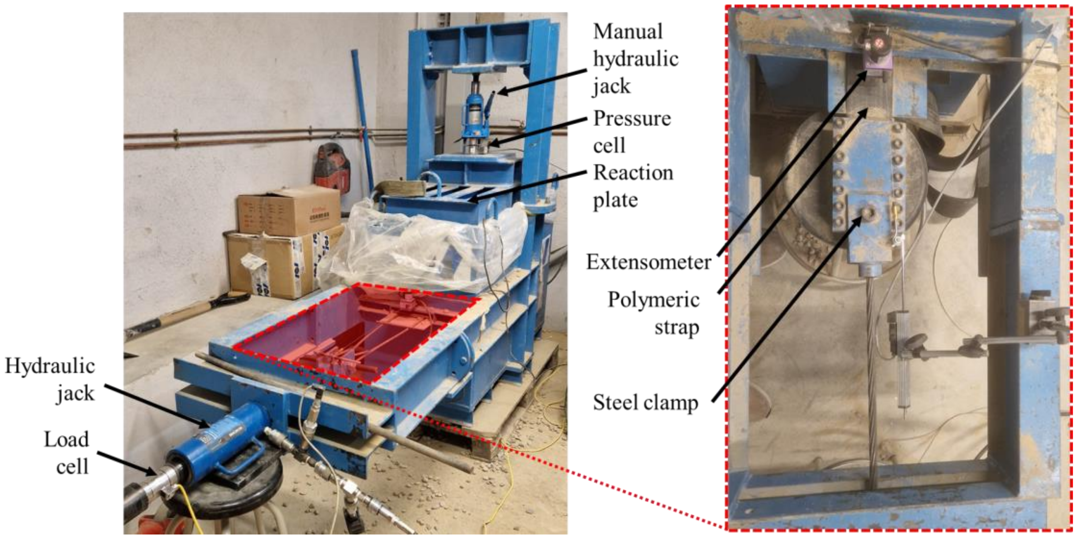

Figure 1. Pullout test box equipment.

3 NUMERICAL MODEL

Numerical simulations were carried out using the finite element program CODE_BRIGHT[vi]. Model dimensions replicate the pullout box dimensions (see Figure 2a). The soil-reinforcement interface was modelled using continuum elements (see Figure 2b). This methodology has been proved to be reliable when modeling RSSs[vii,viii]. Interface properties were determined by reducing the strength properties of the soil via a reduction factor C_i (i.e., $\tan(\delta_{interface}) = C_i \tan(\phi_{soil})$). Soil stiffness remained unchanged between soil and interface materials. Pullout response was achieved by applying a constant displacement of $1.67*10^{-5}$ m/s.

Properties	Soil	Reinforcement
Unit weight (kN/m3)	20	3.5
Elastic modulus (MPa)	20	1451
Poisson's ratio, (-)	0.3	0.3
Cohesion, (kPa)	0	-
Friction angle (°)	37	-
Dilatancy angle (°)	7	-

Table 1. Soil and reinforcement material properties.

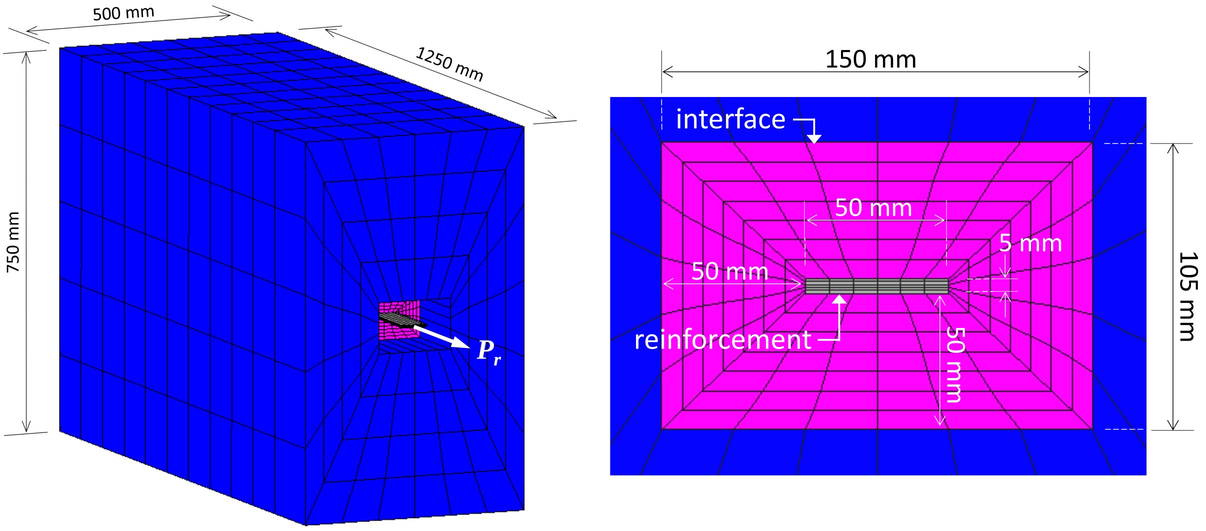

(a) (b)

Figure 2. Numerical model mesh geometry of (a) the whole model and (b) detail of the reinforcement and interface elements (adapted from [ix])

4 RESULTS

Figure 3a shows the pullout force with respect to front- and back-end displacements at variable depths. Simulated results were calibrated by means of the friction factor and reduction coefficient. After a trial-and-error process, optimal F* values were obtained, which properly simulate the stress-strain response. Measured pullout load as well the displacements at which it occurs increase with increased depth. Pullout response is properly modelled at all analyzed depths.

Figure 3b shows the measured and simulated head- and tail-end displacement during the pullout tests. As the testes materials fall into the extensible category, as pullout force increases, the material is gradually extended from front to back. Said extensibility is more notorious at higher confining pressures (z = 3,5 and 7 m), where the head displacements reach approximately 5 mm before the tail-end of the reinforcements begins to tension and displace. To achieve the relative head-tail displacement, special care must be taken when selecting the reinforcement stiffness.

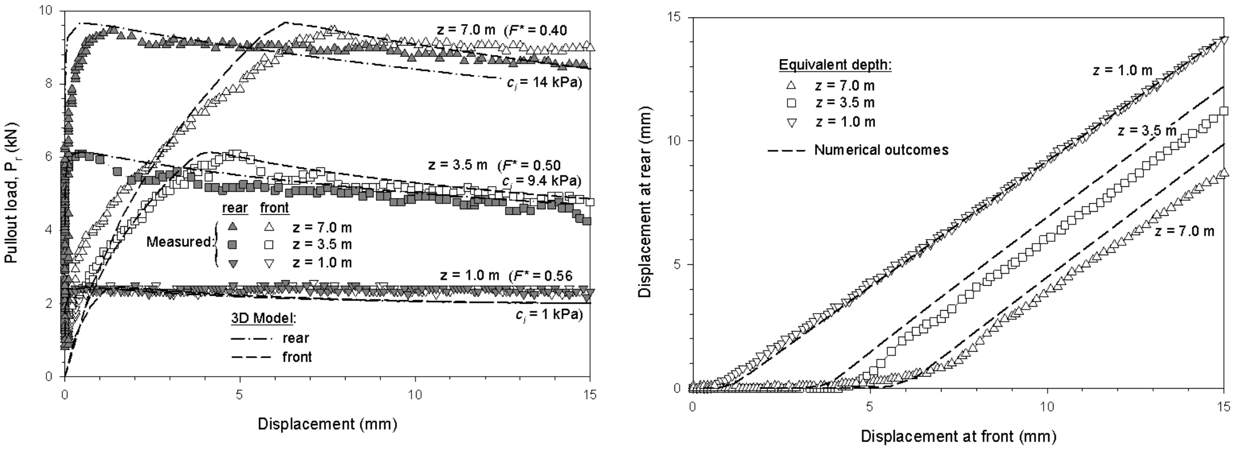

(a) (b)

Figure 3. (a) Measured (symbols) and simulated (dashed-lines) stress-displacement pullout response at variable depths with calibrated F* values and (b) measured and simulated front- and back-end displacements (adapted from [x]).

5 CONCLUSIONS

- Laboratory measured pullout tests with polymeric reinforcements were reproduced using a finite element software package.
- The extensible nature of polymeric materials requires to evaluate deformations at the front- and back-end of the reinforcement. Numerical models properly reproduced front- and back-end displacements while simulating the incremental the pullout force measured in the tests.
- Simulations required an a-priori calibration, mainly focused on reinforcement stiffness and friction reduction factor, to properly reproduce test data.
- Further efforts are being made to assess the effect of temperature and hydraulic variations within the soil mass when undergoing pullout failure.

ACKNOWLEDGEMENTS

The authors wish to thank Aaron Kim from GECO Industrial (Korea, Rep) for providing data for polymeric straps (FASTEN products) from reliability assessment testing records. The authors wish to acknowledge the support of the Department of Civil and Environmental Engineering (DECA) of the Universitat Politècnica de Catalunya·BarcelonaTech (UPC) and the International Centre for Numerical Methods in Engineering (CIMNE) and the funding received from the Spanish Ministry of Economy and Competitiveness through the “Severo Ochoa Programme for Centres of Excellence in R&D” (CEX2018-000797-S-20-4).

REFERENCES

[i] AASHTO. LRFD Bridge Design Specifications, 9th Ed. American Association of State Highway and Transportation Officials (AASHTO), Washington, DC, USA (2020).

[ii] Berg, R.R., Christopher, B.R., & Samtani, N.C. Design and construction of mechanically stabilized earth walls and reinforced soil slopes, Volume I (FHWA NHI-10–024) and Volume II (FHWA NHI-10–025), National Highway Institute, Federal Highway Administration. U.S. Department of Transportation, Washington, DC, USA (2009).

[iii] Lo, S. C. R. Pullout resistance of polyester straps at low overburden stress. Geosynth. Int. 5(4), 361–381 (1998).

[iv] ASTM D6706-01 (2021). Standard test method for measuring geosynthetic pullout resistance in soil. American Society for Testing Materials (ASTM International), West Conshohocken, PA, USA.

[v] BS EN 13738 (2004). Geotextiles and geotextile-related products – Determination of pullout resistance in soil. European Committee for Standardization, Brussels, Belgium.

[vi] Olivella, S., Gens, A., Carrera, J., Alonso, E.E., 1996, 'Numerical Formulation for a Simulator (CODE_BRIGHT) for the Coupled Analysis of Saline Media " Engineering Computations, Vol 13, No 7, pp: 87-112.

[vii] Damians, I.P., Moncada, A., Olivella, S., Lloret, A., Josa, A. (2024). Physical and 3D numerical modelling of reinforcements pullout test. Scientific Reports 14, 7355.

[viii] Damians, I. P., Bathurst, R. J., Olivella, S., Lloret, A., & Josa, A. (2021). 3D modelling of strip reinforced MSE walls. *Acta Geotechnica*, *16*(3), 711-730.

[ix] Damians, I. P., Olivella, S., Bathurst, R. J., Lloret, A., & Josa, A. (2022). Modeling soil-facing interface interaction with continuum element methodology. Frontiers in built environment, 8, 842495.

[x] Damians, I.P., Moncada, A., Olivella, S., Lloret, A., Josa, A. (2024). Physical and 3D numerical modelling of reinforcements pullout test. Sci Rep 14, 7355.

Thermo-Hydro-Mechanical (THM) Modelling of Onkalo Spent Nuclear Fuel Repository

Erdem Toprak[1*], Sebastia Olivella[1.2] , Xavier Pintado[3]

[1]International Center for Numerical Methods in Engineering (CIMNE) Barcelona, Spain

[2]Universitat Politècnica de Catalunya, Barcelona, Spain

[3]Mitta Oy, Helsinki, Finland

*mailto:erdem.toprak@upc.edu

This research contributes to the investigation of the behavior of bentonite based materials (compacted bentonite and pellets) and granular filling (GraFi) materials in an engineered barrier system (EBS) for the disposal of radioactive waste in deep geological repository (DGR) in Finland. This study includes comprehensive experimental characterizations (oedometer, infiltration, water retention curve and thermal conductivity tests) of the materials under thermo-hydro-mechanical (THM) processes. In the case of characterization of the pellets, microstructural behavior has been investigated as well. This paper addresses the modelling activities from three main perspectives: (i) determination of THM model parameters by means of simulation of laboratory scale tests (ii) thermal dimensioning and setting proper TH boundary conditions, (iii) performing long-term THM calculations under different scenarios in order to check long term response of EBS components.

In 3D THM models, the buffer (MX-80 bentonite) and backfill (Italian GraFi, granular filling bentonite) have been simulated with the Barcelona Basic Model. Bentonite pellets have been modelled with the Barcelona Expansive Model (BExM), considering macro-micro behaviour. Rock and canister have been simulated with the linear elastic model. Porosity dependency both in water retention curve and intrinsic permeability functions has been taken into account. Various oedometer and swelling pressure tests have been simulated in order to calibrate HM model parameters of buffer and backfill components.

Thermal and thermo-hydraulic (TH) calculations have been carried out, considering the geometries of canisters containing Loviisa 1-2 and Olkiluoto 3 spent nuclear fuel. The effect of the distance to the boundaries (thermal dimensioning) has been studied.

The long term THM response of the repository under the current material and geometrical configuration has been investigated. A series of cases has been considered to investigate the effect of various aspects related to the design of the vertical disposal method of Olkiluoto 1-2 spent nuclear fuel.

Buffer and backfill design options (filling material in notch and backfill, initial condition of backfill), geological conditions (saline water, rock permeability and heterogeneous rock) and numerical simulation options (different numerical models used to simulate THM behavior of materials, geometrical challenges and meshing) are considered for the sensitivity analyses. Depending on the case, different saturation times have been calculated, different stress developments have been achieved, and different displacements at the buffer-backfill interface have been calculated and different temperature evolutions have been obtained.

Keywords: nuclear waste repository design, engineered barrier system (EBS), THM coupled processes, BBM, double structure model (BExM), CODE_BRIGHT.

1. Thermo-Hydro-Mechanical Processes in Repository

Finnish spent nuclear fuel repository design is based on the vertical emplacement of spent nuclear fuel following the KBS-3V concept (Figure 1a). The copper canisters containing spent nuclear fuel assemblies are emplaced vertically into individual deposition holes (buffer : pellets and compacted clay) drilled into the bottom of deposition tunnels (backfill : granular filling). The canisters are surrounded by a swelling clay material (MX80) separating them from the crystalline host rock. A 3D model geometry has been generated based on the current configuration (Figure 1b).

THM processes are the main processes taking place in the repository during the closure. Most of the performance targets, safety requirements or the design criteria of the repository are associated with long term THM response of the EBS. However, there are secondary processes such as microbial activity; radionuclide transportation, gas migration and geochemical processes that might impact on the response of repository in long term. This paper focuses on long term THM response of EBS components under a particular model configuration.

Thermal process: The source of the heat is the canister. Canister initial power and decay function; the distance between deposition tunnels and individual deposition holes are important parameters for thermal dimensioning [1]. As the thermal conductivity depends on degree of saturation; initial state of the materials (such as initial water content during emplacement) and rock permeability influences the thermal process (HM coupling). Upon the emplacement of the canister, buffer surrounding the canister dries because of heating. During the cooling of the canister, displacements and stresses reduce due to thermal gradient (TM coupling). The peak temperature was set to 95 °C as a dimensioning limit [1]. In previous studies [2 and 3], sensitivity analyses on different modelling parameters (canister power; tunnel and canister spacing, thermal boundary conditions, initial conditions, gap elements, rock permeability among others) has been performed in order to check peak temperature under different model configurations.

Hydraulic process: Buffer and backfill are initially unsaturated. The source of the water is the host rock and possible fractures. Impact of artificial wetting of pillow pellets has been investigated as an alternative hydration option in previous studies [3]. Buffer and backfill water uptake will begin immediately upon emplacement according to distance to the rock wall. As there is a hydraulic gradient between the host rock and the buffer and backfill; desaturation will take place around rock wall (Figure 1a). Swelling pressures will develop in EBS as a consequence of the saturation (HM coupling). Degree of saturation of the inner pellets surrounding the canister will decrease as a result of drying (TH coupling). In order to ensure retardation of radionuclide transportation, low permeabilities ($k_{buffer} < 10^{-19}$ m^2 and $k_{backfill} < 10^{-19}$ m^2) has been set as performance targets for buffer and backfill [5].

Mechanical process: Swelling pressures and displacements will develop as a result of hydration. The magnitude of the swelling pressure of the materials are associated with the nature of the clay mineral and dry density. As buffer has a bigger swelling capacity compare to backfill, the upheave of the buffer will take place. As a performance target, the maximum upheaved backfill volume was set to < 0.7 m^3 [5].During the installation of canister, compression on the buffer below the canister might be expected. Upper part of the buffer will swell and compress the backfill. Therefore, dry density of buffer and backfill will not be constant. Intrinsic permeability depends on porosity (HM coupling). On the other hand, total permeability (the product of intrinsic and relative permeability) increases upon saturation. Particularly, total permeability of the buffer surrounding the canister will change not only because of mechanical processes (swelling and compression) but also the thermal (drying) and hydraulic (saturation) processes. During the cooling (controlled by the canister decay function), mean effective stresses and displacements will reduce gradually because of thermal gradient (TM coupling).

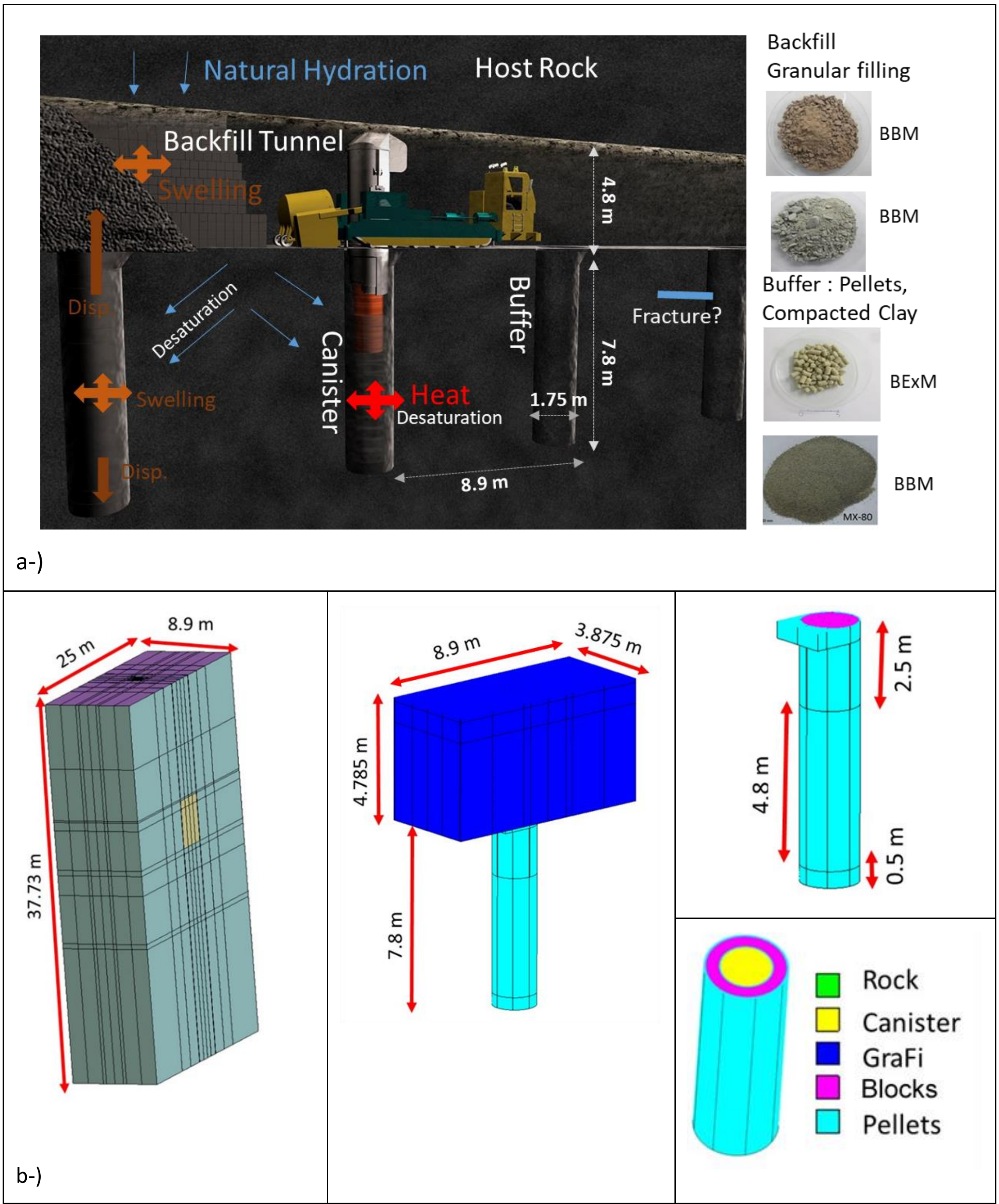

Figure 1. THM processes taking place in KBS3V concept (a), 3D model geometry (b).

2. Material Model Calibrations

The calibration of model parameters of EBS components are given in previous studies : MX80 [2]; pillow pellets [3] and Italian and Bulgarian GraFi [4]. As an example of calibration process, Figure 2 shows simulation of infiltration test performed in Italian GraFi [4]. For MX80 and GraFi materials BBM [6] and for pillow pellets BExM [7] has been considered as geo-mechanical models. Theoretical background and equations of BBM and BExM can be found in [8].

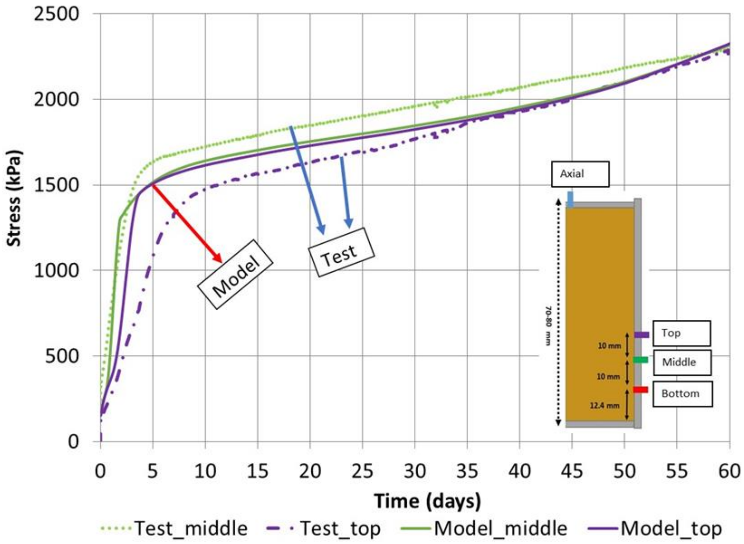

Figure 2. Infiltration test results for Italian GraFi [4].

4. Conclusions

One of the main aims of this study is to show the fulfilment of the performance targets [5], design criterion and safety requirements set for the buffer and backfill under the recent model configuration. Some of the relevant performance targets set for buffer and backfill in the spent fuel repository design are: the allowed maximum temperature (95 °C, Figure 3), maximum upheaved backfill volume (0.7 m^3) and swelling pressure around canister (0.2 MPa $< P_{swell}$ around canister < 10 MPa). The current model under a certain geometrical configuration; with specific TH boundary conditions and with selected materials under given initial conditions fulfils the long term performance targets of EBS components. As shown in the sensitivity analyses, long-term THM response of the repository varies under different scenarios and configurations [3].

Deposition hole	Pillow pellets	Buffer blocks	Canister	15 years

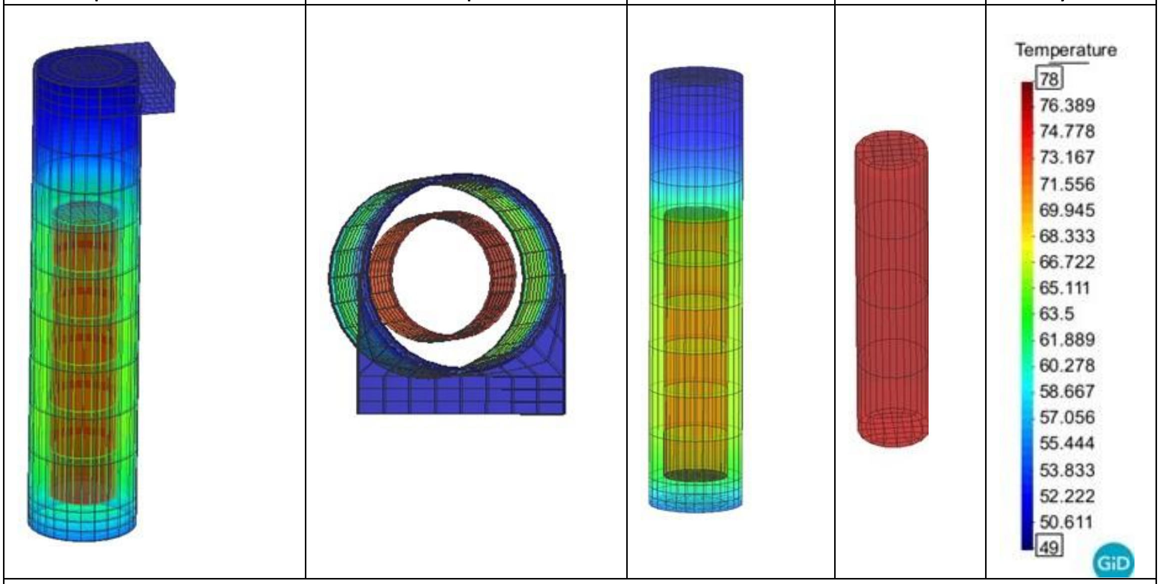

Figure 3. *Distribution (15 years) of temperature in deposition hole in (15 years later emplacement of canister).*

References

[1] Ikonen, K., Kuutti, J. & Raiko, H. 2018. Thermal Dimensioning for the Olkiluoto Repository - 2018 Update. Working Report 2018-26. Eurajoki, Finland: Posiva Oy

[2] Toprak, E., Olivella, S., & Pintado, X. (2016). Coupled THM modelling of engineered barriers for the final disposal of spent nuclear fuel isolation. *Geological Society, London, Special Publications*, *443*(1), 235-251. https://doi.org/10.1144/SP443.19

[3] Toprak, E., Olivella, S., & Pintado, X. (2018). Modelling engineered barriers for spent nuclear fuel repository using a double-structure model for pellets. *Environmental Geotechnics*, *7*(1), 72-94. https://doi.org/10.1680/jenge.17.00086

[4] Toprak, E., Olivella, S., Alcoverro, J., Pintado, X. (2020). Modelling oedometric and infiltration tests on granular filling materials. Eurajoki, Finland: Posiva Oy. Technical Memorandum, kronodoc. POS- 030788

[5] Posiva (2021) Buffer, Backfill and Closure Evolution. Posiva working report 2021-08

[6] Alonso, E.E., Gens, A., Josa, A. (1990). A constitutive model for partially saturated soils. Géotechnique 40(3): 405-430

[7] Gens, A., Alonso, E.E. (1992). A framework for the behaviour of unsaturated expansive clays. Canadian Geotechnical Journal 29(6): 1013-1032

[8] Olivella, S., J. Vaunat, and Rodriguez-Dono. A., Code_Bright 2023 user's guide. 2023.

Acknowledgements

Financial support has been granted by Posiva Oy through a collaboration agreement with CIMNE (Spain). The authors thank to Mika Niskanen for technical assistance and useful discussions.

MODELLING REACTIVE TRANSPORT IN UNSATURATED CONCRETE FOR STORING RADIOACTIVE WASTE

M. Carme Chaparro[*] and Maarten W. Saaltink[†]

[*] CSD Engineers AG,
Schachenallee 29A, 5000 Aarau, Switzerland
E-mail: c.chaparro@csd.ch

[†] Department of Civil and Environmental Engineering,
Technical University of Catalonia (UPC)
Campus Nord UPC, 08034 Barcelona, Spain
E-mail: maarten.saaltink@upc.edu

Key words: Reactive Transport, Multiphase flow, Concrete, Retraso-Code_Bright

Abstract. *Water with high concentration of tritium was leaking from drains situated in concrete cells storing radioactive waste, indicating flow of water into these concrete cells. 2D numerical models together with temperature and humidity measurements suggested that this leak of water was caused by a combination of thermo-hydraulic processes occurring in the unsaturated concrete, such as capillary rise from the groundwater, evaporation, and condensation due to temperature gradients caused by seasonal temperature fluctuations outside. To study the effect of these processes on the mineralogy of the concrete, 1D reactive transport models have been developed following a 2D thermo-hydraulic conceptual model. When minerals are controlled by fast kinetics the model results show that the cement phases precipitate and dissolve clearly following the yearly fluctuations of condensation and evaporation. However, when minerals are controlled by slow kinetics, the reactions are less affected by the hydraulic processes. The models suggest that precipitation-dissolution could be particularly important near the gap of air in the concrete, where water condenses and evaporates more easily.*

1 INTRODUCTION

This study is related to El Cabril, the Spanish facility for the disposal of low- and intermediate- level radioactive waste. At this site radioactive waste is stored in concrete cells. El Cabril motivated this study because, after sealing these cells, water was collected in drains placed at their center, indicating flow of water inside the cell. Moreover, this water had a high concentration of tritium. In a previous work, the same authors[i,ii] demonstrated by means of numerical models that the leakage of tritiated water collected in the drain of the cells could be caused by capillary rise from the phreatic level, evaporation and condensation produced by temperature gradients inside the concrete, which in turn were caused by seasonal fluctuations outside. However, in these previous works, changes in concrete microstructure have not been considered.

So far, no modelling studies have been reported on the geochemistry of concrete affected by temperature gradients, together with evaporation and condensation processes in natural conditions. Hence, the objective of this work is to study the effect of these hydraulic processes on the mineralogy of the concrete used to store radioactive waste at El Cabril.

2 CONCEPTUAL MODEL

Figure 1 displays the conceptual model and a schematization of a concrete cell where the low- and intermediate- radioactive waste is stored. The conceptual model[i,ii], considers that water can ascend from the phreatic level to the wall of the cell due to capillary rise through the unsaturated rock. In summer, the wall of the cell is hotter, and the wall of the container is colder because the air gap acts as thermal insulation. Thus, water can evaporate from the wall of the cell. This vapour diffuses through the air gap due to the temperature gradient between the wall of the cell and the wall of the container. Water condenses at the wall of the container because of its lower temperature. Consequently, water runs off to the drain. In winter, the wall is colder, and the container is hotter. Hence, water evaporates at the container and condenses at the wall. So, again water runs off to the drain. This occurs only in summer and winter because then the temperature difference across the air gap is large enough to produce this phenomenon. In this work, the conceptual model also takes into account chemical reactions in the concrete during the evaporation and condensation processes. To do so, two numerical models have been implemented, one controlled by fast kinetics (where cement phases are practically at equilibrium) and another one controlled by slow kinetics.

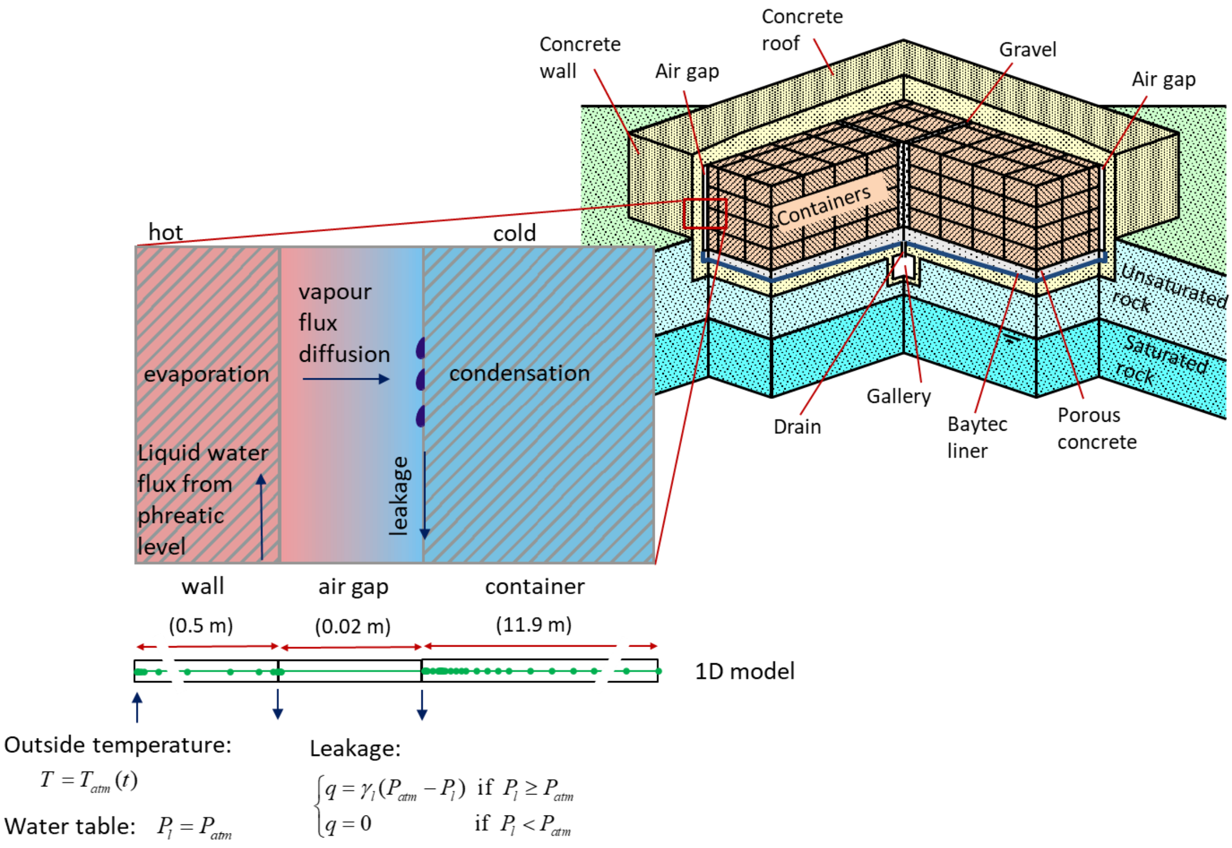

Figure 1: Schematization of a concrete cell, conceptual model and boundary conditions. Situation in summer: water ascends from the phreatic surface, evaporates at the hot side (wall of the cell), vapour diffuses through the air gap and water condensates at the cold side (wall of container)[i,ii].

3 NUMERICAL MODEL

The simulations were carried out using Retraso-CodeBright[iii]. This software package coupled CodeBright[iv] to a module for reactive transport modelling, including aqueous complexation reactions, adsorption, and precipitation-dissolution of minerals.

3.1 Geometry, materials and mesh

An 1D numerical model with 105 nodes and 104 one-dimensional elements has been made (Figure 1). The model considers the wall of the cell, the air gap and the container where the waste is stored. The gap is modelled as one element, and its nodes represent the wall of the cell and the container. The reactions take place in the wall of the cell and container, no reactions occur in the gap.

3.2 Thermo-hydraulic system

The initial temperature of the entire cell is 20ºC and the initial liquid pressure is -0.9 MPa. Temperature is prescribed and varies with time at the wall of the cell, using the daily average temperature measured by the sensors situated outside the cell[i,ii]. This boundary condition is applied to the first node of the wall of the cell. The vertical water flux from and to the groundwater is simulated by a pressure dependent boundary flux taking into account the distance to the groundwater level and the hydraulic conductivity of the concrete. This boundary condition is applied to the second node of the wall of the cell. A leakage boundary condition is applied to the gap of air between the wall and the container allowing water to leave the cell only when liquid pressure exceeds atmospheric pressure. This represents the leakage to the drain (Figure 1).

Retraso-CodeBright solves the mass balance equations for water, air, and energy balance[v]. The thermo-hydraulic parameters of the concrete used in this model are the same used in previous works from the same authors[i,ii].

3.3 Geochemical system

The concrete is composed of C-S-H gel, portlandite, ettringite and calcite as primary phases. The numerical model assumes that aggregates are composed only of quartz. The C-S-H gel is considered a solid solution with varying Ca/Si ratios. This is modelled assuming 5 pure minerals with Ca/Si ranging ratios from 0.83 to 1.67. C-S-H-1667 is used as primary phase and the others as secondary phases. C-A-S-H is also considered a solid solution, with 3 phases with a Ca/Si ration of 1, and Al/Si ratios equal to 0.05, 0.10, and 0.15[vi]. All C-A-S-H phases are considered as secondary phases. The volumetric fractions of the primary phases were calculated from the cement and concrete composition[i,vii].

The composition of the groundwater corresponds to the measured chemical data from a well at approximately 300 m from the concrete cell storing the radioactive waste and with a phreatic level between 4 and 5 m. According to the two conceptual models considered, with fast and slow kinetics, two solution compositions are considered for the concrete pore water. The model called fast kinetics considers the concrete pore water at equilibrium with portlandite, C-S-H-1667, ettringite and calcite. The other components are calibrated according to the measured water composition. In the model called slow kinetics, the concrete pore water is only at equilibrium with calcite and the other components were adjusted to fit the model with the composition of the water collected at the drain. For both models the pH is calculated assuming zero charge balance.

4 RESULTS AND DISCUSSION

4.1 Water composition

In general, both models show that the concentrations follow the yearly temperature fluctuations outside the cell (not shown). The concentration is higher at the hotter side, in summer at the wall of the cell and in winter at the wall of the container, because of evaporation. Calcium concentration is overestimated when portlandite is at equilibrium, indicating that the concentrations in the cement pore water are not at equilibrium with the cement phases. Once the cell was built, it was exposed to atmospheric CO_2 and rainwater during 4 years. Afterwards, it was filled with the radioactive waste and isolated from atmospheric CO_2. However, in that period carbonation could have taken place. Also, the pore water was in contact with the inflowing groundwater due to capillary rise. This could also have affected the composition of the pore water.

The pH calculated by the numerical models oscillates between 12.5 and 13.4 due to changes in water saturation. Both models cannot reproduce the measured pH in the drain. Models predict a pH around 13 but the measured one is around 10. The collected water in the drain could have been in contact with atmospheric CO_2 before the pH was measured or during the measurement, which could drop the pH from 13 to 10. The numerical model does not consider this atmospheric CO_2, because it considers that inside the cell is isolated from the atmosphere.

4.2 Mineral variation

The results for the model with fast kinetics (Figure 2) show a clear yearly mineral variation according to the temperature fluctuations outside the cell. In summer portlandite, C-S-H, ettringite and calcite precipitate in the wall of the cell because of evaporation, and dissolve in the container due to condensation. In winter, the contrary occurs. Portlandite, C-S-H and calcite dissolve in the wall and precipitate in the container. C-A-S-H-05 precipitates when portlandite and C-S-H dissolve, and it dissolves when portlandite and C-S-H precipitate. C-A-S-H precipitates only in winter and in the wall of the cell.

In general, in the model where the cement phases are controlled by slow kinetics (Figure 3) there is less dissolution and precipitation of portlandite, C-S-H and ettringite. In addition, the fluctuations due to the outside temperature are less evident, indicating that reactions are mainly controlled by kinetics and less by evaporation and condensation. However, the amounts of dissolved and precipitated calcite are still high, and they follow the yearly temperature fluctuations, because calcite is at equilibrium. In this model, there is no precipitation of C-A-S-H.

4.3 Porosity

The model predicts no changes in porosity when it is controlled by slow kinetics. There are also no significant changes when the model is at fast kinetics, although the porosity is more affected near to the gap, and in the wall of the container. Similar results are obtained for winter and summer.

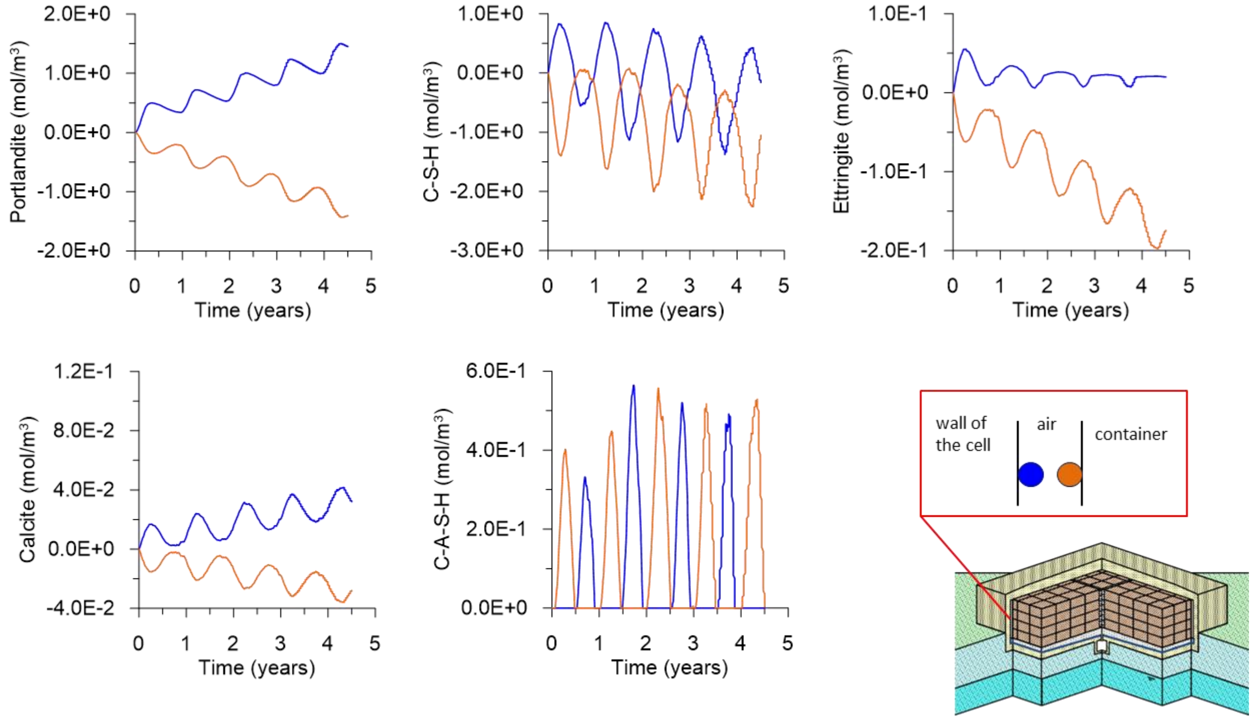

Figure 2: Mineral variation calculated by the fast kinetics model.

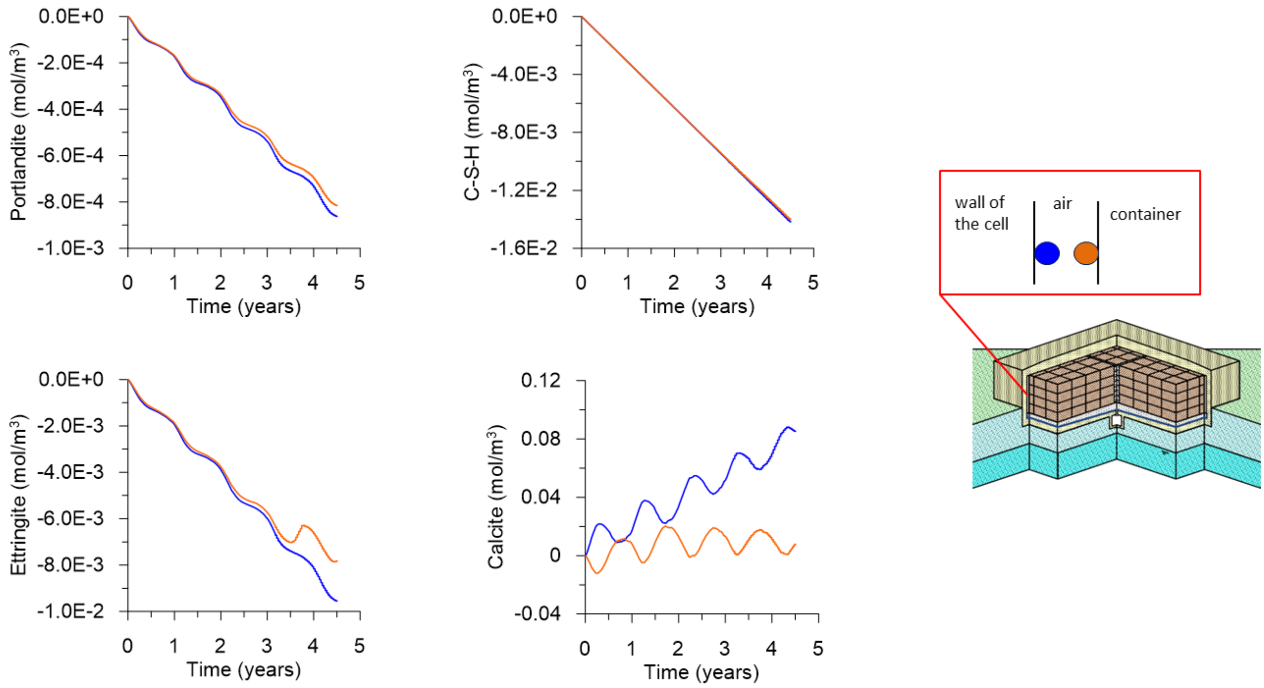

Figure 3: Mineral variation calculated by the low kinetics model.

5 CONCLUSIONS

- The fast kinetics model (equilibrium) shows that minerals precipitated or dissolved according to the evaporation and condensation processes near the air gap. The changes in porosity are more noticeable also near to the air gap.
- The low kinetics model could explain the concentrations measured in the collected water in the drain. The pH could have decreased due to atmospheric CO_2 into the drain. The mineral precipitation-dissolution is controlled by the kinetics of the mineral, and therefore, less controlled for the hydraulic processes (evaporation and condensation).

REFERENCES

[i] Chaparro, M. C. and Saaltink, M. W., 2016. Water, vapour and heat transport in the concrete cells for storing radioactive. Advances in Water Resources, 94:120-130.

[ii] Chaparro, M. C. and Saaltink, M. W., 2022. Tritium transport in non-saturated concrete under temperature fluctuations. Journal of Environmental Radioactivity 251-252, 106969.

[iii] Saaltink, M. W., Batlle, F., Ayora, C., Carrera, J., Olivella, S., 2004. Retraso, a code for modeling reactive transport in saturated and unsaturated porous media. Geologica Acta, 2 (3), 235-251.

[iv] Olivella, S., Gens A., Carrera J., Alonso E. E., 1996. 'Numerical Formulation for a Simulator (CODE_BRIGHT) for the Coupled Analysis of Saline Media " Engineering Computations, Vol 13, No 7, pp: 87-112.

[v] Olivella, S., Carrera J., Gens A., Alonso E. E., 1994. Non-isothermal Multiphase Flow of Brine and Gas through Saline media. Transport in Porous Media, 15, 271:293.

[vi] Myers, R.J., L'Hôpital, E., Provis, J.L., Lothenbach, B., 2015. Effect of temperature and aluminium on calcium (alumino)silicate hydrate chemistry under equilibrium conditions. Cem. Concr. Res. 68, 83e93.

[vii] Chaparro, M.C., Saaltink, M.W., Soler, J.M., 2017. Reactive transport modelling of cement-groundwater-rock interaction at the Grimsel Test Site. Physics and Chemistry of the Earth, 99, 64-76.

EXTENSION OF CODE_BRIGHT WITH AN OBJECT-ORIENTED CHEMICAL MODULE FOR THERMO-HYDRO-MECHANICAL-CHEMICAL MODELS

Maarten W. Saaltink[*†], Anna Ramón[*] and Sebastià Olivella[*]

[*] Department of Civil and Environmental Engineering
Technical University of Catalonia (UPC)
Campus Nord UPC, 08034 Barcelona, Spain
E-mail: maarten.saaltink@upc.edu

[†] Associated Unit: Hydrogeology Group
(UPC-CSIC), Barcelona, Spain

Key words: THMC models, object-oriented programming, Code_Bright.

Abstract. *Code_Bright has been extended with a module for geochemical calculations. This module uses object-oriented-programing to improve on flexibility, extensibility and transportability. The result is a code for THMC (Thermo-Hydro-Mechanical-Chemical) modelling. This new THMC version of Code_Bright has been successfully applied to a simple one-dimensional case that models calcite dissolution due to acid water injection and its effect on porosity and permeability.*

1 INTRODUCTION

In the last years coupled Thermo-Hydro-Mechanical-Chemical (THMC) models have gained importance in many fields of earth and material science, ranging from the laboratory scale, e.g., carbonation in cement[i], to the field scale, e.g. CO_2 injection[ii]. Historically, these models can be seen as a combination of Thermo-Hydro-Mechanical (THM) models in the field of soil and rock mechanics[iii] and Thermo-Hydro-Chemical (THC) models in the field of reactive transport[iv,v]. Code_Bright has played an important role in this development. Code_Bright in its traditional version[vi] is a THM code, which was later coupled to a reactive transport model RETRASO[vii]. This coupled code considers the effect of flow and heat on chemical reactions, but does not consider the opposite effect of chemistry on flow and heat neither on mechanics. Obviously, such coupling is too simplistic for some applications. Moreover, precipitation of gypsum crystals and its effect on mechanical phenomena, such as heave displacements, have been implemented and modeled by Code_Bright[viii,ix]. However, the implementation was done for this particular case and cannot be used for other chemical systems.

This extended abstract presents a fist version of Code_Bright for more sophisticated THMC modeling. It considers the effect of THM models on chemistry and vice versa. Mathematical formulation and numerical solution are briefly discussed in section 2. Chemical calculations are done by an object-oriented chemical module CheProf, explained in section 3. An illustrative example is given in section 4. Finally, section 5 discusses some conclusions.

2 MATHEMATICAL FORMULATION AND NUMERICAL SOLUTION

For THM modelling Code_Bright considers internal energy balance, mass balance of water and of air, momentum balance and/or mass balance of salt[vi] (note that the salt mass balance is considered to be part of THM). These balance equations are associated to different primary state variables, respectively, temperature, pressure of liquid and gas, deformation and mass fraction of dissolved salt. Various constitutive laws and equilibrium restrictions are used to write variables in the balance equation as a function of the primary state variables. Examples are Darcy's law for liquid and gas advective flux as a function of liquid and gas pressure, the retention curve for the liquid phase degree of saturation as a function of capillary pressure (that is, gas minus liquid pressure), and the psychrometric law for vapor mass fraction as a function of temperature and capillary pressure.

The mathematical formulation of reactive transport follows the same approach. Mass balances must be formulated for so called chemical components, which are linear combinations of chemical species[v,vii]. The primary state variables for these mass balances can be the aqueous concentrations of the components or the concentrations a subset of species called primary species. There are various chemical constitutive laws or equations of state, such as the mass action law for equilibrium reactions, kinetic rate laws for kinetic reactions and the extended Debye-Hückel equation for activity coefficients, which are used to calculate concentrations of other (secondary) species and kinetic reaction rates, necessary for the component mass balances. It is worth mentioning that these reactive transport equations depend on THM properties, of which liquid and gas fluxes are generally the most important ones. Contrariwise, though in general to a lesser extent, reactive transport may affect THM properties, such as porosity due to precipitation-dissolution of minerals, density of the liquid due to high salinity and gas production or consumption due to chemical reactions. Moreover, in some cases chemical reactions may involve water and these reactions should be added to the water mass balance, which is part of the THM equations.

Code_Bright uses the finite element method for the spatial discretization and finite differences for the temporal discretization. All THMC balance equations use the same spatial and temporal discretization. The Newton-Raphson method is used for the solution of the non-linear equations[vi], which iteratively solves the following set of linear equations:

$$\boldsymbol{J}^i(\boldsymbol{x}^{i+1} - \boldsymbol{x}^i) = -\boldsymbol{f}^i \tag{1}$$

where superscript i refers to iteration, $\boldsymbol{x}$ is a vector of the primary state variables of all nodes, $\boldsymbol{f}$ is a vector of balance equations of all nodes and $\boldsymbol{J}$ $(= \partial\boldsymbol{f}/\partial\boldsymbol{x})$ is the Jacobian matrix. In order to obtain an exact solution, the Jacobian matrix does not have to be exact and one may just use an approximation. However, an inexact Jacobian affects numerical behavior as it can cause divergence problems or increase number of iterations to reach convergence. The Jacobian matrix can be subdivided into parts for the THM and the reactive transport (indicated by subscript C):

$$\boldsymbol{J} = \begin{pmatrix} \dfrac{\partial\boldsymbol{f}_{THM}}{\partial\boldsymbol{x}_{THM}} & \dfrac{\partial\boldsymbol{f}_{THM}}{\partial\boldsymbol{x}_{C}} \\ \dfrac{\partial\boldsymbol{f}_{C}}{\partial\boldsymbol{x}_{THM}} & \dfrac{\partial\boldsymbol{f}_{C}}{\partial\boldsymbol{x}_{C}} \end{pmatrix} \tag{2}$$

The purely THM part $(\partial\boldsymbol{f}_{THM}/\partial\boldsymbol{x}_{THM})$ has already been coded in the THM version of Code_Bright. The purely reactive transport part $(\partial\boldsymbol{f}_{C}/\partial\boldsymbol{x}_{C})$ has been added. The other parts ($\partial\boldsymbol{f}_{C}/\partial\boldsymbol{x}_{THM}$ and $\partial\boldsymbol{f}_{THM}/\partial\boldsymbol{x}_{C}$) have not been included yet in the present version, that is, they are assumed to equal zero, which may affect numerical behavior.

3 AN OBJECT-ORIENTED CHEMICAL MODULE

The THMC version of Code_Bright needs to calculate the chemical speciation for each node, that is, the concentration of all chemical species from the chemical primary state variables (concentrations of components or of primary species). For this we use CheProf, a module written in Fortran 2003 using the technique of Object-Oriented Programming (OOP) and based on the work of Bea et al.[x]. OOP has various advantages. It has flexibility, that is, it is easy to change, it has extensibility, that is, it is easy to increase functionality and it has transportability, it is easy to implement in different codes.

An important part of OOP is the class diagram, shown in figure 1. Basically a "Chem" consists of a LocalChem (local chemistry) and a pointer to a ChemSys (chemical system). A LocalChem consists of the (state) variables, such as concentrations of all species and volume fractions of phases. A ChemSys contains all equations of state, such as mass action laws, kinetic rate laws, definitions of components and activity models. A ChemSys consists of zero or several Components, zero or several Reactions and one or more Phases. Each reaction, if it is kinetic, has a RateLaw, that can be of the type Monod or Lasaga. Each Phase has one or more Species and one PhaseModels, which are further subdivided according to the way activities are calculated, e.g., assuming ideal mixtures or the extended Debye Hückel equation.

More information can be downloaded from https://github.com/upc-ghs/CheProf-for-Users. This website also contains some other codes, that use CheProf. An interesting one for THMC Code_Bright users is CheProfRW, which can be used to prepare files for the chemical input from results obtained by Phreeqc[xi], a widely used code for aqueous geochemical calculations.

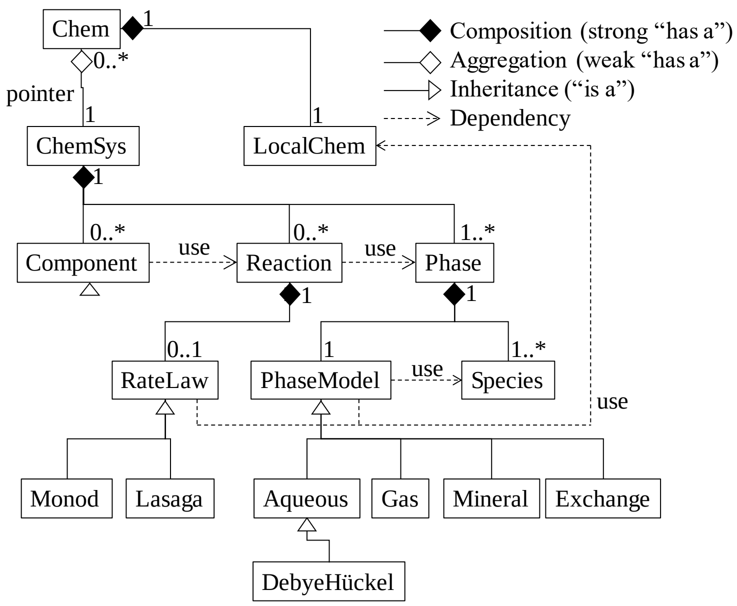

Figure 1: Class diagram of CheProf

4 ILLUSTRATIVE EXAMPLE

A first version of THMC Code_Bright has been developed, which can be downloaded from the Code_Bright website (https://deca.upc.edu/en/projects/code_bright). To illustrate its functioning and verify its correct implementation a simple one-dimensional model has been made. Details and input files can also be downloaded from the Code_Bright website. The chemical system is typical for calcite ($CaCO_3(s)$) dissolution and consists of five equilibrium reactions:

$H_2O \leftrightharpoons H^+ + OH^-$

$H^+ + CO_3^{2-} \leftrightharpoons HCO_3^-$

$2H^+ + CO_3^{2-} \leftrightharpoons CO_2(aq) + H_2O$

$Ca^{2+} + H^+ + CO_3^{2-} \leftrightharpoons CaHCO_3^+$

$CaCO_3(s) \leftrightharpoons Ca^{2+} + CO_3^{2-}$

Water flows from left to right with a prescribed uniform Darcy flux. The inflowing water is acid and dissolves the calcite. As a result, porosity and permeability increases according to Kozeny´s law. In order to obtain a clear effect of the calcite dissolution, long simulated times are used: 500 years, corresponding to 67 to 100 flushed pore volumes, depending on the porosity. Results are compared with DSA1D, a simple code for 1D reactive transport that also uses the chemical module, CheProf, but that does not consider porosity and permeability changes (https://github.com/upc-ghs/CheProf-for-Users).

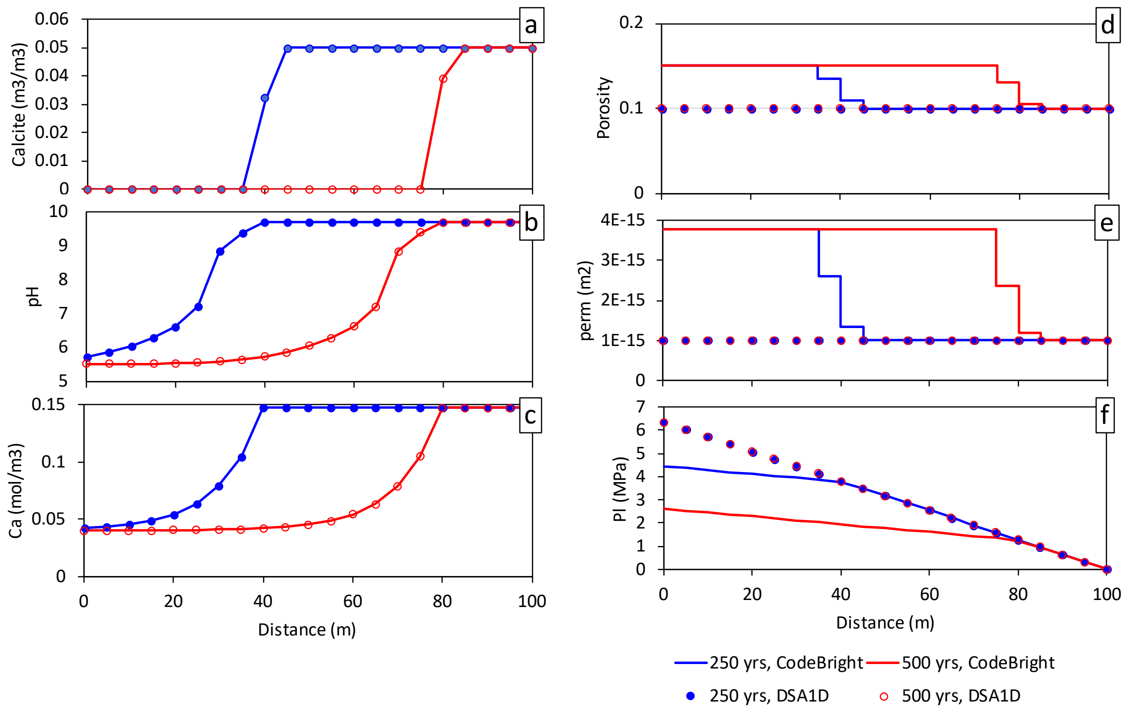

Figure 2: Results of the illustrative example after 250 (blue) and 500 years 8 (red): Calcite volume fraction (a), pH (b), Aqueous Ca concentration (c), porosity (d), intrinsic permeability (e) and Liquid pressure (f). Results of Code_Bright (lines) are compared with those of DSA1D (circles), that does not consider porosity and permeability changes due to precipitation-dissolution reactions.

Figure 2 shows the results. Calcite dissolves at sharp fronts situated at 40 m after 250 years and 40 m after 500 years (Figure 2a). Before these front pH and Ca concentrations are low (figure 2b and 2c), because the lack of calcite cannot buffer the chemical composition of the water. Calcite volume fraction, pH and Ca concentrations calculated by DSA1D and Code_Bright are practically identical (Figures 2a, 2b and 2c), which verifies the correct implementation of reactive transport in Code_Bright. This is not the case for porosity, intrinsic permeability and liquid pressure (Figure 2d, 2e and 2f). The Code DSA1D has a constant porosity and permeability. Therefore, as the Darcy flux is constant, the pressure gradient is constant as well. In contrast, Code_Bright simulates a porosity change from 0.10 for the zone with calcite to 0.15 for the zone without (Figure 2d). As a result, intrinsic permeability increases from $1 \cdot 10^{-15}$ m^2 to almost $4 \cdot 10^{-15}$ m^2 and liquid pressure gradient decreases accordingly. Note, that the calcite volume fractions are given for nodes (Figure 2a), whereas porosities are given for elements (Figure 2d).

5 CONCLUCIONS AND DISCUSSION

A first version of Code_Bright capable of handling THMC modelling has been made. The non-linear balance equations of all nodes at each time step are treated as one mathematical system that are solved numerically with the method of Newton-Raphson, which is considered a robust method, although it may require the solution of large systems of linear equations. Some parts of the Jacobian matrix are neglected, which in theory can affect negatively numerical performance. We expect that numerical performance will improve if proper derivatives are added to these parts of the Jacobian. As THMC models are complex, more research is necessary to gain insight and improve on numerical performance.

A module was added for geochemical calculations, that uses object-oriented programing (OOP). Because of the OOP adding features on chemistry are relatively easy. In fact, most time was spent on writing and changing code related to the residual ($-\boldsymbol{f}$) and the Jacobian ($\boldsymbol{J}$) of equation (1). The overall code may still have to be extended with many other features. For instance, the possibility of reactive gasses (e.g., O_2, CO_2 and H_2) are not yet considered, but is under development.

This new THMC version of Code_Bright has been successfully applied to a simple one-dimensional case that models calcite dissolution due to acid water injection. This model takes into account the effects of dissolution on porosity, permeability and pressure gradient. Nevertheless, more examples and benchmark are needed to evaluate the use of Code_Bright to THMC models.

REFERENCES

[i] Socié, A., N. Seigneur, B. Bary, S. Poyet, Touzé, 2023. A fully coupled Hydraulic Mechanical Chemical approach applied to cementitious material damage due to carbonation. npj Materials Degradation, 7(60). https://doi.org/10.1038/s41529-023-00378-x.

[ii] Gaus, I., P. Audigane, L. André, J. Lions, N. Jacquemet, P. Durst, I. Czernichowski-Lauriol, M. Azaroual, 2008. Geochemical and solute transport modelling for CO_2 storage, what to expect from it? International Journal of Greenhouse Gas Control, 2(4), 605-625. https://doi.org/10.1016/j.ijggc.2008.02.011.

[iii] Rutqvist, J., L. Börgesson, M. Chijimatsu, A. Kobayashi, L. Jing, T.S. Nguyen, J. Noorishad, C.-F. Tsang, 2001. Thermohydromechanics of partially saturated geological media: governing equations and formulation of four finite element models. International Journal of Rock Mechanics and Mining Sciences, 38(1), 105-127. https://doi.org/10.1016/S1365-1609(00)00068-X.

[iv] Steefel, C. I., D. J. DePaolo, P. C. Lichtner, 2005. Reactive transport modeling: An essential tool and a new research approach for the Earth sciences. Earth and Planetary Science Letters, 240(3-4), 539-558. https://doi.org/10.1016/j.epsl.2005.09.017.

[v] Steefel, C. I. (2019). Reactive Transport at the Crossroads. Reviews in Mineralogy and Geochemistry, 85(1), 1-26. https://doi.org/10.2138/rmg.2019.85.1.

[vi] Olivella, S., A. Gens, J. Carrera, E. E. Alonso, 1996. Numerical Formulation for a Simulator (CODE_BRIGHT) for the Coupled Analysis of Saline Media. Engineering Computations, Vol 13, No 7, pp: 87-112.

[vii] Saaltink, M.W., F. Batlle, C. Ayora, J. Carrera, S. Olivella, 2004. RETRASO, a code for modeling reactive transport in saturated and unsaturated porous media. Geologica Acta, 2(3), 235-251.

[viii] Ramon, A., Alonso, E. E., 2013. Heave of a railway bridge: modelling gypsum crystal growth. Géotechnique, 63(9), 720-732. https://dx.doi.org/10.1680/geot.12.P.035.

[ix] Ramon, A., Alonso, E. E., Olivella, S., 2017. Hydro-chemo-mechanical modelling of tunnels in sulfated rocks. Géotechnique, 67(11), 968-982. https://doi.org/10.1680/jgeot.SiP17.P.252.

[x] Bea, S. A., J. Carrera, C. Ayora, F. Batlle, M.W. Saaltink, 2009. CHEPROO: A Fortran 90 object-oriented module to solve chemical processes in Earth Science models. Computers & Geosciences, 35(6), 1098-1112. https://doi.org/10.1016/j.cageo.2008.08.010.

[xi] Parkhurst, D.L., C.A.J. Appelo, 2013. Description of input and examples for PHREEQC version 3-A computer program for speciation, batch-reaction, one-dimensional transport, and inverse geochemical calculations. U.S. Geological Survey Techniques and Methods, book 6, chap. A43, Denver: U.S. Geological Survey, 497 pages. http://pubs.usgs.gov/tm/06/a43/.

THERMAL ANALYSIS OF THE FULL-SCALE IN-SITU SYSTEM TEST (FISST) IN FINLAND. ROCK THERMAL PROPERTIES

Pintado, X.[*] and Niskanen, M.[†]

[*] Mitta Engineering Oy
Riihimiehentie 3, 01720 Vantaa, Finland
E-mail: xavier.pintado@mitta.fi, web page: https://mitta.fi/en/
[†] Posiva Oy
Satamatie 22, 27160 Eurajoki
E-mail: mika.niskanen@posiva.fi, web page: http://www.posiva.fi

Key words: GiD interface, THM coupled analysis, Geological media

Abstract. *The spent nuclear fuel produced in the nuclear power plants in Finland is going to be stored in a network of caverns at 420 m depth. The spent nuclear fuel generates heat that must be conducted through the host rock to avoid excess of temperature which might cause mineralogical changes in the clay barriers located between the canister containing the spent nuclear fuel and the host rock, losing part of their sealing properties. Rock thermal properties were assessed carrying out the simulation of an "in situ" test performed in ONKALO® (Finland). The results gave an upper limit of the maximum temperature expected in the contact between the canister containing the spent fuel and the clay barrier surrounding the canister. The analysis was thermal, without considering the favourable effect of the hydration, which increases the thermal conductivity of the clay barrier and facilitates the heat diffusion.*

1 INTRODUCTION

This contribution presents the thermal analysis of the Full-Scale In-Situ System Test (FISST) currently ongoing in the ONKALO® demonstration area[i], part of the Finnish spent nuclear fuel disposal facility under commissioning phase. Demonstration tunnel hosting FISST is located at a depth of approximately 420 m. The test is carried out with two canisters equipped with heating elements to simulate the decay heat power generated by the spent fuel. The space between the canisters and the rock was filled with blocks and pellets manufactured with Wyoming-type bentonite. The deposition tunnel was filled with blocks and pellets manufactured with two types of bentonites from Italy and Bulgaria respectively[ii].

The test was instrumented with different types of sensors. Sensors measuring temperature (thermocouples), relative humidity (capacitive hygrometers), pore pressure (piezometers), total pressure (total pressure sensors) and electric resistance tomography (ERT) system were chosen based on the evaluation of suitable sensors and instrumentation methods done in the EU project Modern 2020 and also from experiences in Prototype Repository[iii] and other "in situ" experiments. Part of the sensor data is used for comparing with the early evolution simulation results of the EBS system.

2 CONCEPTUAL MODEL

The geometry of the test was implemented (Figure 1). This geometry follows the Posiva's Geological Structure Model v. 04122023. The geometry was created from CAD drawings provided by Posiva. These drawings were transformed to files to be able to use by the preprocessing in GiD[iv], the mesh generator used for carrying out the pre-post processing in the computer code that performs the simulations, CODE_BRIGHT[v]. The position of the fractures is presented in Anna et al.[vi] and added in the pre-process file.

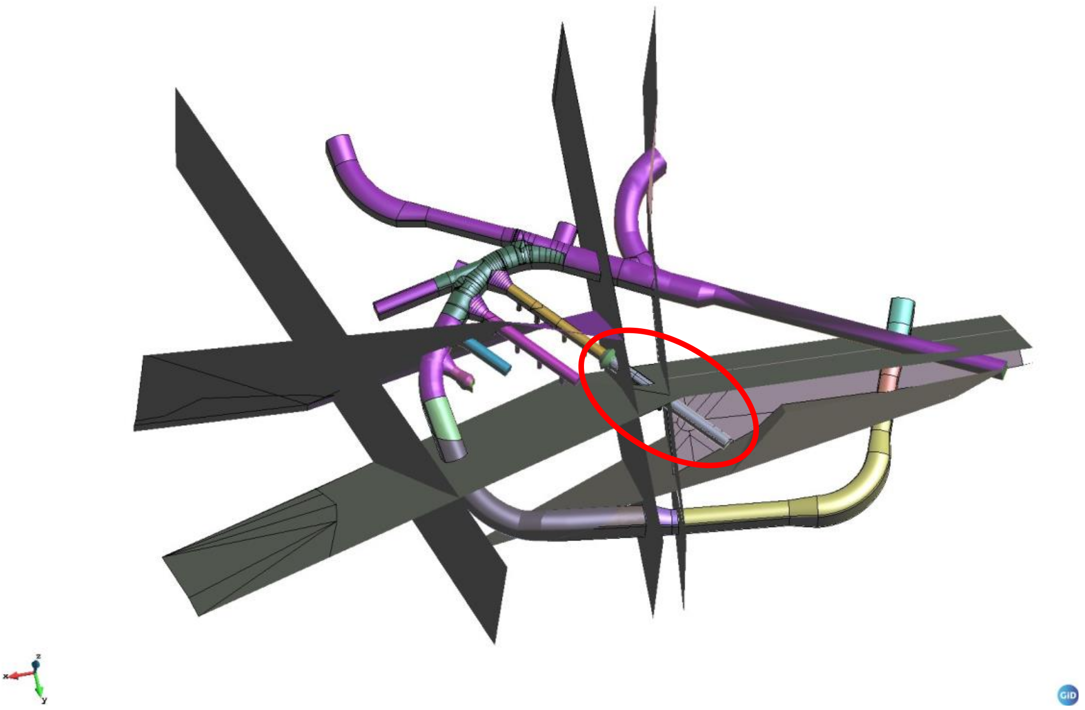

Figure 1: FISST emplacement with the fractures and network fractures' system.

The sensors in rock were emplaced in three drillholes in rock, with a total number of sensors of 27 (9 sensors in each drillhole, Figure 2).

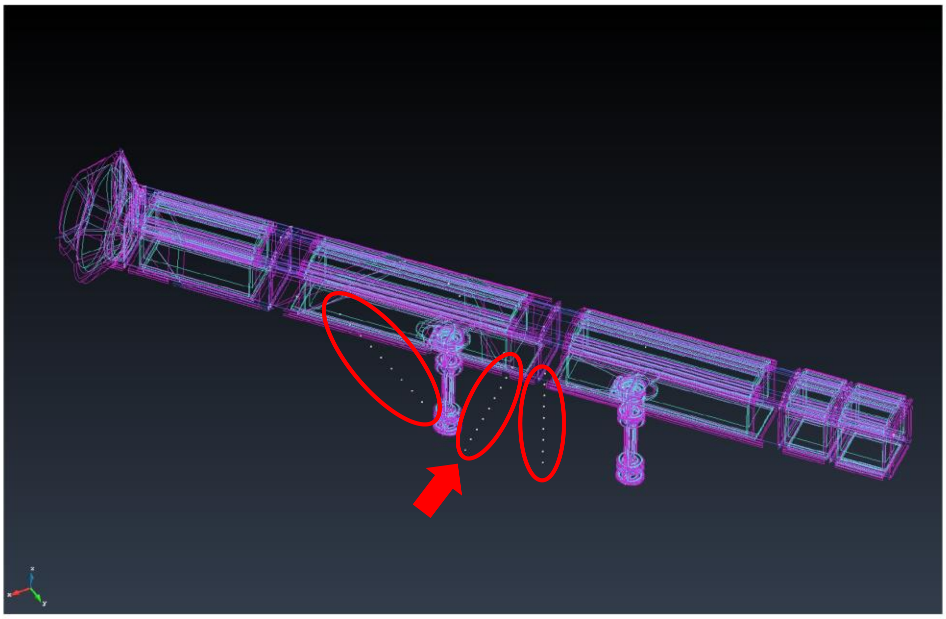

Figure 2: Position of the rock sensors in FISST test.

The finite element mesh had 166 265 nodes and 948 412 linear tetrahedra elements in volumes. The mesh was mixed structured (deposition holes) and non-structured (rest of the volumes and fractures) for making easier the generation of the mesh. The position of the sensors was also implemented in the mesh and their position coincided with nodes of the mesh.

Only the energy balance equation was solved, so the parameters of the materials were only the density, thermal conductivity and specific heat. These parameters, presented in Table 1, must be the average of the parameters of soil components (air, water and clay or rock). The porosity considered was 10^{-10} to be able to have homogeneous materials.

Material	Density (kg/m^3)	Thermal conductivity (W/mK)	Specific heat (J/kg)
Canister	8 930	390	390
Buffer (pellets)	1 075	0.20	694
Buffer (ring blocks)	2 040	1.25	1 324
Buffer (disc blocks)	1 988	1.20	1 316
Backfill (Italian pellets)	1 221	0.24	1 480
Backfill (Italian blocks)	1 888	1.25	1 339
Backfill (Bulgarian pellets)	1 201	0.23	1 430
Backfill (Bulgarian blocks)	1 866	1.30	1 292
Rock	2 743	2.82	764

Table 1: Thermal properties of the materials

The boundary conditions were an injection of heat with a power of 409 W/m^3 (equivalent to 1 700 W/canister) in the heaters and constant temperatures on top and at the bottom of the geometry. The initial temperature of the model followed the geothermal gradient, which value was 1.4°C/100 m[vii].

3 RESULTS

Figure 3 presents the evolution of the temperature in three positions of the drillhole signaled in Figure 2.

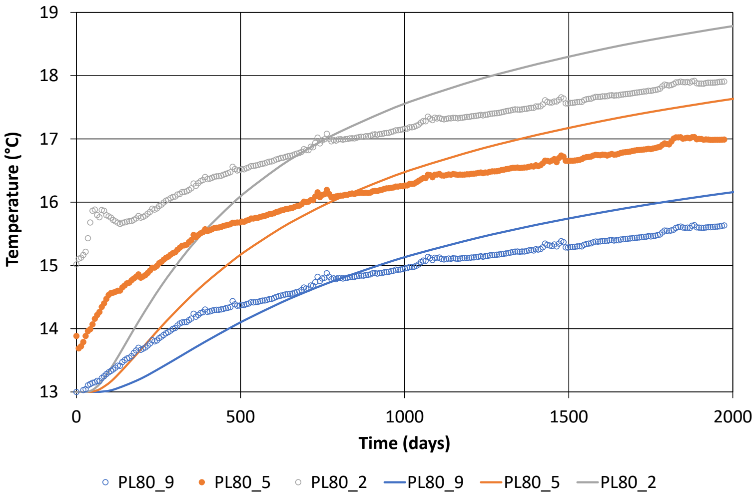

Figure 3: Position of the rock sensors in FISST test

Figure 4 presents the temperature distribution after 2083 days of heaters switched on.

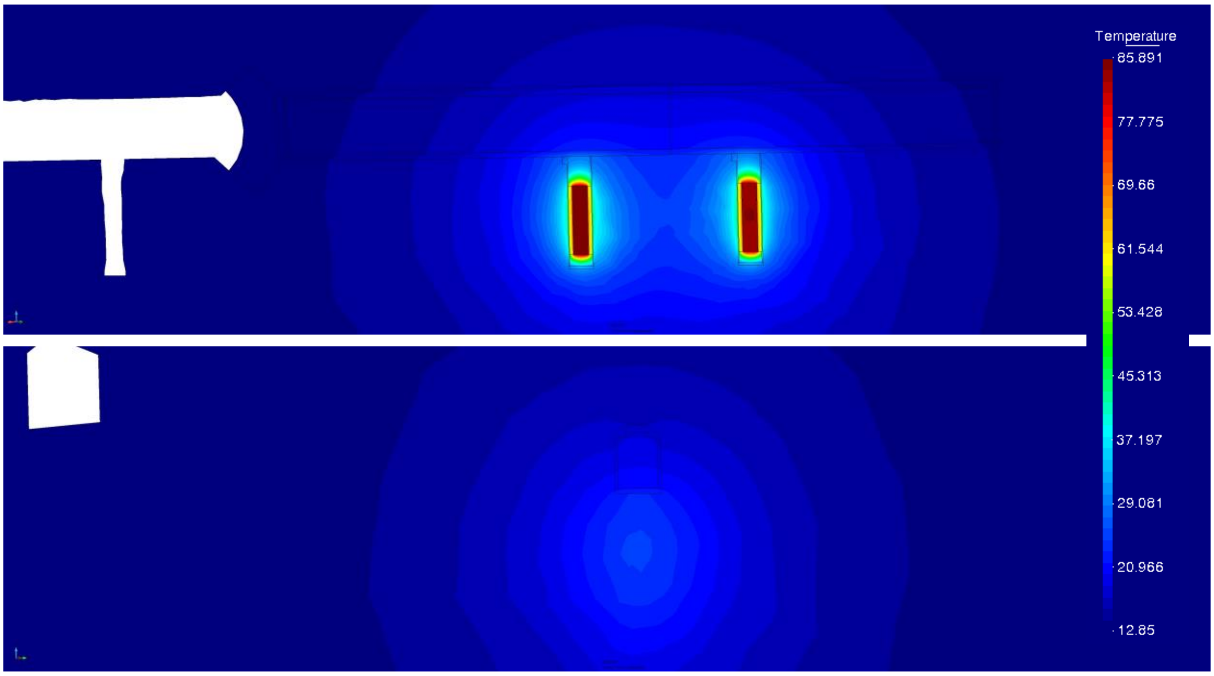

Figure 4. Sections at t=2 083 days. Looking at the end of the tunnel

4 CONCLUSIONS

- The capacity of the mesh generator to include the measurement points allows to generate meshes more realistic and facilitates the calibration of the models.
- Thermal properties of rock can be adjusted with the "in situ" tests.
- Thermal analysis overestimates the temperatures due to the increase of the thermal conductivity of the buffer is not considered.
- Necessary to adjust better the initial conditions of the rock.
- It is possible to consider the model as Digital Twin.

REFERENCES

[i] Posiva. "Final disposal tests." Posiva website. https://www.posiva.fi/en/index/finaldisposal/finaldisposaltestsfisstytk.html (Retrieved May 21, 2024).

[ii] Tsitsopoulos, V., Holton, D., Appleyard, P., Thompson, S., Baxter, S., Niskanen, M., 2023, "Thermal hydraulic and mechanical modelling of the full-scale in situ test (FISST)" Engineering Geology, Vol 322, pp. 107165.

[iii] Svemar, C., Johanesson, L-E, Grahm, P., Svensson, D., Kristensson, O., Lönnqvist, M., Nilsson, U., "Prototype Repository Opening and retrieval of outer section of Prototype Repository at Äspö Hard Rock Laboratory. Summary report" SKB report TR 13-22. Stockholm, Sweden.

.[iv] CIMNE. “GiD SIMULATION.” GiD SMULATION. https://www.gidsimulation.com/ (Retrieved May 20, 2024).

[v] DECA-UPC. “CODE_BRIGHT 2023 User’s guide.” CODE_BRIGHT Department of Civil and Environmental Engineering. https://deca.upc.edu/en/projects/code_bright (Retrieved May 20, 2024).

[vi] Anna, R., Laitinen, Mustonen, S., Kosunen, P., Joutsen, A. Mellanen, S., Ikonen, A., Hollmen, K., Nuijten, G., 2016, “Design and Construction of Equipment and Experimental Deposition Holes, in ONKALO Demonstration Tunnel 2” Posiva Working report 2016-27, Eurajoki, Finland.

[vii] Hartikainen, J., 2006, “Numerical Simulation of Permafrost Depth at Olkiluoto” Posiva Working report 2006-52, Eurajoki, Finland.

HM SIMULATION OF LABORATORY AND IN-SITU EXPERIMENTS IN THE SANDWICH PROJECT

Matthias Hinze*, Larissa Friedenberg* and Klaus Wieczorek*

* Gesellschaft für Anlagen- und Reaktorsicherheit (GRS) gGmbH
Repository Research Department
Theodor-Heuss-Straße 4, 38122 Braunschweig, Germany
E-mail: matthias.hinze@grs.de, web page: https://www.grs.de/en/

Key words: Hydraulic shaft sealing, Sandwich principle, Mont Terri Rock Laboratory

Abstract. *This study summarizes the modelling results obtained during the first phase of the Sandwich project, in which the Sandwich shaft sealing system is investigated in a large-scale in-situ test together with laboratory and semi-technical-scale experiments. The accompanying modelling work comprises a bentonite model calibration and validation using laboratory measurements as well as the simulation of the in-situ experiment by using the Barcelona Expansive Model implemented in CODE_BRIGHT.*

1 INTRODUCTION

The international joint project "Sandwich" deals with the investigation of a special hydraulic shaft sealing system. A Sandwich seal consists of alternating sealing segments (DS) of bentonite and equipotential segments (ES) of sand with a much higher hydraulic conductivity. The advantage of the Sandwich sealing system compared to monolithic shaft seals is the even distribution of incoming fluid over the cross-section of the shaft, leading to a more homogeneous hydration and swelling of the DS (Figure 1). Particularly, liquid bypassing the seal via the excavation damaged zone (EDZ) or penetrating the seal inhomogeneously is absorbed and distributed by the ES[i,ii].

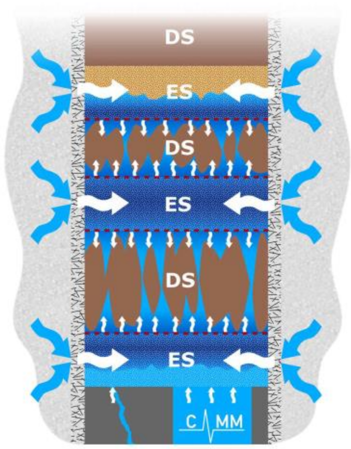

Figure 1: Scheme of the hydraulic behavior of the Sandwich sealing system[ii]

The Sandwich project comprises an extensive multi-scale laboratory program with material characterization experiments, MiniSandwich tests and semi-technical-scale experiments (Figure 2). Investigations on a large scale are realized by an in-situ experiment at the Mont

Terri Rock Laboratory consisting of two shafts in which Sandwich sealing system are installed and monitored while being hydrated (Figure 2, right).

The experimental investigations are accompanied by numerical modelling work on multiple scales. Selected simulation results obtained by GRS using CODE_BRIGHT are presented in the following.

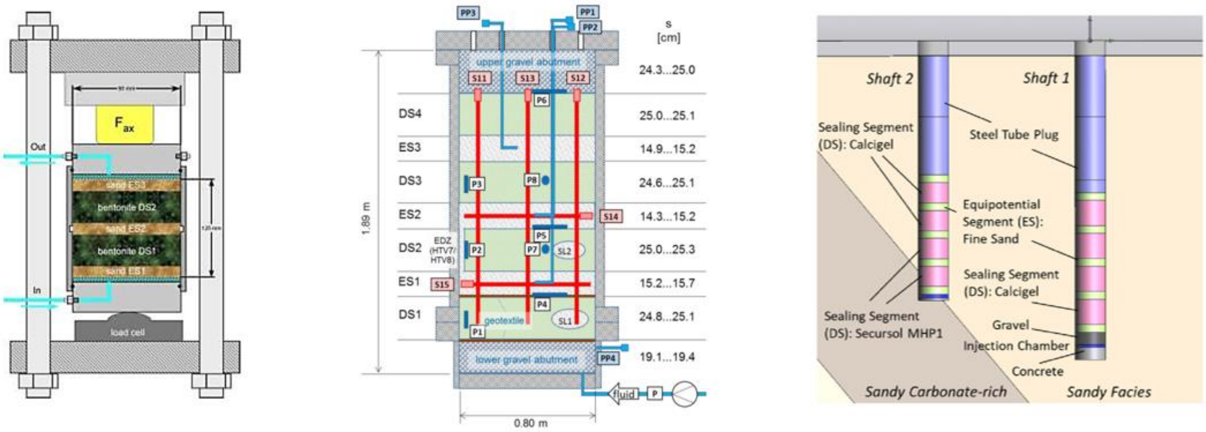

MiniSandwich
(125 x 90 mm)

Semi-technical scale experiment
(189 x 80 cm)

In-situ experiment at Mont Terri

Figure 2: Multi-scale experimental approach within the Sandwich project

2 MODELLING APPROACH

The modelling work covers a hydraulic-mechanical (HM) coupled approach. The focus is on the simulation of the Sandwich sealing system behavior, especially on the interaction between the ES and DS, and later, on the interaction of the whole sealing system with the surrounding host rock Opalinus clay (OPA).

For the simulation of the complex HM-coupled behavior of the bentonite, the “Barcelona Expansive Model (BExM)” available in the official CODE_BRIGHT version is applied. It covers a double-structure approach assuming a macrostructural and microstructural level (Figure 3) with different material properties and interaction mechanisms[iii,iv]. With the BExM, hydration and consequent swelling of bentonite materials can be simulated. The feature of an individual retention behavior of the microstructure was not applied yet. Thus, the microstructure is assumed to be mostly saturated and in hydraulic equilibrium with the macrostructure.

The fine-grained sand in the ES as well as the Opalinus clay are currently modelled by using a linear elastic constitutive law.

From the extensive experimental laboratory program, a good amount of data is available for calibrating the material parameters needed in the BExM[ii]. Thus, the modelling work started with calibration simulations of swelling pressure tests and one MiniSandwich experiment. With the calibrated parameter set, the hydration of Shaft 1 of the in-situ experiment was simulated.

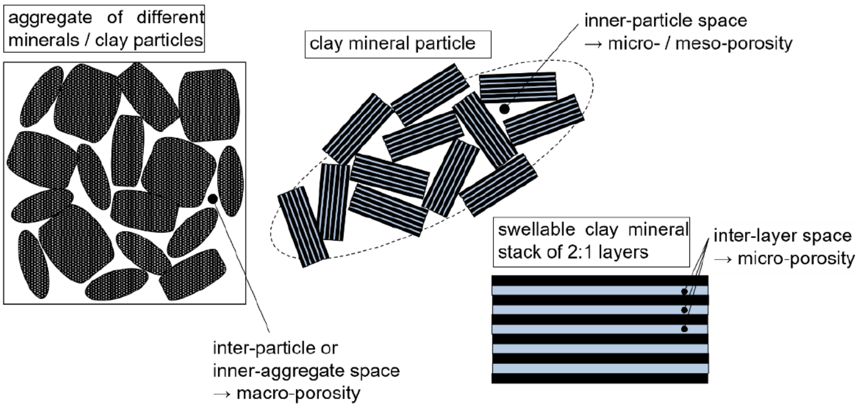

Figure 3: Schematic concept of porosity levels in granular bentonite[ii]

3 MODEL CALIBRATION OF THE BEXM

3.1 Swelling pressure tests

Various swelling pressure tests were simulated with the aim to obtain a consistent parameter set for tests at different conditions. Particularly, it was intended to extract one porosity-permeability relation and one relation between dry density and initial pre-consolidation pressure for all tests and keep the other parameters constant. Since no parameter set was existing for the used calcium bentonite “Calcigel”, the material parameters from the FEBEX bentonite were applied as a basis. During the calibration process, several parameters were adjusted. The details can be found in the final report of the first phase of the Sandwich project[ii].

Experimental measurements of the water retention behavior performed during the project showed that the suction of Calcigel would be more a function of water content than of saturation. Accordingly, updated retention curves were used for samples at different initial dry densities[ii].

In Figure 4, results are shown for the in-situ installed dry density of 1.54 g/cm^3 with the originally calibrated retention curve. The simulation results show a convincing fit of the measurement data. Measured saturations greater than 1 can obviously not be captured by the simulation. The simulated evolution of the axial pressure build-up nicely matches the trend of the measurements. The final parameter set can be found in Wieczorek et al. (2024).

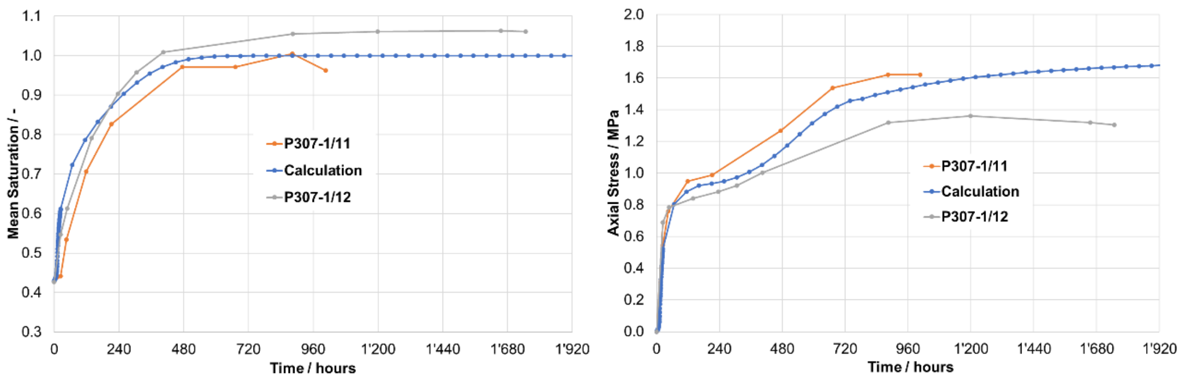

Figure 4: Comparison of measurements and numerical results for swelling pressure tests with an initial dry density of 1.54 g/cm^3. Left: mean saturation. Right: axial stress.

3.2 MiniSandwich Oe8

As a next step, the laboratory test MiniSandwich Oe8 was simulated to validate the beforehand calibrated parameter set. This MiniSandwich experiment was chosen, since its conditions and settings (bentonite, dry density, initial saturation) represent the situation of Shaft 1 in the in-situ experiment (Figure 2, right). The test setup and geometric model are shown in Figure 5. The boundaries of the axisymmetric model are mechanically fixed in normal direction. Hydration of the specimen from the bottom is represented by a pressure condition (rapid increase to 0.1 MPa) at the lower boundary.

The numerical results show a very good accordance with the measurement data for the cumulative liquid inflow and the axial stress evolution, see Figure 6. However, the calibration process must not be considered finished. More data to confirm the porosity-permeability relationship are needed, as well as tests with higher hydration pressures. The simulation is very sensitive to the pressure gradient in the model, which might cause issues for higher hydration pressures. Moreover, an experimental program of suction-controlled consolidation tests with Calcigel is currently being planned to allow for a direct measurement of the mechanical parameters used in the BExM and the consideration of a desaturated microstructure is being investigated.

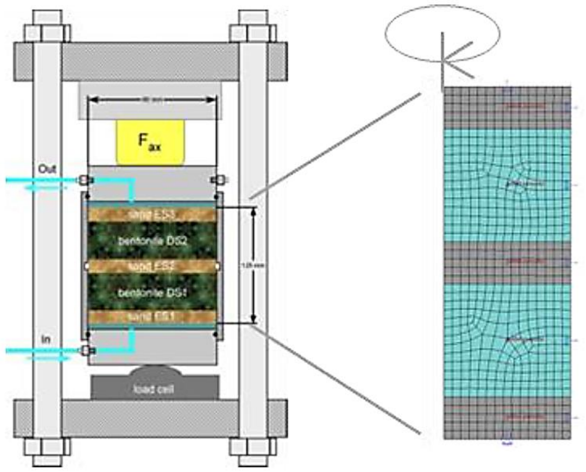

Figure 5: Setup of the MiniSandwich Oe8 test and axisymmetric model for the simulation

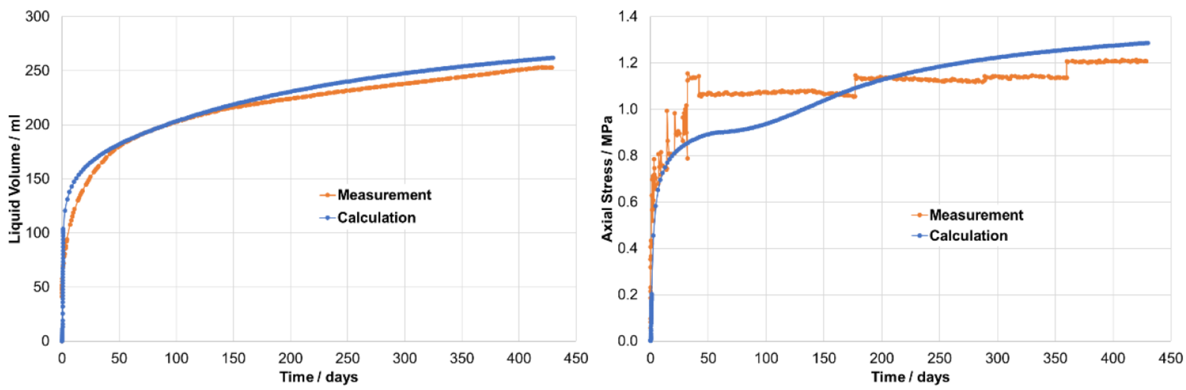

Figure 6: Comparison of measurements and simulation results for MiniSandwich Oe8.
Left: total liquid volume uptake. Right: axial stress.

4 SIMULATION OF SANDWICH SHAFT 1

The parameter set obtained from the calibration process was applied for the simulation of Shaft 1. An axisymmetric model was chosen which is shown in Figure 7. It includes (besides the materials of the sealing system) the OPA and the concrete floor of the niche. Initial and boundary conditions are also displayed in Figure 7. The suction of 2 MPa on the top boundary represents the ventilation of the niche. Information on the complete parameter set used for the simulation can be found in Wieczorek et al. (2024)[ii]. The simulation includes the excavation of the shaft, its ventilation and the subsequent installation of the sealing system. The hydration from the shaft bottom and its evolution follows the course of the in-situ experiment (Figure 7).

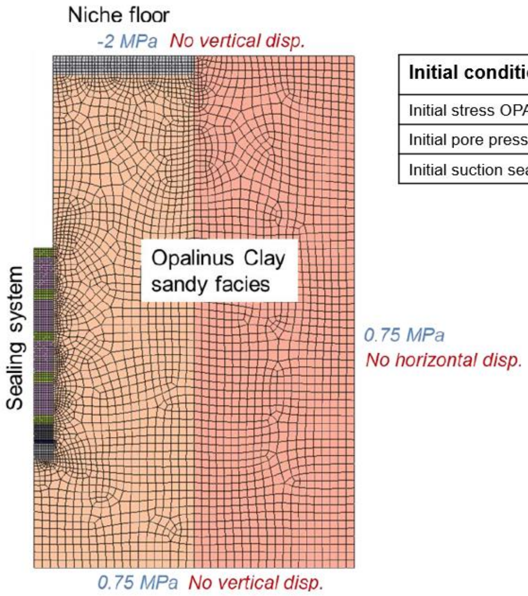

Initial conditions	
Initial stress OPA	7 MPa / 3MPa
Initial pore pressure OPA	0.75 MPa
Initial suction sealing system	133 MPa

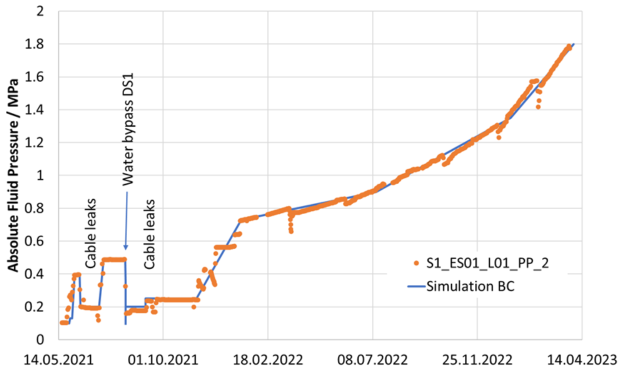

Figure 7: Geometry, hydration history, mesh, initial and boundary conditions of the Shaft 1 model[ii]

Figure 8 shows the liquid saturation in the model for selected time instances. Right before seal construction, the OPA and concrete are almost everywhere saturated. Only a small desaturated zone at the nice floor and the shaft wall can be observed due to ventilation. The bentonite material has an initial saturation of around 40 %. At the start of hydration, already some water uptake of the sealing system from the surrounding OPA can be observed due to the high suction of the bentonite. The high permeability of the ES allows for a quick transfer of water to the DS leading to a constant suction in the ES. The ES remain rather dry, until the bentonite in the adjacent DS approach full saturation. The simulation comprises around 5 years of the experimental course and ends in March 2023. In the whole sealing system, the suction has decreased over time. However, the sealing system is still unsaturated. In the lower segments, water uptake occurs due to hydration, whereas in the upper segments the water uptake from the host rock continues. The liquid flow from the rock to the shaft and water uptake of the sealing system leads to an increased desaturated area in the rock mass.

Comparing the hydraulic simulation results to in-situ measurement data[ii] shows a generally good agreement. The expected processes can be reproduced by the numerical model. However, the measurements show full saturation of the lowest DS at the end of March 2023, which is not reproduced by the simulation. The most likely explanation is the need for an improved porosity-permeability relation of the bentonite material.

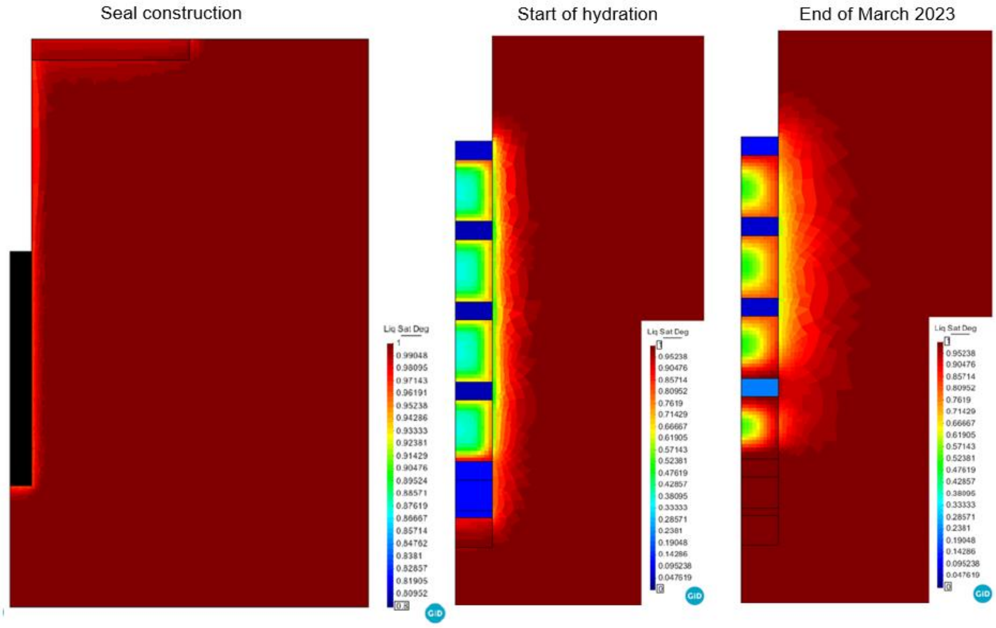

Figure 8: Liquid saturation results for different time steps in the simulation of Shaft 1[ii]

5 CONCLUSIONS AND OUTLOOK

This contribution presents a multi-scale modelling approach which allows for the simulation of the hydro-mechanical behavior of a Sandwich shaft sealing system interacting with the surrounding argillaceous rock mass. The bentonite model parameters are obtained through calibration from swelling pressure tests and validated against a laboratory-scale MiniSandwich experiment. Using the resulting parameter set for the simulation of the Sandwich in-situ experiment yields a good qualitative representation of the experimental measurements. However, the results also suggest an improvement of the calibration procedure. Therefore, further laboratory tests are designed to access parameters of the BExM, and the application of the most recent implementation of the BExM in CODE_BRIGHT, allowing for a desaturated microstructure and a liquid exchange between structural levels, is considered.

ACKNOWLEDGEMENTS

The Sandwich project is supported by the German Federal Ministry for the Environment, Nature Conservation, Nuclear Safety and Consumer Protection under contract 02E12163B.

REFERENCES

[i] Emmerich, K. et al.: Joint project: Vertical hydraulic sealing system based on the Sandwich principle - preproject (Sandwich-VP): Joint final report. DOI 10.2314/KXP:1692488228, 2019.

[ii] Wieczorek, K. et al.: Sandwich - HP, Vertical Hydraulic Sandwich Sealing System, Final Report. Ed.: Gesellschaft für Anlagen- und Reaktorsicherheit (GRS) gGmbH: Köln, GRS-745, February 2024.

[iii] Alonso, E. E., Gens, A., Josa, A.: A constitutive model for partially saturated soils. Géotechnique, vol. 40, no. 3, pp. 405–430, DOI 10.1680/geot.1990.40.3.405, 1990

[iv] Olivella, S., Vaunat, J., Rodriguez-Dono, A.: CODE_BRIGHT. Version 2022, Universitat Politècnica de Catalunya: Barcelona, 2022.

THM SIMULATION OF PROCESSES IN GENERIC FINAL REPOSITORY CONCEPTS

Matthias Hinze* and Larissa Friedenberg*

* Gesellschaft für Anlagen- und Reaktorsicherheit (GRS) gGmbH
Repository Research Department
Theodor-Heuss-Straße 4, 38122 Braunschweig, Germany
E-mail: matthias.hinze@grs.de, web page: https://www.grs.de/en/

Key words: THM coupled analysis, CODE_BRIGHT, Geological media, Final repository

Abstract. *This contribution presents some results of THM simulations with CODE_BRIGHT for one- and two-dimensional generic models of a nuclear waste repository in argillaceous host rock.*

1 INTRODUCTION

The deep geological disposal of high-level radioactive waste requires a prediction of the long-term behavior of a repository including (among others) thermal-hydraulic-mechanical (THM) coupled processes that must be considered in numerical simulations. It was the aim of the BenVaSim[i] project to investigate the basic processes, with special regard to flow processes, in simplified models of repository components to perform an international benchmarking for common THM simulators. Within the project, several one-dimensional repository models were considered at different levels of complexity. While the simulator results where in great accordance for the case of the HM modelling tasks, much larger differences in simulation results of different codes occurred for the considered THM problems due to different simulator frameworks. This observation led to the follow-up project BenVaSim II, which aims, on the one hand for an improved compilation of model assumptions for the one-dimensional problems considered in the first project phase, and, on the other hand to extend the benchmarking initiative to more complex, particularly two- and three-dimensional problems related to generic repository concepts. It is the aim of this contribution to present the results that the authors obtained within the project by simulations performed with CODE_BRIGHT. Particularly, THM simulation results for the improved one-dimensional problem as well as thermo-mechanical (TM) and thermo-hydraulic (TH) simulations of a two-dimensional section through a waste canister and the surrounding backfill and host rock are given and interpreted.

2 ONE-DIMENSIONAL MODEL AND THM COUPLED ANALYSIS

2.1 Model assumptions, conditions, and parameters

The considered (quasi) one-dimensional model (Figure 1) represents a horizontal section through a deposition drift and the surrounding argillaceous host rock (40 m in length) oriented perpendicular to the drift direction. It consists of a canister section representing the mixed behavior of canister and backfill (2 m) and a host rock section (38 m).

The mathematical model includes the equations associated to energy balance, stress equilibrium and the mass balances of the solid skeleton as well as the fluid components water and air. The constitutive model includes Fourier's law, a linear elastic solid material law with additional linear thermal expansion and Bishop-type effective stress and advective fluid fluxes following a generalized Darcy's law with constant intrinsic permeability and van-Genuchten-type liquid and gas phase interactions. The associated model parameters are given in Table 1.

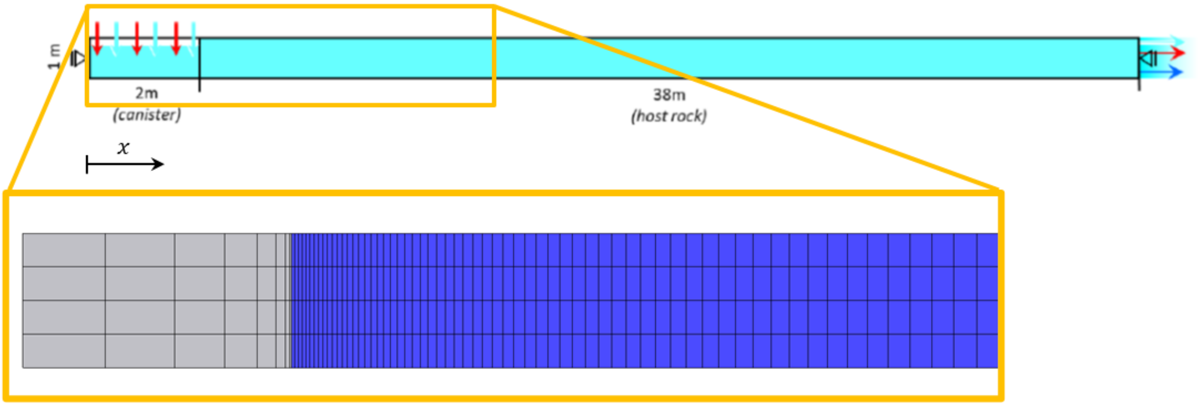

Figure 1: Model geometry and mesh details (1D model)

solid phase properties	**1D model**		**2D model**		
	can. sect.	host rock	canister	backfill	host rock
general parameters					
specific density [kg/m³]	3,450	2,700	6,700	2,700	2,700
initial porosity [-]	0.37	0.17	0.01	0.45	0.12
thermal parameters					
thermal conductivity [W/(m K)]	11.57	2.3	16	2	2
specific heat capacity [J/(kg K)]	830	900	500	900	900
linear elastic constitutive parameters					
Young's modulus [MPa]	150	8,000	195,000	100	5,000
Poisson's ratio [-]	0	0	0.3	0.1	0.3
hydraulic parameters					
intrinsic permeability [m²]	1.75E-18	1.0E-20	1.0E-25	1.0E-16	1.E-20
van Genuchten gas entry pressure [MPa]	12	30	0.1	10	10.9
van Genuchten shape parameter [-]	0.5	0.28	0.5	0.4	0.29
residual liquid saturation [-]	0.03	0.16	0	0	0.01
residual gas saturation [-]	0	0	0	0	0
coupling parameters					
lin. thermal expansion coefficient [1/K]	5.9E-6	3.6E-6	1.7E-5	2.5E-5	2E-5
Biot coefficient [-]	1	0.8	-	-	-

Table 1: Model parameters (1D and 2D model)

The model boundaries are assumed to be mechanically fixed in normal direction. Energy and fluid exchange is only possible via the right-hand boundary at a constant fluid pressure of 4 MPa and a constant temperature of 25 °C. The global initial temperature is also 25 °C and the global initial total stress has the value 8 MPa. The canister section is initially partly saturated with a liquid saturation of 0.75 and a gas pressure of 0.1013 MPa. The host rock section is initially fully saturated at a fluid pressure of 4 MPa. A heat and gas source is evenly distributed to the canister section representing the heat production from the waste and hydrogen production due to canister corrosion. The heat source with an initial power of 1.5 W is linearly decreasing to zero within 10,000 years and the gas production starts to increase linearly after 5,000 years, reaches its maximum of 10^{-9} kg/s after 10,000 years and decreases linearly to zero within the following 5,000 years.

2.2 Results

From the simulation results, the quantities temperature, horizontal displacement, liquid pressure and gas pressure have been evaluated as temporal evolutions at different horizontal locations (Figure 2). The heat input leads to a temperature increase in the whole model for about 150 years with a subsequent temperature decrease to the initial temperature until the end of the heat production phase. The temperature increase results in an initial pore pressure increase in the host rock at constant gas pressure followed by a fluid pressure decrease resulting from the ongoing saturation of the (initially partly saturated) canister section and another fluid pressure increase until an intermediate pressure equilibrium in the whole model is reached after about 2,000 years. The host rock desaturation phase is accompanied by a slight material contraction followed by an expansion (as well equilibrating after 2,000 years). Moreover, the triangular evolution of the gas production in the canister section between 5,000 years and 15,000 years is visible in the fluid pressure and displacement evolutions.

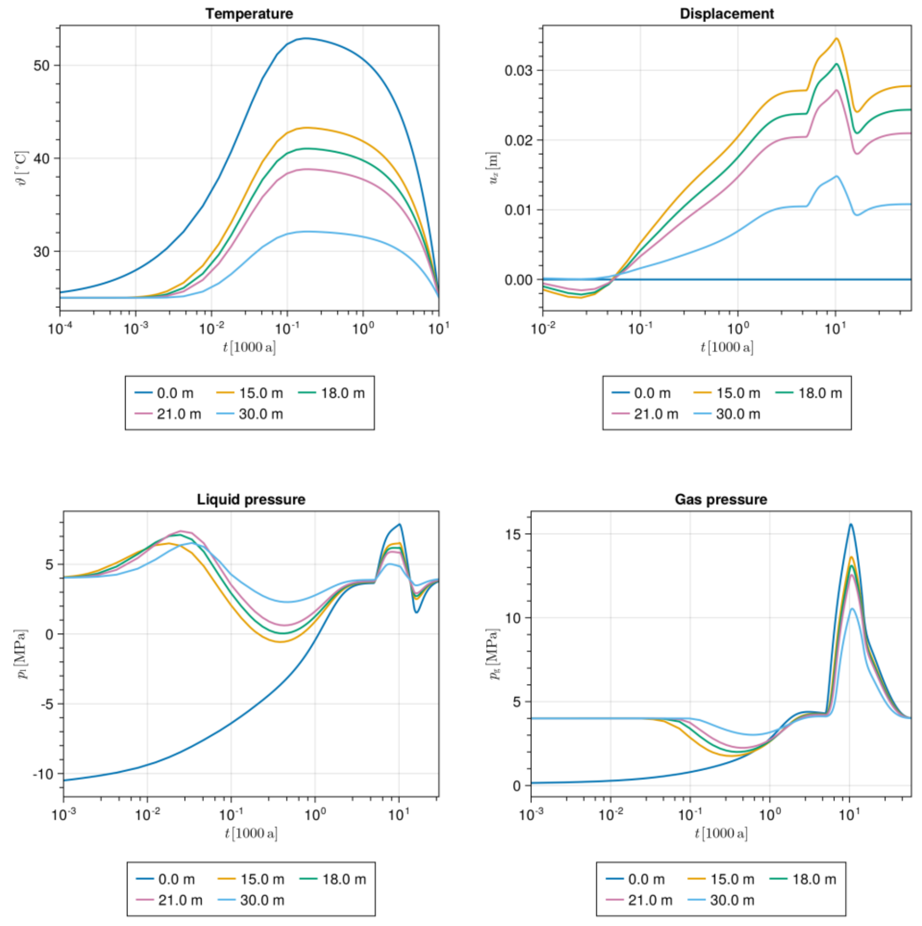

Figure 2: Point evolution of temperature, displacement, liquid, and gas pressure (1D model)

3 TWO-DIMENSIONAL GENERALIZATION AND INCREASING PROCESS COUPLING COMPLEXITY

3.1 Model assumptions, conditions, and parameters

The two-dimensional model (Figure 3) describes a cross-section of a horizontal disposal drift considering canister and backfill as two different materials together with the surrounding argillaceous host rock. Prior to a fully coupled THM simulation, it is the aim to gradually increase the complexity of the problem. The different modelling steps are given by:

TM → TH (Richards) → TH (two-phase flow) → THM (Richards) → THM (two-phase flow)

The first two modelling steps are considered hereafter. For the TM problem, the energy balance, solid mass balance and stress equilibrium equations are solved. The constitutive assumptions are given by Fourier's law and linear elasticity with additional linear thermal expansion. A constant temperature of 28 °C is assumed at the top and bottom boundary and initially throughout the entire model. No heat flow is possible through the left and right boundary. The left, bottom and right boundary are mechanically fixed in normal direction and a vertical compressive total stress of 14 MPa is applied to the top boundary. The initial stress state is given by a compressive vertical total stress of 14 MPa and compressive horizontal total stresses of 10 MPa. A heat source distributed to the area of the canister is considered. The initial heat power of 51 W/m³ decreases linearly to zero within 1,000 years.

To tackle the TH problem, the energy and water mass balance equations are solved. The liquid phase follows Darcy's law and a constant gas pressure of 0.1013 MPa is assumed. The thermal boundary conditions and the heat source are identical to the conditions in the TM problem. No fluid flow is allowed through the left and right boundary. A constant liquid pressure of 0.1013 MPa is assumed for the top and bottom boundary and initially for the host rock. An initial liquid saturation of 0.2 is given for the backfill. All parameters considered for the two-dimensional TM and TH problem are shown in Table 1.

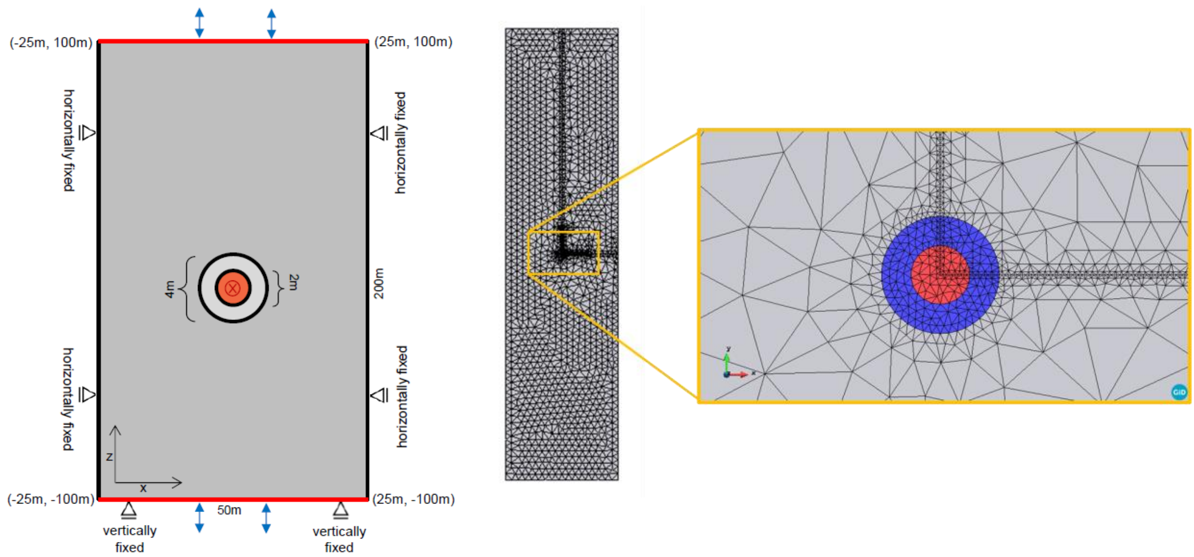

Figure 3: Model geometry and mesh details (2D model)

3.2 Results

The results of the TM and TH simulations are given by the evolution of field quantities at different distances from the canister center along the horizontal symmetry axis and by profiles along this axis at different time instances. Temperature and displacement evolutions and profiles for the TM simulation are given in Figure 4. The heat source generates a temperature increase during the first 200 years followed by a decrease to the initial temperature after 2,000 years. The temperature increase leads to a reversible expansion of the canister and the host rock while the backfill is being contracted. The assumption of thermo-elastic material behavior leads to a recovery of the initial mechanical state after the heat source has lapsed.

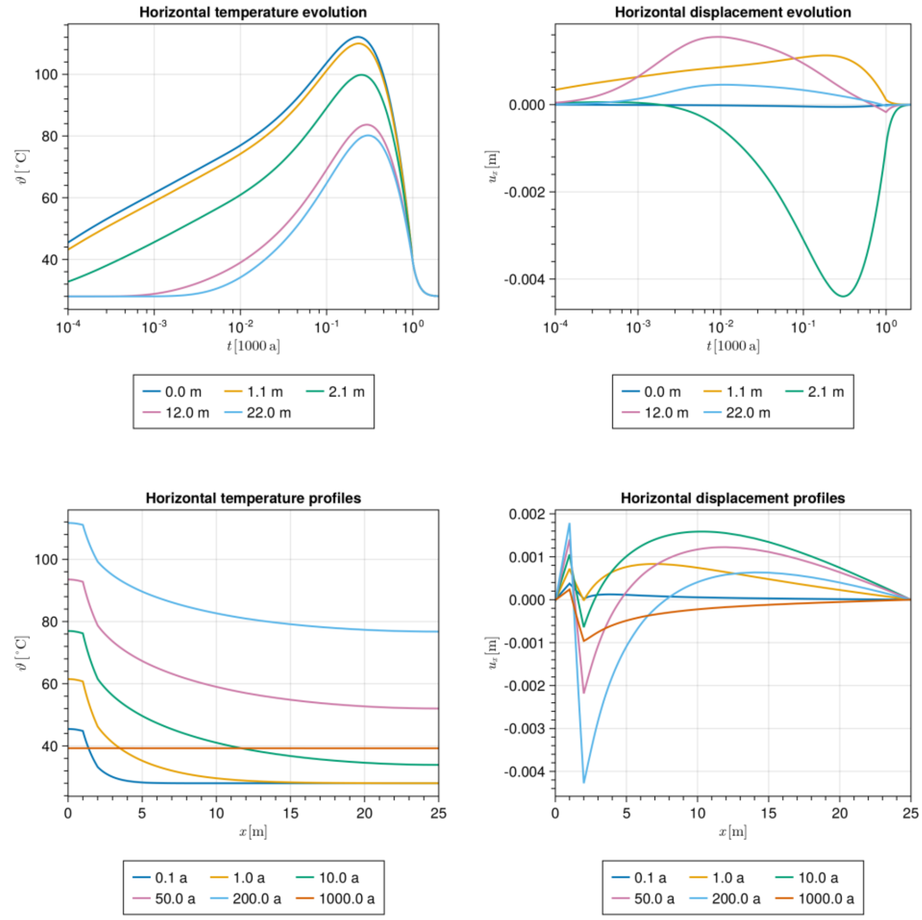

Figure 4: Evolution and profiles of temperature and displacement for the TM simulation (2D model)

The liquid pressure evolution and profiles for the TH simulation are given in Figure 5. The temperature evolution is similar as given in Figure 4 for the TM simulation. The temperature increase leads to a liquid pressure increase in the host rock in some distance from the drift contour. Near the interface to the backfill, the host rock is slightly desaturated as it provides liquid for the backfill saturation. After full saturation has been reached in the backfill, a further pressure increase occurs in the entire model as long as the temperature increases. The initial pressure is regained after the heat source has lapsed.

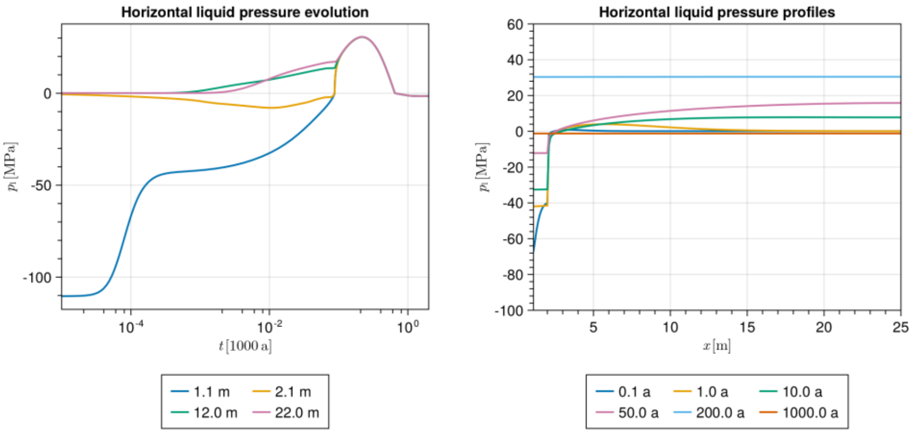

Figure 5: Evolution and profiles of liquid pressure for the TH simulation (2D model)

4 CONCLUSIONS AND OUTLOOK

The simulations of the considered one- and two-dimensional THM models of nuclear waste repository systems using CODE_BRIGHT show reasonable values of the computed field variables in space and time and particularly capture phenomena such as backfill saturation, host rock de- and resaturation, thermal expansion and thermal pressure increase. The chosen model assumptions and parameters refer to a drift disposal concept in argillaceous host rock. However, not all model assumptions are intended to represent real conditions in a repository but to allow for a comparison of simulation results of different codes, which is the superior goal of the benchmarking project BenVaSim II.

The next step is the fully coupled THM simulation of the considered two-dimensional model and the introduction of more complex material models and anisotropy. Moreover, a three-dimensional model of the neighborhood of a disposal drift will be studied.

ACKNOWLEDGEMENTS

The project BenVaSim II is supported by the German Federal Ministry for the Environment, Nature Conservation, Nuclear Safety and Consumer Protection under contract 02E12022B.

REFERENCES

[i] Lux, K.-H., Rutenberg, M., Feierabend, J., Czaikowski, O., Friedenberg, L., Maßmann, J., Pitz, M., Sentis, M., Graupner, B., Hansmann, J., Hotzel, S., Kock, I., Rutqvist, J., Hu, M., Rinaldi, A.P. (2021) International Benchmarking for Verification and Validation of TH2M Simulators with Special Consideration of Fluid Dynamical Processes in Radioactive Waste Repository Systems (BenVaSim) Synthesis report. DOI: 10.13140/RG.2.2.28998.34887.

AN APPROACH FOR THE MODIFICATION OF MODELLING CRUSHED SALT COMPACTION PROCESSES

Larissa Friedenberg[*] and Sebastià Olivella[†]

[*] Gesellschaft für Anlagen- und Reaktorsicherheit (GRS) gGmbH
Theodor-Heuss-Straße 4, 38122 Braunschweig, Germany
E-mail: larissa.friedenberg@grs.de

[†] Department of Civil and Environmental Engineering
Technical University of Catalonia (UPC)
Campus Nord UPC, 08034 Barcelona, Spain

Key words: Crushed salt compaction, rock salt repository, backfill, constitutive modelling

Abstract. *This paper presents an approach for the modification of the dislocation creep model in CODE_ BRIGHT with the aim to improve the numerical reproduction of crushed salt compaction processes. Phenomenological functions are implemented to overcome the fixed geometrical dependence on the idealized grain/grain structure. A triaxial compaction test was simulated to show the improvements gained due to the modification.*

1 INTRODUCTION

The investigation of crushed salt compaction is part of the research in frame of a repository for high-level nuclear waste in the host rock salt. Crushed salt will be used as backfill and sealing material for open drifts and shafts and will act as a long-term stable barrier. With time, the crushed salt gets compacted due to the convergence of the rock salt, reducing crushed salt's initial high porosity of about 30 % to a final porosity comparable with rock salt (≤ 1 %).

For the long-term safety assessment of a repository in rock salt, a qualified prognosis of the long-term compaction behavior of crushed salt is crucial. It requires a fundamental process understanding and a reliable numerical reproduction and projection into future.

The validation, verification, and calibration of constitutive models for crushed salt is done by re-simulating laboratory experiments. The experimental program of the KOMPASS-II project dealt with the isolated investigation of influencing factors in triaxial long-term compaction tests[i]. The tests are simulated using the constitutive model for crushed salt available in CODE_BRIGHT. The results showed some discrepancies between the numerical simulation and the measurement data, especially for the creep behavior[i].

Based on the process understanding gained from the experimental investigations in the KOMPASS-II project, it is strived for an optimization of the constitutive model formulation in CODE_BRIGHT enhancing the reproduction of crushed salt compaction processes.

This paper presents an approach for modifying the numerical simulation of crushed salt compaction using CODE_BRIGHT. The approach addresses the dislocation creep equation.

2 CONSTITUTIVE MODEL FOR CRUSHED SALT IN CODE_BRIGHT

The constitutive model for the simulation of crushed salt compaction processes covers an additive approach of various mechanisms: linear elastic deformations (EL), fluid assisted diffusional transfer mechanism (FADT), dislocation creep (DC) and viscoplastic deformations

(VP)[ii]. The model is formulated in terms of strain rates:

$$\dot{\varepsilon} = \dot{\varepsilon}_{EL} + \dot{\varepsilon}_{FADT} + \dot{\varepsilon}_{DC} + \dot{\varepsilon}_{VP} \tag{1}$$

Since this paper focuses on the dislocation creep (DC) mechanism, only the main components of this mechanism will be shown here. A summary of the whole constitutive model for crushed salt can be found in Olivella & Gens (2002)[ii].

The dislocation creep model is formulated based on a viscoplastic approach:

$$\dot{\varepsilon}_{ij}^{DC} = \frac{1}{\eta}\Phi(F)\frac{\partial G}{\partial \sigma'_{ij}} \tag{2}$$

Where G is the flow rule, F a stress function, Φ a scalar function and η the viscosity. G and F are written in terms of stress invariants $q = (3^*J_2)^{0.5}$ and $p = I_1/3$.

$$F = G = \sqrt{q^2 + \left(\frac{-p}{\alpha_p}\right)^2} \tag{3}$$

$$\Phi(F) = F^n \tag{4}$$

$$\eta = \eta_{DC}^d, \ \ \alpha_p = \left(\frac{\eta_{DC}^v}{\eta_{DC}^d}\right)^{1/(n+1)} \tag{5}$$

The exponent n comes from the rock salt power law. The parameter α_p contains information based on material properties and the idealized geometry which are described by the volumetric and deviatoric viscosities, η^v_{DC} and η^d_{DC}, respectively (Equation 6 and 7). The information of idealized geometry is incorporated by geometrical functions (g^v_{DC} and g^d_{DC}) which depend on void ratio and can be described by the functions g and f. These basic functions g and f are derived by the definition of the idealized grain geometry as shown in Figure 1. They are pre-defined by a dependence on void ratio e.

$$\frac{1}{\eta_{DC}^v} = A(T)g_{DC}^v(e) \tag{6}$$

$$\frac{1}{\eta_{DC}^d} = A(T)g_{DC}^d(e) \tag{7}$$

$$g_{DC}^v(e) = 3(g-1)^n f \tag{8}$$

$$g_{DC}^d(e) = \left(\frac{\sqrt{1+g+g^2}}{3}\right)^{n-1}\left(\frac{2g+1}{3}\right)f + \frac{1}{\sqrt{g}} \tag{9}$$

$$g = \frac{1}{(1-f)^2} = \frac{d^2}{x^2} \tag{10}$$

$$f = \sqrt{\frac{2e}{3(1-e^{\frac{3}{2}})(1+e)}} = \frac{\sqrt{2}s}{d} \tag{11}$$

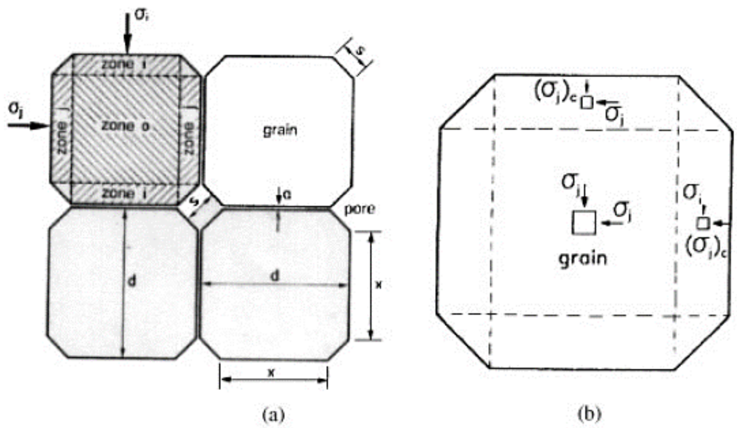

Figure 1: Idealized grain geometry as basis for the derivation of the constitutive model for dislocation creep. a) composition of ideal grains. b) stress concentration zones[ii]

3 MODIFICATION APPROACH

The basis of an idealized geometry to develop a constitutive model is a common approach and based on microstructural observations[ii]. However, it lacks some generality since the compaction process can change the arrangement of grains, as well as the grain shape due to breakage, deformation and/or dissolution/precipitation processes.

Numerical simulations of triaxial compaction tests performed in the KOMPASS-II project showed deviations to the measurement data, especially for the creep part[i]. As an approach for optimizing the constitutive model formulation and giving more flexibility regarding the geometry definition, it is proposed to formulate g^v_{DC} and g^d_{DC} in terms of phenomenological functions which can be calibrated on experimental data. Figure 2 is a plot of g^v_{DC} and g^d_{DC} in dependence of the void ratio as implemented in CODE_BRIGHT.

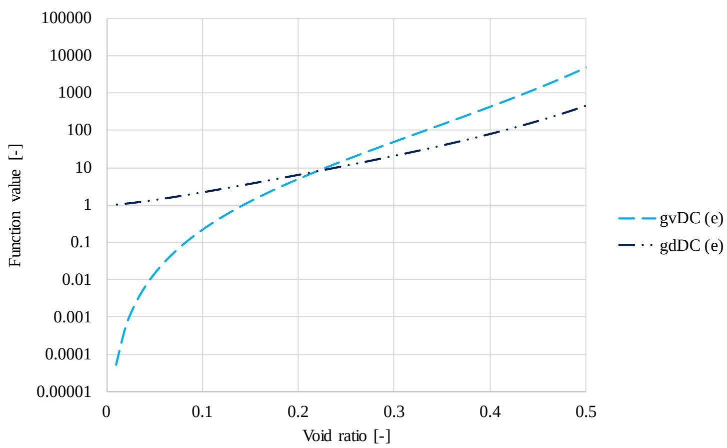

Figure 2: Geometrical functions for the dislocation creep mechanism as implemented in CODE_BRIGHT. Light blue: volumetric part. Dark blue: deviatoric part.

Based on the trend of the originally implemented functions, an exponential approach is proposed for the phenomenological functions:

$$g^v_{DC} = \exp(a * e^b) - 1 \tag{3}$$

$$g^d_{DC} = \exp(c * e^d) \tag{4}$$

Where e is the void ratio, a, b, c and d are parameter.

These proposed functions can be calibrated against experimental data from triaxial tests considering volumetric and deviatoric strain rates, respectively. An example is shown for the triaxial compaction test TUC-V2 described in the following section.

4 NUMERICAL SIMULATION OF THE TRIAXIAL LONG-TERM COMPACTION TEST TUC-V2

One test of the experimental program in the KOMPASS-II project is the triaxial long-term compaction test TUC-V2. It ran over a period of 750 days and covers 5 phases with different boundary conditions (Figure 3). The test addresses different levels of mean stress, deviatoric stress cycles and temperature changes.

Figure 3b shows the axisymmetric model applied for the simulation of TUC-V2. The constitutive model described in Equation (1) is applied.

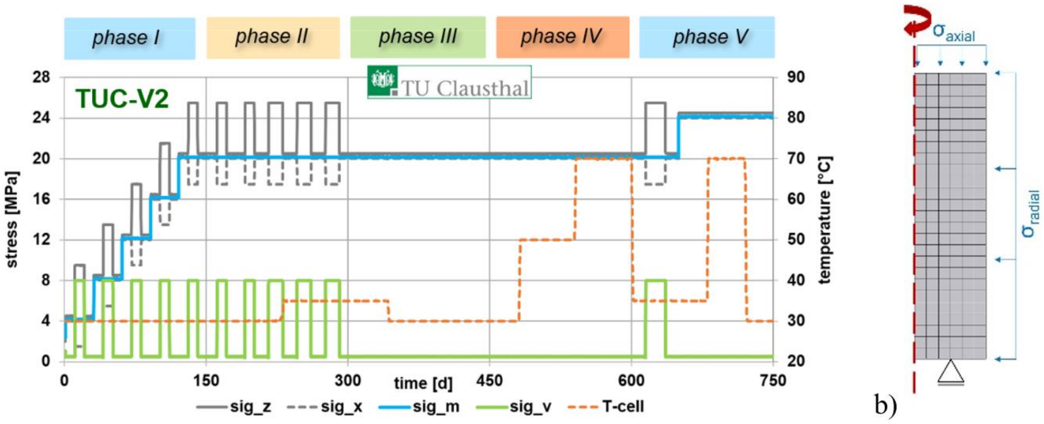

a) b)

Figure 3: Triaxial long-term compaction test TUC-V2[i]. a) Loading history. b) Numerical model.

Two simulations are performed: one with the original formulation for dislocation creep and a second one with the proposed phenomenological functions which are calibrated against the experimental data. Therefore, the only difference between these two simulations are the functions g^{v}_{DC} and g^{d}_{DC}.

Figure 4 shows the experimental data derived for the volumetric and deviatoric part, respectively, the original formulation for the geometrical functions and the calibrated phenomenological functions. For the phenomenological approach the parameter are chosen as: a = 1000; b = 3.1; c = 50; d = 2. Especially for the volumetric part (Figure 4a), the phenomenological function shows a very good accordance with the experimental data.

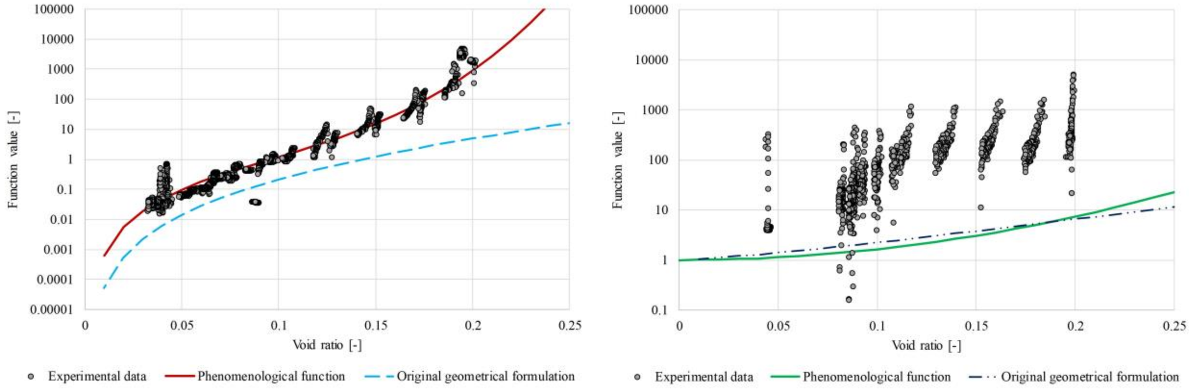

Figure 4: Calibration of phenomenological functions against experimental data. a) Function gvDC. b) Function gdDC

The comparison of numerical results against measurements of TUC-V2 are shown in Figure 5 for the volumetric strain and in Figure 6 for the deviatoric strain. The simulation with the original geometrical function strongly underestimates the volumetric compaction but overestimates the deviatoric deformation. The results using the phenomenological approach are in accordance with the measurement data for the volumetric part. Here, the function is calibrated very nice against the experimental data leading to a very good reproduction of the volumetric deformation behavior. For the deviatoric part, the phenomenological approach leads to an improvement of the numerical reproducibility, however, is not satisfactory. The numerical model gives a high respond to the deviatoric load changes which are not visible in the measurements.

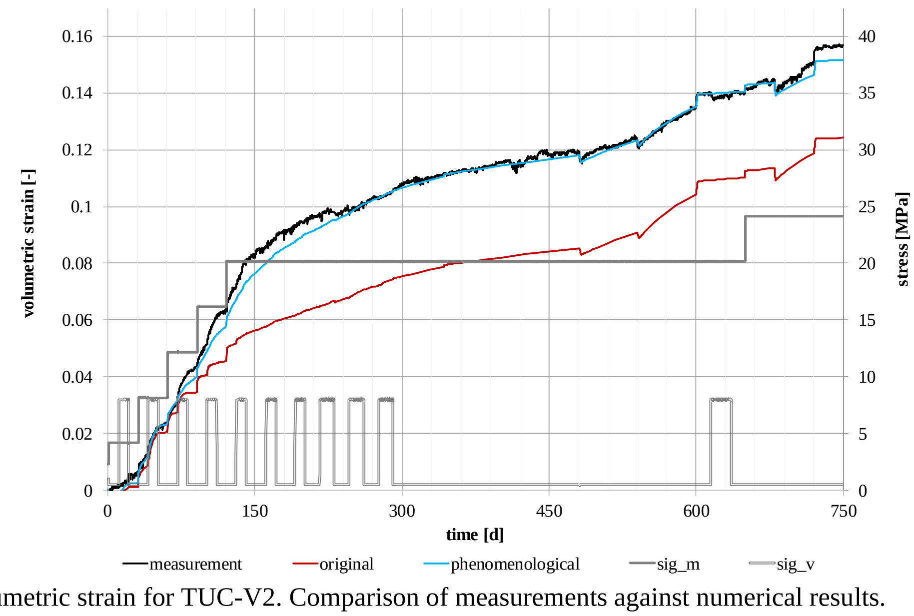

Figure 5: Volumetric strain for TUC-V2. Comparison of measurements against numerical results.

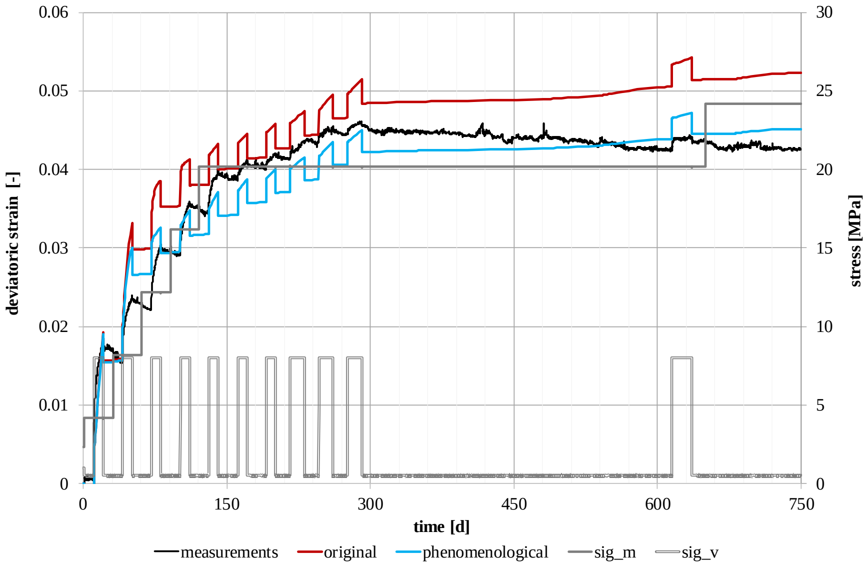

Figure 6: Deviatoric strain for TUC-V2. Comparison of measurements against numerical results.

5 CONCLUSION AND OUTLOOK

This paper presents an approach for the modification of the dislocation creep model in CODE_BRIGHT with the aim to improve the numerical reproduction of crushed salt compaction processes. Two phenomenological functions are implemented, one for volumetric and one for deviatoric deformations, to replace the stiff original geometrical formulation based on an idealized grain structure. The phenomenological functions are calibrated against experimental data from the triaxial long-term compaction test TUC-V2 to receive the four free parameters. The comparison of numerical results with the original and the modified formulation showed an improvement of numerical reproduction using the new approach. Especially, the volumetric deformation behavior is in good accordance with the measurement data, due to a sufficient calibration of the volumetric phenomenological function. Also, for the deviatoric deformation behavior improved results are presented. However, there is still potential for improvement in the calibration of the deviatoric phenomenological function which may lead to better agreement with the measurement data.

All in all, the presented approach gives flexibility in the constitutive model for crushed salt and shows sufficient first results. The approach will be followed up and further developed.

REFERENCES

[i] Friedenberg, L. Bartol, J., Bean, J., Beese, S., Coulibaly, J. B., Czaikowski, O., Bresser, J. de, Düsterloh, U., Eickemeier, R., Gartzke, A.-K., Hangx, S., Jantschik, K., Laurich, B., Lerch, C., et al.: Compaction of Crushed Salt for the Safe Containment - Phase 2, KOMPASS-II. Gesellschaft für Anlagen- und Reaktorsicherheit (GRS) gGmbH: Köln, 2024.

[ii] Olivella, S., Gens, A. 2002. A constitutive model for crushed salt. International Journal for Numerical and Analytical Methods in Geomechanics, 26(7), 719–746. https://doi.org/10.1002/nag.220

MODELLING BARRIER HYDRATION AND SWELLING UNDER SALINITY CONDITIONS

A. Ramon*, S. Olivella* and A. Rodríguez-Dono*

* Department of Civil and Environmental Engineering
Universitat Politècnica de Catalunya - BarcelonaTech (UPC)
Campus Nord UPC, 08034 Barcelona, Spain

Centre Internacional de Metodes Numerics a l'Enginyeria (CIMNE),
Campus Nord UPC, 08034 Barcelona, Spain

E-mail: anna.ramon@upc.edu, sebastia.olivella@upc, alfonso.rodriguez@upc.edu

Key words: Chemistry, Expansion, Bentonite barriers, THMC coupled analysis, CODE_BIGHT

Abstract. *Chemical processes in rocks and soils influence the mechanical and hydraulic behaviour of the geological medium. For instance, the occurrence of cation exchange in clayey materials may result in a modification of the swelling capacities. The mineralogical composition of a soil or rock mass and, also, the chemical composition of the groundwater define the chemical processes that may take place in the field. Knowing in detail the chemistry involved in a geotechnical problem is relevant because the development of chemical reactions can influence on the hydraulic and mechanical behaviour of the geological media. This is the case of the modification of the swelling potential or the triggering of an expansive or shrinkage response of the soil after a variation in the salinity of groundwater and, also, when cation exchange occurs in clayey soils (e.g. [i]). The implications of these effects of chemistry are relevant, for example, for the design of engineered barrier systems for nuclear waste repositories. A formulation to address and to model the effects of chemistry on geotechnics is available. The general chemical formulation considers the mass balance of chemical species in terms of the chemical components present in the medium. The solution of the reactive transport takes into account the presence of equilibrium and kinetic chemical reactions in the medium. The existence of equilibrium reactions implies the solution of an additional chemical speciation, coupled with the general chemical problem, which considers the mass action laws of equilibrium. Reaction kinetics is directly considered in the source or sink terms of the balance equations. The chemical formulation is implemented in a coupled manner with the* thermo-hydro-mechanical (*THM) program CODE_BRIGHT. The implementation of the chemical subroutines follows an object oriented programming which permits independent structures. This leads to a more flexible and versatile code for future developments. An example based on the hydration and expansion of a bentonite barrier will be described.*

1 INTRODUCTION

In general terms, the mineralogical composition of a soil or rock mass and, also, the chemical composition of the groundwater define the chemical processes that may take place in the field.

Knowing in detail the chemistry involved in a geotechnical problem is relevant because the development of chemical reactions can influence on the hydraulic and mechanical behaviour of the geological media. This is the case of the modification of the swelling potential or the triggering of an expansive or shrinkage response of the soil after a variation in the salinity of groundwater and, also, when cation exchange occurs in clayey soils (e.g. [i]). The implications of these effects of chemistry are relevant, for example, for the design of engineered barrier systems for nuclear waste repositories.

In another context, the dissolution of soluble minerals present in the rock mass or soil and the precipitation of crystals also have an influence on the hydraulic and mechanical behaviour of geological media. These phenomena have been described by several authors and often lead to severe expansions that are capable of damaging infrastructures and buildings. For instance, the growth of selenite, in the presence of pyrite, induced the expansion of sub-floor fills and resulted in the heave of more than 12000 houses in Ireland [ii], and the crystallization of ettringite and thaumasite, when sulphate attack develops within compacted sulphated soils, may results in important expansions damaging road bases and embankments ([iii] and [iv]). The extreme expansions observed in anhydritic rocks are another example in which dissolution and precipitation processes play an important role in the geotechnical behaviour ([v] and [vi]).

The extended abstract addresses the numerical modelling of chemical processes coupled to THM problems in geological media. A numerical model capable of simulating general chemical processes and the mechanical and hydraulic effects generated by them will be summarised. Details on the equations and hypothesis considered in the model will be described. An application example involving the chemical processes and its effects on the hydraulic and mechanical behaviour will be presented.

2 MODEL DESCRIPTION

The development of chemical processes has been formulated within a general framework for coupled THM analysis for saturated and unsaturated porous materials. The THM analysis addresses the resolution of the balance equations of the solid phase, water, air, momentum of the medium and internal energy in a coupled manner. To be able to consider the coupled chemical modelling, the formulation should describe the mass balance of chemical species, which will have to be resolved also in a coupled manner with the rest of balance equations.

The chemical formulation has been designed to be able to model geotechnical problems dealing with general chemical systems. In that direction, the formulation takes into account that the chemical system of the "chemical-geotechnical problem" analysed is characterized by all the liquid and solid chemical species present in the medium, and the involved chemical reactions. However, the mass balance of chemical species is formulated considering the chemical components of the system instead of all the individual species. A benefit of this is the reduction of the number of equations that have to be solved and the simplification of the structure of the equations because of the cancellation of some sink/source terms. In addition, the model can consider the occurrence of kinetic and/or equilibrium chemical reactions.

After the substitution of the mass balance of total solid, the mass balance equation for each liquid and solid chemical species can be written in matrix notation:

$$\phi \frac{D}{Dt}(\mathbf{m}_l S_l) + (1-\phi)\frac{D}{Dt}(\mathbf{m}_s) + (\mathbf{\nabla} \cdot \mathbf{J}_l')^T = \mathbf{U}\mathbf{S}_{kin}^T \mathbf{r}_{kin} \qquad (1)$$

for constant solid density, including precipitation. The equation has the same structure than the standard mass balances equations for THM analysis. The right hand term of the equation accounts for the source/sink term that comes from the occurrence of the chemical reactions. **S** and **U** are the stoichiometry and component matrices of the chemical system, ϕ is the porosity of the medium, S_l is the water saturation degree of the medium and the term $(\nabla \cdot \mathbf{J}_l')^T$ accounts for the rates of advective and dispersive flow. $\mathbf{m}_l$ and $\mathbf{m}_s$ are the vectors of the concentrations of the species.

The solution of the balance of chemical species is performed in a coupled manner with the rest of THM balance equations and provides the concentrations of components. When equilibrium reactions exist, the concentrations of the chemical species are calculated following a chemical speciation. Then, the formulation addresses the chemical speciation with the resolution of the implicit equation defined from the mass action law for the equilibrium chemical reactions

$$\mathbf{S}\log\mathbf{a} - \log\mathbf{k} = 0 \tag{2}$$

where **a** is the vector of the activities of each chemical species and **k** is the vector of the equilibrium constants of the chemical equilibrium reactions.

The model also allows taking into account the effects of the chemical coupling on the mechanical and hydraulic behaviour of the geological media. For instance, the model allows to reproduce the effects of the chemistry of groundwater on the swelling behaviour of clayey materials and also, its hydraulic implications. This is considered in the formulation of the Barcelona Basic Model (BBM) following the equations 3 and 4

$$\kappa_s = \kappa_{s0} f_s(s) f_p f_{chem}(I) \tag{3}$$

$$f_{chem}(I) = \left(\frac{2b\tanh^{-1}(aI+d)+c}{2b\tanh^{-1}(aI_0+d)+c}\right) \le 1\,;\, I_0 = 0 \tag{4}$$

where the term f_{chem} incorporates the chemical effects for the definition of the parameter k_s of the BBM model. f_{chem} depends on the ionic strength of groundwater, I , and the constants a, b, c and d. The ionic strength is calculated during the coupled resolution. The relationship described in equation 4 is inspired on de proposal to calculate swelling pressure described in [i].

In addition, the model formulation also describes the swelling deformations and pressures induced by the precipitation of minerals and, also, its hydraulic implications. In this regard, the formulation considers that the precipitation of salts can occur filling the existing porosity and that it can also lead to a volume change in excess of the precipitated crystal volume. The model simulates these latter chemical effects on the mechanical and hydraulic behaviour following the approaches described in [vii], [viii] and [ix].

All these chemical developments are included in the Finite Element program for THM analysis of porous media CODE_BRIGHT [x]. The design of all the chemical subroutines is programmed using the Object Oriented Fortran to get independent programming structures. This provides a more flexible and versatile code in view of future extensions of the formulation.

3 EXAMPLE OF APLICATION

One well known case in geotechnics involving chemical processes is the hydration of the clayey barriers used for nuclear waste disposal in underground galleries. The chemistry characteristics of the interstitial water has an effect on the swelling potential of the material. [i] proposed a relationship to describe the effect of chemistry on the swelling pressure developed based on data test.

The coupling between the hydro-mechanical behaviour and the chemical processes taking place during the hydration and swelling of a bentonite barrier under different salinity conditions has been analysed with the numerical model described. The chemical system considered during the simulations was characterized by 5 chemical species: Na^{+}, CL^{-}, Ca^{+2}, NaCl(aq) and $CaCl_2$(aq). Two equilibrium chemical equations completed the definition of the chemical system.

A synthetic 2D numerical simulation of a typical bentonite barrier was used to verify the chemical formulation coupled with the general THM code. The chemical module CheMech of CODE_BRIGHT was used for the calculations. Figure 1a shows the geometry of the model considered in the calculations. The FEBEX test ([xi]) showed in Figure 1b inspired the geometry of the model considered. The model considers that the barrier is made of bentonite blocks (figure 1a). The joints between the blocks are described in the geometry by means of a material with similar properties than the bentonite. The differences are a higher porosity and a reduced compressibility. The host rock is not simulated as a separate material, the rock is considered by means of boundary conditions applied at the outer boundary of the bentonite barrier. An entrance of water is defined at the "virtual" contact between the host rock and the bentonite barrier. The generation of heat by the canister (indicated in green in Figure 1a) is simulated by means of a heat flux imposed at the exterior boundary of the canister.

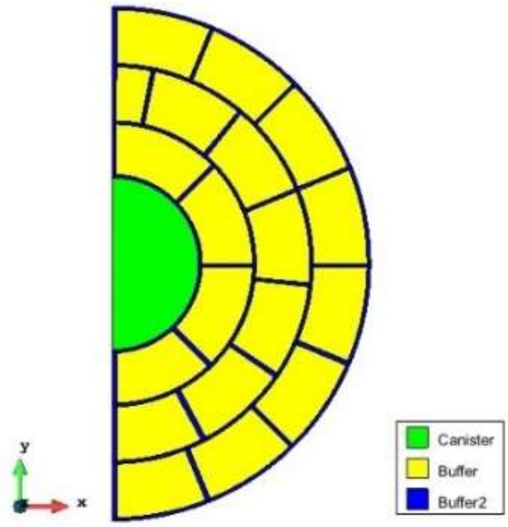

Figure 1. (a) Geometry of the model, 8b) FEBeX test (Gens et atl., 2009)

Four different solute compositions were imposed at the outer boundary of the bentonite barrier (cases "THM", "THMC1", "THMC2" and "THMC3"). The case "THM" corresponds to the case with equilibrium. The three waters with salts considered in the analysis contained intermediate salinities between two stablished well known "waters": a water in equilibrium with the mineralogical composition of bentonite and the brine (for brine I = 1.62 mol/kg). Respectively for the 4 cases analized, the ionic strength of the cases is 0.0, 0.28, 0.57, 0.96 mol/kg.

The numerical analysis verified the capabilities of resolution of reactive transport and mixing of solutes in porous media. A homogeneous distribution of dissolved salts was obtained along the simulated geometry in all the cases. The simulation described the chemical processes taking place and, also, the different development of swelling behaviour of the barrier over time under each salinity (material Buffer 2 in Figure 2). Figure 3 shows the special distribution of contraction and expansion strains during the test. Reddish colours stand for calculated contraction strains whereas expansions are represented by bluish colours. Contraction strains occur within the bentonite blocks near the canister and also within the joints. The development of swelling deformations starts at the external boundary of the outer blocks, at the rock-bentonite contact.

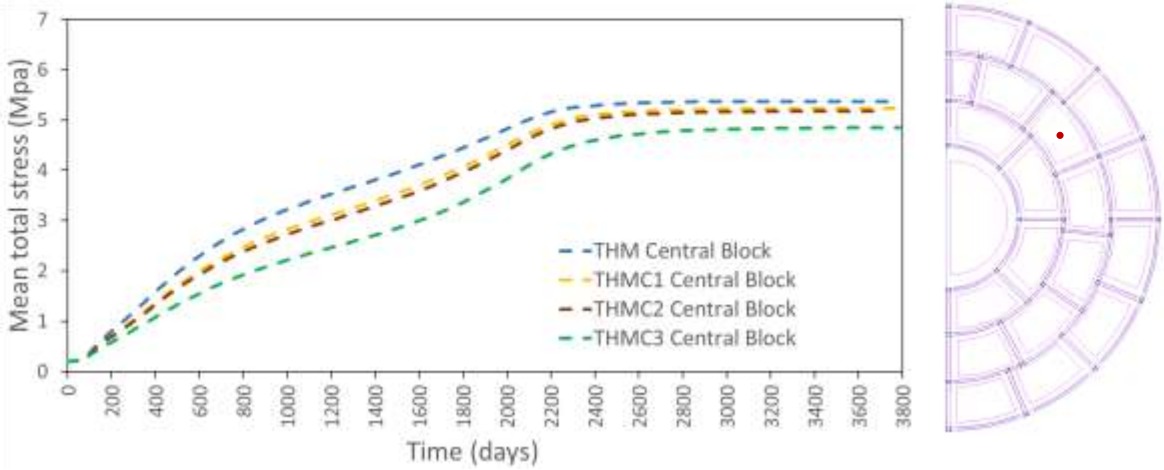

Figure 2. (a) Comparison of mean stress over time under different salinities calculated at the point indicated in (b)

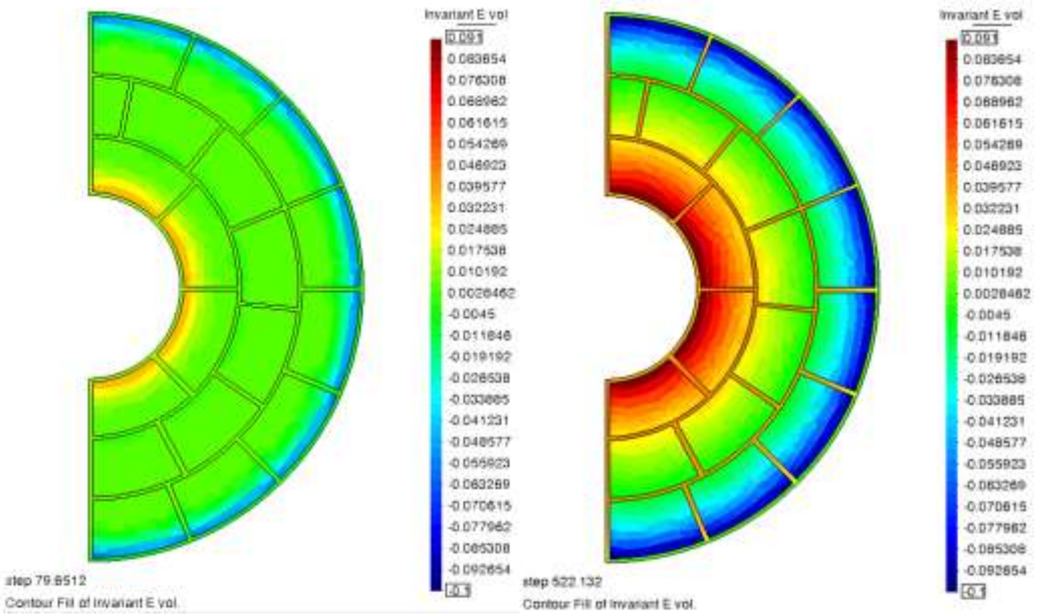

Figure 3. Distribution of volumetric deformations during the simulation of the in-situ test for two times

The code requires additional developments to permit the simulation of more complex mechanical couplings. However, the preliminary results of simulations of the expansion in clayey material are promising. The numerical analyses show that the model, apart from solving reactive transport, is also capable to reproduce the expansions generated by the precipitation of salts.

5 CONCLUSIONS AND DISCUSSION

The importance of the chemistry involved in geotechnical problems and its damaging effects have been highlighted. In that direction, an approach for coupled thermo-hydro-mechanical and chemical analysis has been presented for simulating the chemical processes involved in geotechnical situations. The chemical model is formulated to address general chemical systems dealing with an unlimited number of liquid and solid chemical species.

The development of swelling behaviour in clayey barriers induced by different salinity conditions has been selected as an example to illustrate the type of processes to be investigated. The simulation of the chemical processes involved shows the type of couplings of the THM chemical code. The independent programming structures of the chemical formulations is based on the object oriented Fortran. This design facilitates the implementation of future advanced formulation developments in the THMC code.

REFERENCES

[i] Yustres, A., Jenni, A., Asensio, L., Pintado, X., Koskinen, K., Navarro, V., Wersin, P. 2017. Comparison of the hydrogeochemical and mechanical behaviours of compacted bentonite using different conceptual approaches. Applied Clay Science, 141: 280-291.1.

[ii] Ryskin, M. & Maher, M.L.J. 2021. The pyrite heave problem: New insights from trace-element analysis. Geotechnique Letters. 4(5). 10.1680/jgele.21.00016.

[iii] Rajasekaran, G., 2005. Sulphate attack and ettringite formation in the lime and cement stabilized marine clays. Ocean Engineering, 32, 1133-1159.

[iv] Alonso, E. E. and Ramon, A. 2013. Massive sulfate attack to cement-treated railway embankments. Géotechnique 63, No. 10, 857 – 870

[v] Alonso, E.E., Berdugo, I.R. and Ramon, A. 2013. Extreme expansive phenomena in anhydritic-gypsiferous claystone: the case of Lilla tunnel. Géotechnique 63 No. 7, 584 – 612

[vi] Ramon, A. and Alonso, E. E. 2018. Heave of a Building Induced by Swelling of an Anhydritic Triassic Claystone. Rock Mech. Rock Engng.: 51, Issue 9, pp 2881–2894.

[vii]Ramon A, Alonso EE. 2013. Heave of a railway bridge: modelling gypsum crystal growth. Géotechnique 63(9):720–732. https:// doi. org/ 10. 1680/ geot. 12.P. 035

[viii] Olivella, S. & Alonso, E. E. (2008). Gas flow through clay barriers. Géotechnique 58, No. 3, 157–176, http://dx.doi.org/10.1680/geot.2008.58.3.157.

[ix]Ramon A, Alonso EE, Olivella S. 2017. Hydro-chemo-mechanical modelling of tunnels in sulfated rocks. Géotechnique 67(11):968–982. https ://doi.org/10.1680/jgeot .SiP17 .P.252

[x] Olivella, S., Gens, A., Carrera, J. & Alonso, E. E. 1996. Numerical formulation for a simulator (Code_Bright) for the coupled analysis of saline media. Engng Comput. 13, No. 7, 87–112.

[xi] Gens, A., Sánchez, M., Guimarães, L. D. N., Alonso, E. E., Lloret, A., Olivella, S., Villar, M. V., & Huertas, F. (2009). A full-scale in situ heating test for high-level nuclear waste disposal: Observations, analysis and interpretation. Geotechnique, 59(4), 377–399.